PROBABILISTIC MICROMECHANICS OF WOVEN CERAMIC MATRIX COMPOSITES

By

MARLANA GOLDSMITH

A DISSERTATION PRESENTED TO THE GRADUATE SCHOOL
OF THE UNIVERSITY OF FLORIDA IN PARTIAL FULFILLMENT
OF THE REQUIREMENTS FOR THE DEGREE OF
DOCTOR OF PHILOSOPHY

UNIVERSITY OF FLORIDA

2013

To my family

ACKNOWLEDGMENTS

I wish to express my sincere gratitude to my advisors, Dr. Bhavani Sankar and Dr. Raphael Haftka, for their invaluable guidance. Their ability to provide a balance of both freedom and direction greatly contributed to my learning experience throughout the completion of this work. I would also like to thank Dr. Ashok Kumar, Dr. John Mecholsky, and Dr. Robert Goldberg for serving on my committee and reviewing my work.

I am also very thankful for the time I spent at NASA GRC with Dr. Goldberg. The support of Dr. Goldberg, Dr. Peter Bonacuse, and Dr. Subodh Mital during my time at NASA GRC is greatly appreciated and the background and foundation they established for the research was extremely valuable to my work. I would also like to thank Dr. Kim Bey for hosting me at NASA Langley for a few weeks, and for the support and helpful discussions.

Thanks also to members of the Center for Advanced Composites and other graduate students for their valuable input and suggestions. To my family, especially my husband and parents, thanks for being a constant source of support and encouragement.

Finally, I'd like to thank the NASA Graduate Student Research Program (NNX10AM49H) for the funding of this work.

TABLE OF CONTENTS

page

LIST OF TABLES

LIST OF FIGURES

Abstract of Dissertation Presented to the Graduate School
of the University of Florida in Partial Fulfillment of the
Requirements for the Degree of Doctor of Philosophy

PROBABILISTIC MICROMECHANICS OF WOVEN CERAMIC MATRIX COMPOSITES

By

Marlana Goldsmith

December 2013

Chair: Bhavani Sankar
Cochair: Raphael Haftka
Major: Aerospace Engineering

Woven ceramic matrix composites are a special class of composite materials that are of current interest for harsh thermo-structural conditions such as those encountered by hypersonic vehicle systems and turbine engine components. Testing of the materials is expensive, especially as materials are constantly redesigned. Randomness in the tow architecture, as well as the randomly shaped and spaced voids that are produced as a result of the manufacturing process, are features that contribute to variability in stiffness and strength. The goal of the research is to lay a foundation in which characteristics of the geometry can be translated into material properties.

The research first includes quantifying the architectural variability based on 2D micrographs of a 5 harness satin CVI (Chemical Vapor Infiltration) SiC/SiC composite. The architectural variability is applied to a 2D representative volume element (RVE) in order to evaluate which aspects of the architecture are important to model in order to capture the variability found in the cross sections. Tow width, tow spacing, and tow volume fraction were found to have some effect on the variability, but voids were found to have a large influence on transverse stiffness, and a separate study was conducted to determine which characteristics of the voids are most critical to model. It was found

that the projected area of the void perpendicular to the transverse direction and the number of voids modeled had a significant influence on the stiffness.

The effect of varying architecture on the variability of in-plane tensile strength was also studied using the Brittle Cracking Model for Concrete in the commercial finite element software, Abaqus. A maximum stress criterion is used to evaluate failure, and the stiffness of failed elements is gradually degraded such that the energy required to open a crack (fracture energy) is dissipated during this degradation process. While the varying architecture did not create variability in the in-plane stiffness, it does contribute significantly to the variability of in-plane strength as measured by a 0.02% offset method. Applying spatially random strengths for the constituents did not contribute to variability in strength as measured by the 0.02% offset.

The results of this research may be of interest to those designing materials, as well as those using the material in their design. Having an idea about which characteristics of the architecture affect variability in stiffness may provide guidance to the material designer with respect to which aspects of the architecture can be controlled or improved to decrease the variability of the material properties. The work will also be useful to those desiring to use the complex materials by determining how to link the architectural properties to the mechanical properties with the ultimate goal of reducing the required number of tests.

CHAPTER 1
INTRODUCTION

1.1 Background Information

Composite materials are made from two or more materials that, when combined, offer advantages not achieved by their monolithic equivalents such as those used on the thermal protection system of the space shuttle. They have become widely used across many industries including automobiles, marine applications, and civilian and military aerospace applications. Woven, or textile, composites are a special form of composite materials used frequently for structural applications. Yarns are interlaced with one another, and then infiltrated by a polymer, metal, or ceramic matrix.

Woven ceramic matrix composites (CMCs), in particular, are candidate materials for thermal protection systems and turbine engine applications due to their high strength and fracture toughness at high temperatures. However, there is a large amount of variability associated with the stiffness and strength. Traditionally, a very large number of coupons are tested in order to accurately quantify the material properties and their variability. This process is expensive, especially when considering the extremely high cost of CMCs and other advanced materials. Additionally, the constituents used and the manufacturing processes are constantly changing and being improved upon. By the time one material is completely characterized by experiments and approved for use, a new and potentially significantly improved material may be available. Using virtual testing (numerical models that provide information otherwise gathered from experiments) has the potential to decrease the amount of coupons needed for testing. However, we must first understand which geometrical, or architectural, properties are

important contributors to the variability in stiffness and strength and how to best model them.

For this work, the composite system under investigation is a CVI (chemical vapor infiltration) SiC/SiC eight ply 5HS (harness satin) weave material. This composite is capable of withstanding high temperatures (greater than 2000°F), and has good oxidation resistance compared to its C/SiC and melt infiltrated SiC/SiC counterparts. Both of these characteristics are important for the turbine engine and thermal protection systems it may be used in. Initial evaluation of the composite system has shown large amounts of variability in the mechanical properties [1]. The engineering and materials science community are beginning to recognize the importance of handling physical uncertainties of the material in determining the structural response [2]. The exact source of variability is unknown, but believed to be due to randomness in the architecture (tow spacing, tow size, tow nesting), as well as the unevenly shaped and spaced voids created as a result of the randomness in architecture and the nature of the manufacturing process. The matrix is deposited by a chemical process which is very different than the application of epoxy that is more customary for polymer matrix composites. This chemical process also creates variability through the generation of voids. There is also variability in the constituent properties. However, the variability due to these properties is thought to be small relative to previously unexamined architectural properties.

Recently, methods of determining which aspects of the architecture affect variability have been explored. Some of these methods include a multi-scale approach in which relationships are developed that link the lowest level (unidirectional composite)

to the mid-level (woven composite), and finally to the highest level (laminated woven composite) [3]. While this approach may be effective in determining average mechanical properties, it does not explicitly account for the effects of pore size, shape, and location as well as other microstructural variations which should not be neglected. The importance of accounting for these factors explicitly in woven CMCs has recently been studied in a qualitative sense [1]. However, there is still a need to account for these factors in a quantitative sense. Analytical approaches accounting for certain details such as waviness or constituent volume fractions have been developed, but again they do not model porosity explicitly [4]. While these approaches may work very well for some woven composites, it is likely that they do not adequately represent woven composites containing very large voids, like those observed in the SiC/SiC composite.

Models that explicitly include the variability at the constituent level can be used to determine the variability in effective mechanical properties. The effects of architecture in CMC's have been analyzed in the past. However, the methods typically involved a degradation of matrix properties to account for voids, and variability in the microstructure was estimated, rather than rigorously quantified [5]. This assumption does not account for the size, shape, and the interaction of the voids with one another which can affect the stiffness of the composite, as was shown by Huang and Talreja for unidirectional fiber reinforced composites [6]. The analysis in this work will model the voids explicitly to obtain a better physical understanding of the role the voids and other aspects of the architecture have in determining the stiffness and strength.

Evaluation of strength has added complications compared to the evaluation of stiffness. First, it is necessary to define what constitutes failure. Loss of stiffness or

yielding (which can be considered failure initiation) in the material and ultimate failure (involving the evolution of damage) of the material are two major failure considerations. The point at which yielding occurs is important because the material can no longer provide the same structural support. It is important to understand how to model the yielding before ultimate failure can be modeled and understood.

1.2 Objectives

The main objectives of this research are given below.

1. Characterizing architectural (microstructural) variability: Rather than making assumptions about the architectural variability, the goal was to use 2D micrographs to characterize the architectural variability found in the composite structure.

2. Variability in stiffness: The information obtained about the architectural variability was used to determine which details of the architecture (tow size, tow spacing, and voids) are relevant to model in order to understand variability in stiffness.

3. Modeling variability in the composite and the effects of voids: After determining which characteristics of the composite are most relevant to model, it was important to find a way to best account for those characteristics. It was found that voids had the largest influence on transverse stiffness. The goal was then to determine an appropriate way to model the voids to capture their influence on the composite stiffness.

4. Variability of in-plane tensile strength: The extent to which variable architecture affects variability in the in-plane tensile strength is unclear. It is common to relate the variability of the constituents' strength to the variability in the composite strength. The goal was to assess whether or not the varying architecture should be used to model variability in the strength of the composite.

1.3 Outline of Text

The organization of the work is as follows. Chapter 2 presents an overview of woven ceramic matrix composites and how they and other composites have been analyzed in the past with respect to stiffness, strength, and varying architecture. Chapter 3 describes the quantification of the composites variable architecture, and describes how it was applied to a representative volume element in order to determine

which aspects of the architecture were important to model while trying to capture the variability in stiffness. It was found that voids have the most significant impact on the stiffness. Chapter 4 then describes which characteristics of the voids are important to consider (aspect ratio instead of just volume fraction, for example) when determining the transverse stiffness and provides suggestions for how the complex voids can be simplified. In Chapter 5, a readily available damage model is chosen and described in order to assess the relative impact of modeling variable architecture compared to the impact of modeling only random constituent strength. Chapter 6 concludes with a highlight of the important findings and suggestions for future work.

CHAPTER 2
BACKGROUND AND LITERATURE REVIEW

2.1 Ceramic Matrix Composites

Aircraft and spacecraft components that undergo extreme thermo-structural loads have reached some material limitation in terms of strength and weight. Current metallic alloys can withstand approximately 1100°C. However, capabilities of 1200-1400°C are desired. Monolithic ceramics have been used in the past, but their brittle behavior prohibits their use in applications which requires the material to tolerate some damage before catastrophic failure. Ceramic matrix composites (CMCs) are materials that may be able to meet the necessary requirements for thermal protection systems and aero-propulsion components such as combustors and nozzle flaps [7]. They are capable of withstanding these extreme temperatures, and are approximately 30-50% less dense then comparable metals and less prone to damage caused by environmental factors. They also have high toughness for sufficient damage tolerance [8].

Ceramic matrix composites are not manufactured using the well-known methods for polymer matrix composites in which an epoxy or resin is applied to fibers formed into a given configuration, followed by a curing process. The application of the matrix material is usually done through various chemical processes such as chemical vapor infiltration (CVI), melt infiltration, directed metal oxidation, sintering, or pyrolysis. The CVI process (which was used for the composite studied in this work) involves CVI reagents that are pumped into a furnace containing the fiber preform. The gaseous reagents infiltrate the preform and react when they reach the fibers to build up the solid matrix [9]. This process often leaves many large voids, or pores, in the material, which will be further discussed throughout this work. An additional process, melt infiltration,

can be done after the CVI process, which helps to reduce the amount of porosity. For some cases this is undesirable due to the limits it imposes on maximum use temperatures dictated by resulting free silicon formed during the melt infiltration process.

Two common CMCs being studied are C/SiC and SiC/SiC. SiC/SiC has an advantage over C/SiC in that it is more oxidation resistant. Additionally, there is not a large thermal expansion mismatch in the SiC/SiC system, thus reducing cracking during processing. For this work, the composite system under investigation is a CVI (chemical vapor infiltration) SiC/SiC eight ply 5HS (harness satin) weave composite. The composite has continuous Sylramic-iBN (iBN is the fiber coating) fiber tows (20 end per inch) woven into a five-harness woven fabric perform in a [0°/90°] pattern. A silicon-doped boron nitride coating is deposited on the surface of the individual fibers in the tows. The fiber preform is then infiltrated with a CVI-SiC matrix which fills the tows and forms a thin matrix coating around the tows [1].

2.2 Architectural Variability and Voids in Composites

2.2.1 Methodologies for Determining Mechanical Properties

Composite properties (specifically the mechanical properties such as Young's modulus, Poisson's ratio, and the shear modulus) can be determined a few different ways, depending on the desired fidelity of the results and the allotted time for obtaining results. Micromechanics methods use information about the constituents of the composite to determine the mechanical properties of composites. Both analytical and numerical techniques are widely used.

There are numerous analytical techniques and many are capable of obtaining accurate results. However, it is important to consider the assumptions associated with a

particular technique, because not every methodology works for every type of composite. Some of the more basic methodologies make an iso-stress or iso-strain assumption to compute the stiffness. In reality, the stiffness would lie somewhere between the results for these two assumptions. Others have combined the iso-stress and iso-strain assumptions in various ways to obtain reasonable results [10–12]. Laminate theory is also commonly used to determine mechanical properties. The mosaic model in which the composite is broken into segments that look like blocks with several layers is one example of analytical analysis that uses laminate theory [13]. The generalized method of cells is a semi-analytical model that uses displacement field equations to pass information between different levels of the composite scale (for example micro-level to meso-level) [14]. The main numerical technique used to determine mechanical properties is finite element analysis. Periodic boundary conditions applied to a repeating unit cell that represents the overall behavior of the composite are widely used to determine the stiffness matrix as described in more detail in Chapter 3 [15–18].

2.2.2 Modeling of Architectural Variability

The importance of quantifying and understanding the effects of architectural variability has been recognized as an area of importance in understanding how structures fail under various loading conditions [2]. There is a large body of work with various attempts at capturing the effects of architectural variability for polymer matrix composites (PMCs) [19–21]. Others are working on this problem for CMCs which may behave quite differently given the differences in processing techniques [22–25]. It is typical to limit the various types of architectural variability being studied in order to keep the problem tractable. For example, Woo and Whitcomb [21] studied the effects of tow misalignment and Chang [19] investigated tow geometry changes as a result of draping.

With architectural variability occurring across many scales (micro-level fiber and matrix), meso-level (tow and matrix), and macro-level (structure), and also varying depending on the material and manufacturing process, it is important to be aware of the different assumptions made in each individual's study of architectural variability. For example, as stated previously, voids play a significant role in the behavior of the 5HS CVI SiC/SiC composite currently being studied. It is typical for the voids to be treated such that they degrade the properties of the material they are found in [5,11,26]. For example, if the void content of the matrix is 5%, the stiffness used will be degraded by 5% of its nominal value. However, this is not always an appropriate assumption [1,27,28].

While some limit the amount of variability in properties studied, early work at NASA included probabilistic analysis of numerous aspects of variability. Some of these variables included constituent mechanical properties and strength, volume ratios, and architectural variability such as ply misalignment [26]. Micromechanics and laminate theory were used and variability was propagated to different levels in programs such as ICAN (Integrated Composites Analyzer), and CEMCAN (Ceramic Matrix Composite Analyzer) [11,29]. Using these methods produced results that indicated the sensitivity of stiffness and strength to variables that describe the composite. For example, it was observed for a CMC that the in-plane stiffness is sensitive to the fiber volume fraction [30]. While these methods are good for producing results quickly and may be very useful in the initial design process, their fidelity is somewhat low, which may limit the amount of information the models can provide in terms of understanding the physical effects of architectural variability, for example.

A major issue facing those attempting to model effects of architectural variability is the lack of statistical data [2]. It is commonplace to make assumptions about the varying architecture because of the limited amount of data available characterizing the physical uncertainties. When characterizing the uncertainties, a simple random variable can be used which has some probability distribution. If there is enough data, you can have a random field of variables in which the correlation between all of them can be found which allows for a more detailed description of the variability. Cases in which this much data is available are rare. However, Bonacuse [23] was able to use an optical microscope to make images of a 5HS CVI SiC/SiC composite and take measurements of some of the geometry. This work was used to determine how to model the architectural variability in this paper, and further details are provided in Chapter 3.

2.2.3 Modeling Voids

Voids can play a significant role in the determination of material properties, especially for the 5HS CVI SiC/SiC composite as will be shown in this work. The effects of voids have been studied in the past with a variety of methods and goals. There is a large body of work in which the results are related mostly to void volume fraction [31–34]. The relationships found may be relevant for some applications, but as will be shown later, the volume fraction of the voids is not the only thing that must be considered in the woven ceramic matrix composite under consideration in this work. For example, Sejnoha and Zeman [16] observed that neglecting voids in a plain-weave C/C composite over predicts the stiffness measured in experiments by as much as 30% for 20% porosity. They also note that little to no work has been done to properly account for the presence of voids. Some researchers have developed analytical equations based on elasticity to describe the effects of voids [32,35]. One main drawback is that they are usually limited to

uniformly sized and distributed voids, which is not always what is physically observed. The voids considered here in this work are unevenly distributed and many have large aspect ratios. Others have shown the importance of the microstructure including Tsukrov and Kachanov [36] who accounted for elliptical voids with arbitrary orientations and eccentricities. This work is limited to a 2D anisotropic solid and the holes are non-interacting.

Huang and Talreja [6] demonstrated that the void shape and size was an important factor to consider, especially for transverse and shear stiffness of a unidirectional composite. They also observed that long, flat voids are most detrimental to the transverse stiffness. This agrees well with preliminary analysis on the woven CVI (Chemical Vapor Infiltration) SiC/SiC composite where void volume fraction is not the sole mechanism of stiffness degradation [1]. Uniform distribution of voids was assumed for the analysis which was shown to compare well for experimental data in unidirectional composites. However, woven composites appear to have significantly greater variability in void size and distribution as compared to unidirectional composites. Voids were also shown to significantly affect the strength of a composite [27] as demonstrated in polymer matrix composite under uniaxial loading conditions. While the voids decreased the stiffness, they increased the strain to failure. However, it should be pointed out that this was only observed in the uniaxial tension case of an idealized unit cell and the authors stated that further study needed to be completed.

2.3 Analysis of Failure, Damage, and Strength

For the purpose of discussions in this work, failure, damage, and strength are defined as follows. Failure will generally be used when talking about a particular constituent material, for example SiC. Failure occurs when the stress in that constituent

has reached its maximum allowable stress. The materials used are linear-elastic until failure. After failure occurs, there is an onset of damage which is also referred to as post-peak softening. Essentially, after maximum stress is reached, the material begins to soften based on parameters in a given damage model that will be described later. For this discussion, the term strength will be applied to the stress at which the composite is considered to have failed. The following sub-sections provide an overview of what researchers in the past have used to model failure, damage, and strength of the composites of interest to them

2.3.1 Description of Strength

The way in which strength is defined is dependent on the type of information desired from the analyst or engineer. If an analyst is only concerned with catastrophic failure, the strength may be defined as the stress at which the material or structure ruptures. Others may be interested in when the proportional limit stress is reached (the stress at which material no longer behaves in a linear-elastic manner or the onset of non-linearity in the material's stress-strain curve), or the maximum allowable tensile stress. The stress-strain curves used generally come from experiments, numerical models (such as finite element analysis), or a combination of the two.

Strength can also be defined with numerical models that do not generate stress-strain curves. For example, in Zhu, Sankar and Marrey [37], the strength was defined as the global stress at which the first element failed. This is a conservative definition but can be altered to define the strength as the global stress at which a certain percentage of elements has failed. The concept is similar to one of the most common methods of determining strength in a laminate, the first ply failure (FPF). The FPF concept defines the strength as the global stress at which the first ply reaches its failure limit [38]. As

with first element failure, this is a conservative approach that may not reveal the composite's complete capabilities. The FPF concept has been improved upon through considerations of mechanism based failure as an increase in progressive damage has gained interest as discussed in Section 2.4.2 [39]. These first element and first ply failure methods are simple and appropriate for some analyses, especially in early stages of design. However, it does not consider the progressive nature of failure. That is, when one element or ply fails, the load can redistribute throughout the composite, allowing for larger global stresses and strains.

2.3.2 Failure and Progressive Damage

The modeling of failure and damage in the composite allows for virtual generation of the stress-strain curves used by engineers to identify points such as the offset yield strength. While many methods have been proposed for modeling the progressive damage and failure in composites, there are two unifying topics. These include an element or ply discount approach which is typically stress-based, and continuum damage mechanics. Each has their strengths and limitations, and their usefulness depends on the application.

Stress-based methods involve comparisons of stress, either in an element or in a ply, to the strength of the material [40,41]. In this method, usually an incremental-iterative technique is used, which means an iteration is performed at each load or displacement increment, but small increments in between are also used to ensure stability. Failure criteria are evaluated at each increment and material properties are degraded by a factor determined by the analyst if failure is detected. The two main methods for property degradation using this method are the total discount approach and the limited discount approach [42]. The total discount approach is executed by

evaluation of failure criteria, followed by degrading the entire stiffness tensor of the material. In contrast, the limited discount approach degrades only part of the stiffness tensor, depending on the failure mode. For example, if the fiber in a composite fails, the longitudinal stiffness would be degraded while the others would maintain their load-bearing capabilities. This allows for the First Ply Failure approach to be extended to include progressive damage. Rather than assuming the maximum allowable stress has been reached at FPF, the mechanical properties of the failed ply can be degraded, and the loads can be redistributed to other plies. For example, in early work by Ochoa and Engblom [43] and later work by Knight [44], for each load increment the lamina stresses were checked for failure based on several different failure criteria that were related to the mode of failure. If the stress in the fiber direction exceeds the allowable stress, the stiffness in the fiber-direction is degraded. A similar process was completed for a plane woven composite in work by Blacketter et.al. [45]. In this case, elements of a finite element model were degraded based on which material the element was prescribed (composite tow or matrix) and which mode it failed in (tensile, transverse, shear, etc.). One limitation of this method is that the degradation is sudden (occurs all at once as opposed to gradual degradation), and does not correspond to any physical explanation other than perhaps accounting for the mode of failure. It has been shown that the choice of degradation factors has a significant impact on the results [46,47] and thus this method may not be ideal toward gaining predictive capabilities with respect to generating stress-strain curves.

Methods such as continuum damage mechanics also involve checking the failure criteria, and degrading material properties. However, it is done in a way that represents

the physics of the damage occurring. Continuum damage mechanics typically involves the use of a damage variable which introduces damage by degrading the stiffness tensor on the basis of a damage law [48,49]. The way in which the stiffness matrix is degraded varies, and there is no universal method that is appropriate for all materials or all applications. The choice of damage evolution may come from experimental data fitting which would limit capabilities in virtual design of a material [50]. In work by Pineda et.al., Schapery Theory which is based on the energy potential required for structural changes to occur is used [51]. Other models are based on relationships due to observed cracking or fracture. For example, Talreja [40] has developed a method in which crack density can be related to damage evolution. This type of analysis is not appropriate for the present work because observations of cracks in the material are not available.

Another method of determining damage evolution is based on the fracture mechanics concepts of fracture toughness and strain energy release rate of the material [52,53]. This method is valuable for this work because it is derived from information about material properties (fracture toughness and strain energy release rate) that can generally be found in the literature. Since it is a popular method, it is also already implemented in many finite element analysis packages, including Abaqus which has a model titled Brittle Cracking for Concrete [54]. This model is based on early work that was done for concrete, but it can be applied to brittle materials in general [55]. It is similar to the work by Barenblatt that used traction separation laws to define the damage [56]. Elements that are failing can be thought of as cracks. When the maximum tensile stress is reached, the stress does not fall to zero all at once, but gradually

decreases as the crack width increases (the element length increases). The amount of energy needed to open the crack, and the way in which the energy dissipates dictates the post-peak softening behavior. This method also has similarities to cohesive zone modeling [57]. The key advantage offered by implementing the continuum damage mechanics method over cohesive zone modeling is that the location of the crack does not need to be known a priori. More comprehensive mathematical and physical details of progressive damage based on the Brittle Cracking Model for Concrete are found in Chapter 5.

CHAPTER 3
EFFECTS OF ARCHITECTURAL VARIABILITY ON THERMO-MECHANICAL PROPERTIES OF A WOVEN CERAMIC MATRIX COMPOSITE

The goal of this chapter is to first quantify the architectural variability found in three two-dimensional cross sections of the 5HS SiC/SiC composite. Then, the variability is applied to an RVE (representative volume element) to determine which aspects of the architecture need to be modeled in order to capture the variability found in the stiffness of the cross sections.

3.1 Characterization of the Composite

3.1.1 Geometric Parameterization and Model Assumptions

The sketch in Figure 3-1 is a 3D representation of the weave for a 5HS unit cell. The composite has continuous Sylramic-iBN fiber tows (20 ends per inch) woven into a five-harness woven fabric preform in a [0°/90°] pattern. A silicon-doped boron nitride coating is deposited on the surface of the individual filaments in the tows. The fiber preform is then infiltrated with a CVI-SiC matrix which fills the tows and forms a thin matrix coating around the tow.

The microstructure of the composite has been shown to have significant randomness, resulting in large variability in the mechanical properties. A 2D micrograph of one cross section of the composite, obtained by Goldberg, et al. is shown in Figure 3-2 [1]. The black areas in the interior of the cross section represent voids (the black area on the borders of the image are not voids), which vary in location, size, and shape. Other 2D cross sections are not identical to the one shown, but rather, exhibit different random distributions of the voids and the microstructural characteristics such as tow size, shape, and spacing. Therefore, some simplifying assumptions, explained in the

following paragraphs, were made to develop an understanding of the composite at a basic level.

For this work, the focus was on modeling a representative volume element (RVE) of the 8 ply 5 HS composite in order to keep the size of the problem tractable while capturing the important statistical characteristics. Due to the large amount of variability, it is difficult to define an RVE in the traditional manner, in which the RVE is a statistically equivalent representation of the larger cross section. Preliminary work involved the use of only one unit cell (one ply), which consists of a weft tow crossing over four warp tows, as shown in Figure 3-3 [58]. The weave of one 2D unit cell consists of five elliptical transverse tows, and one longitudinal tow that follows a sinusoidal curve. The configuration of the unit cell is based on tow spacing in the in-plane and transverse directions (s and ΔY, respectively), transverse tow width (w), transverse tow height (h), longitudinal tow amplitude (A), and longitudinal tow wavelength (λ), as labeled in Figure 3-4. The in-plane tow spacing, tow width, and tow height are randomly assigned as described later. The longitudinal tow is a sine curved described by the equation

$$Y = A*\sin\left(\frac{2\pi}{\lambda}X + \frac{\pi}{2}\right)$$

where the longitudinal tow amplitude (A) is 0.07 mm (obtained by estimation from micrographs), and the wave length (λ) and position (X) vary and are functions of the randomly prescribed tow width and tow spacings. The spacing in the transverse direction (ΔY) also varies depending on the position, X, for each tow. For multiple stacked unit cells an additional variable called the tow offset is introduced. The tow offset can be defined as two unit cells being stacked on top of one another, and then

shifted by a given tow length. This tow offset is also referred to as ply shifting. Figure 3-4 illustrates a tow offset of 2.

After the tows are placed, the matrix is grown uniformly around the tows, until a prescribed matrix volume fraction is reached. Essentially, one layer of pixels representing matrix material is added at a time. This is similar to what occurs during chemical vapor infiltration in which the matrix accumulates on top of the tows (albeit not uniformly). This allows for the voids to be explicitly modeled in locations where the voids are likely to occur. While the non-uniform matrix distribution seen in Figure 3-2 is not captured precisely, the method approximates the manufacturing process of matrix deposition in that the voids generated are a result of the tow placement [1]. However, the unit cell neglected the presence of any ply shifting/tow nesting (uneven tow alignment as illustrated in Figure 3-4) that is exhibited in the actual composite, resulting in artificial cross sections that did not realistically represent the void geometry. All voids were small and compact, as opposed to a few having a large aspect ratio. The ply shifting is one cause of the voids with large aspect ratios.

In order to capture the ply shifting a larger RVE was modeled, made up of two unit cells with a uniform tow offset or shifting for all RVEs. With more plies, the ply shifting would change within each layer. This variability in shifting and tow nesting is currently being neglected since it cannot be rigorously quantified in the same manner as the other variables being investigated. The 2D representation of a 5HS RVE is shown in Figure 3-5. The figure is a result of using two unit cells, with one flipped upside down (as done by the material manufacturer), and shifted by one tow length. Note that the 1-

direction is in-plane longitudinal, the 2-direction is out-of-paper transverse, and the 3-direction is through-thickness transverse.

Another assumption was made in regards to modeling the composite in 2D as opposed to 3D. The goal of the work is not to accurately predict thermo-mechanical properties, but rather gain an understanding of which features of the material architecture improve or worsen the thermo-mechanical properties. Relevant preliminary conclusions regarding this matter can be drawn with a 2D analysis. Another important goal was to explicitly represent the voids in finite element analysis based on where they naturally occur due to variation in the weave architecture. In a recent survey of available 3D modeling tools, it was found that there are no tools with a completely generalized capability that would be suitable for the current modeling task of generating a matrix with naturally occurring voids as a result of perturbations in the weave geometry [59]. A 2D plane strain representation of the woven composite is not completely accurate. However, since the purpose of the paper is to gather information on modeling the architectural variation and to determine how the variation affects the thermo-mechanical properties in a general sense, a 2D assumption was deemed appropriate [1]. In addition, the resulting mechanical properties due to 2D analyses discussed in the paper do not deviate significantly from limited experimental results available for a similar composite [28].

3.1.2 Statistical Distributions and Correlations

The parameters chosen to be randomly varied were selected based on availability of statistical data, and whether or not there was significant variation in the parameter. Image processing techniques were used to extract information about the tows [23]. The geometric parameters for which statistical data was available were

transverse tow width (*w*), transverse tow height (*h*), and transverse tow spacing in the longitudinal direction (*s*), as labeled in Figure 3-4. The data used can be found in the Appendix A [23]. Other architectural parameters, such as tow spacing in the through thickness direction and longitudinal tow amplitude are either dependent on the variables used, or were approximated based on visually fitting the geometry to the cross sections. The variables that do not yet have statistical data (like longitudinal tow amplitude) were held constant.

The random generation of the variables was based on the statistical data in three different cross sections (similar to that shown in Figure 3-2), resulting in approximately 225 data points (each tow provided a data point). While the data from the three cross sections cannot provide accurate statistical distributions, the goal is to explore how the variability should be modeled. For this purpose, the data is sufficient. However, to calculate accurate probabilities, more data would be necessary. It was found that the tow spacing and tow width fit best (according to the lowest standard error in the fit) to a normal distribution. Plots of the empirical cumulative distribution functions (CDF) and the normal cumulative distribution functions are displayed in Figure 3-6 and Figure 3-7. The tow height fit best to a Weibull distribution, and a normal distribution fits well also. In Figure 3-8, both a Weibull and Normal CDF are plotted with the empirical CDF. By visual inspection they both fit closely. The square error, computed by

$$Error = \sum_{i}^{n} \left(p_{data,i} - p_{CDF,i} \right)^2$$

where n is the number of data points, p_{data} is the cumulative probability at an individual data point and p_{CDF} is the cumulative probability for a given distribution such as normal or Weibull, was found to be 0.0013 and 0.0027 for the Weibull and normal distributions,

respectively. Since correlation is taken into account (as described in the next paragraph) it is more convenient to use a normal distribution for all variables, and the error introduced by using this distribution is very small. The parameters of the distributions are given in Table 3-1.

An issue that further complicates the problem is that the variables not only vary between the cross section, but they have a variation within each cross section as well. If each tow in the cross section is given a unique geometry, it is important to consider correlation (a measure of the strength of the linear relationship between two variables) between the variables in order to avoid producing unrealistic cross sections. Therefore, each transverse tow is assigned an individual, but correlated, tow width, tow height, and tow spacing. Since there are five tows in the RVE, this results in a total of fifteen variables (five tow widths, five tow heights, and five tow spacings). Using correlated parameters ensured that inherent architecture variation due to the manufacturing process would be accounted for and the generation of unrealistic cross sections would be minimized.

3.1.3 Generation of Artificial Cross Sections

The number of cross sections chosen for the finite element analysis was based on how much data is needed for the potential response surfaces (discussed in a following section). For the finite element analysis, which is used to determine the magnitude of thermo-mechanical property variability, 38 artificial cross sections were generated. The number of cross sections necessary depends on the order of the polynomial response surface and is explained in Section 3.2.2. In order to determine the statistical distribution of mechanical properties, 1000 artificial cross sections were randomly generated. The number of artificial cross sections is chosen based on the

desired accuracy, or standard error (approximately 0.3%). The 1000 artificial cross sections were generated to determine the constituent volume fractions for each one. However, the mechanical properties from these cross sections will be determined with a response surface, rather than analyzing each one individually. A typical artificial cross section is shown in Figure 3-5.

A summary of the characteristics of the three sample cross sections from which the statistics were obtained is presented in Table 3-1. For the individual cross sections, the mean and standard deviation of width, spacing and height is provided, with standard deviations in parentheses. Table 3-2 and Table 3-3 show characteristics of the artificial cross sections. The volume fractions and geometric parameters of tow width (*w*), tow spacing (*s*), and tow height (*h*) from the actual composite and artificial cross sections are in good agreement.

The correlation coefficients (based on 24 data points) of the significantly correlated parameters (correlation coefficient is greater than 0.4) are displayed in Table 3-4. The statistical significance is in parentheses (the likelihood that the correlation coefficient arose by chance). For example, spacing between the first and second tow (spacing 1) and spacing between the third and fourth tow (spacing 3) have a correlation coefficient of -0.47. This can be interpreted by saying that when spacing 1 increases, spacing 2 decreases, but not necessarily in a one to one ratio. It is likely that the spacing and width have some degree of correlation because when the composites are manufactured they are restricted to a certain width. Therefore, depending on the tow sizes, the spacing has to adjust to accommodate for all of the tows.

3.2 Analysis Methods

3.2.1 Finite Element Analysis Model Description

The RVEs were generated as red, green, and blue images with a Python code (e.g. Figure 3-5), which were then meshed with open source software, OOF2 [60]. Any color scheme can be used so long as their differences can be recognized by OOF2. OOF2 allows the user to import an image and define the different materials by color selection. It then creates a mesh of a desired size with homogenous elements (each element has only one material associated with it). The mesh was then imported into the commercial software, ABAQUS, for finite element analysis [54]. A combination of linear triangular and quadrilateral plane strain elements was used. The material properties assigned were determined by Goldberg, et al. [1] using standard micromechanics formulations for unidirectional composites and are shown in Table 3-5. While there may be variation in the thermo-mechanical properties of the tows, it is thought to contribute less to the overall variability than the architecture. Therefore the thermo-mechanical properties of the tows are held constant. Since the RVE is modeled in 2-D, the longitudinal and transverse tows were treated as separate materials. The yarn/matrix interphase is not explicitly modeled in the present study. The tows are modeled as homogenous orthotropic materials, with resultant properties based on the fiber, matrix, voids, and interphase in the tows. The matrix was assumed to be an isotropic material.

A finite element analysis based micromechanics approach was used to determine the effective elastic moduli, Poisson's ratios and coefficients of thermal expansion (CTEs) of the RVE. The constitutive equations of the composite can be written as

$$\underset{6\times1}{\{\sigma\}} = \underset{6\times6}{[C]}\left\{\underset{6\times1}{\{\varepsilon\}} - \underset{6\times1}{\{\alpha\}}\,\Delta T\right\}$$

where the stresses and strains are macroscopic or volume averaged quantities, *C* is the stiffness matrix, *α* is the matrix of CTEs and *ΔT* is the temperature difference measured from the reference temperature. A summary of micromechanical analysis procedures is given below.

Periodic boundary conditions are applied such that one of the macro strains is non-zero and all other strains and *ΔT* are zero. The macro-stresses are calculated by averaging the micro-stresses in the RVE. Using the six macro-stresses one can determine the first column of *C*. The procedure is repeated for the other five macro strains (engineering strains) to calculate the entire *C* matrix. From *C* one can calculate the elastic constants using the relations of the type

$$[C]^{-1} = [S] = \underset{(6\times6)}{\begin{bmatrix} S_{11} & \dots & S_{16} \\ \dots & \dots & S_{26} \\ S_{61} & \dots & S_{66} \end{bmatrix}}$$

In order to determine the CTEs the periodic boundary conditions are applied such that all macro-strains are suppressed and a known *ΔT* is applied to the RVE. Additional inputs to the finite element analysis are the CTEs of the tow and matrix phases. By substituting the macro-stresses in (1) one can solve for the CTEs as

$$\{\alpha\} = -\frac{1}{\Delta T}[C]^{-1}\{\sigma\} = -\frac{1}{\Delta T}[S]\{\sigma\}$$

Since plane elements in the 1-3 plane were used for the FE analysis slight modification of the procedures were required. Using plane strain elements the boundary conditions corresponding to macro-strains ε_1, ε_3, and ε_{13} could be easily implemented.

The generalized plane strain condition could also be used for the case $\varepsilon_2 = 1$. The transverse shear strains $\gamma_{12} = 1 \text{ and } \gamma_{32} = 1$ cannot be implemented using the plane strain elements. The transverse shear strains cannot be implemented using the plane strain elements. Plate elements with only u_2 degree of freedom in the 2-direction were used for the two transverse shear strain cases [37]. Since ABAQUS does not provide the transverse shear stress for plate elements, the displacement at each node combined with shape functions was used to extract the stress in each element manually.

3.2.2 Response Surfaces

In order to quantify the statistical distribution of thermo-mechanical properties to specific variability in the architecture, many analyses are often necessary (depending on desired accuracy). While the computational time of the individual analyses mentioned previously is not unmanageable, the mesh generation is very time consuming (~40 minutes per model). One thousand models were necessary for the work in this paper, necessitating a method in which many analyses could be performed in a short amount of time.

When it is desired to determine the response at a large number of data points, it is typical to perform analyses at a small set of data points, which are then fit with a polynomial response surface. For this work, a linear polynomial response surface was used, necessitating *2(n+1)* analyses where n is the number of variables, and twice the minimum amount of variables *(n+1)* was used to improve the accuracy of the response surface. The relationship between the variables and the thermo-mechanical properties is given by

$$response = c_1 x_1 + c_2 x_2 + \ldots + c_n x_n + c_{n+1}$$

where c_n is the coefficient and x_n is the variable. The coefficients indicate the sensitivity of the response to a given variable.

In the current work, 15 random variables were chosen, as explained in a previous section, in addition to constituent volume fractions for a total of 18 variables. Preliminary work demonstrated the importance of including the volume fractions [58]. As shown later in this paper, volume fractions carry a heavier weight than the architectural variations in the influence of certain mechanical properties, which is important since volume fractions are typically easier to work with. For a linear response surface in 18 variables, 38 high fidelity models are necessary. For the selection of the variable values of the 38 FEA models, Latin Hypercube Sampling was used. This technique ensures representation of a realistic variability by generating non-repetitive samples that are evenly distributed in the design space.

3.3 Results and Discussions

3.3.1 Finite Element Analysis

The goal was to model the variability in the thermo-mechanical properties of the real cross sections by varying the architectural properties in an RVE. The tensile moduli of the full cross sections are provided in Table 3-6 for comparison to the RVE analysis. The three full cross sections analyzed are based on actual cross sectional images of a 5HS SiC/SiC composite. The thermo-mechanical properties of 38 artificial cross sections were determined with finite element analysis as described in the previous section. The mean and standard deviation of the thermo-mechanical properties are shown in Table 3-7. It is important to note that values in the 2-direction, such as E_2, may be lacking in accuracy due to the 2-D assumption. In reality the behavior of E_2 would be similar to that of E_1 due to the balanced weave of the actual composite. The in-plane

stiffness E_1 and shear stiffness G_{12} compare well (less than 10% error) to experimental results found in the literature on a similar material, melt infiltrated CVI 5HS SiC/SiC composite [28]. The material has a smaller void volume fraction which is the likely cause of the discrepancy. The transverse stiffness E_3 is over-predicted by approximately 33% compared to approximate experimental results, which is likely related to the use of constant ply shifting, as explained later. The response surface results presented in Table 3-7 are explained in the following section. Note that the variability in RVE properties is smaller than that exhibited by the full cross sections. An explanation for the discrepancy is given in Section 3.3.3.

While the full extent of the variability of the full cross sections is not captured, some initial observations can be made from the RVE results. It is known that voids have a significantly more detrimental effect on the out of plane moduli than the in-plane moduli for varying void content as well as for flat shapes [6]. Therefore, it is not surprising that with varying geometry, which inherently alters the void volume fraction, the coefficient of variation in the through thickness modulus is almost three times that of the coefficient of variation of the in-plane modulus. Huang and Talreja [6] also observed that the voids would have the most significant impact in the out-of-plane shear modulus (G_{13}), which is also observed here. While the out-of-plane CTE is smaller than that of the in-plane CTE, the coefficients of thermal expansion were shown to be insensitive to the variations in architectural parameters. This is due to the fact that the coefficients of thermal expansion of the constituents are approximately the same. If the coefficients of thermal expansion were drastically different between the constituents, there would be more variability due to architectural variation and voids.

3.3.2 Effects of Architectural Variability

After completing the finite element analysis, the mean values and the approximate variability associated with them is determined. Fitting a response surface to the data provides two additional pieces of information. First, the response surface indicates the magnitude of the effect each variation has on the property being examined (based on the magnitude of the coefficients). Secondly, the response surface allows the statistical distribution of the properties to be estimated (for example, Normal or Weibull distributions).

Several options were explored regarding which variables should be used in the response surface. Initial work involved fitting the response surface to every architectural variation required for the formation of the RVE (5 tow widths, 5 tow heights, and 5 tow spacings), as well as the volume fractions [58]. However, this does not provide useful information since each individual tow parameter cannot be controlled by a manufacturer. Instead, the individual variations in tow parameters will provide information about the amount of variability, but it is more practical to discuss the architectural variations in an average sense. Therefore, the response surface variables selected were: 1) average tow width, 2) average tow spacing, 3) average tow height, 4) tow volume fraction, 5) void volume fraction, 6) standard deviation in the width, 7) standard deviation in the spacing, and 8) standard deviation in the height. The matrix volume fraction was not used since it is directly dependent on the tow and void volume fractions. Therefore the number of variables for the response surface was reduced from 18 to 8 in order to gain a better understanding of the impact of the architectural variations. The use of the average tow properties in the fit provides general information about how much tow properties affect the mechanical properties on average. Using the

standard deviation of the tow properties in each RVE gives additional information on how much the variation in tow properties within each RVE affects the mechanical properties.

After selecting the pertinent variables, a linear polynomial response surface was fit to the finite element results. One response surface was created for each mechanical property. A response surface was not generated for the CTE since the variability was insignificant. The sensitivity of each modulus to certain variables (labeled as "coefficient") is displayed in Figure 3-9. The numbers are the coefficients for each response surface. Only coefficients with a test-statistic greater than 2 were used. Also, note that since some parameters are correlated, one coefficient may be dependent on another. For example the average tow width is related to the tow volume fraction. The response surface, however, does not directly account for the dependencies which should be considered upon interpreting the results. The moduli were most sensitive to the average tow width, average tow spacing, tow volume fraction, and void volume fraction. There was minor sensitivity to the amount of variability in tow spacing due to the effect that it has on the void shape and size. The tow width, tow spacing, and variation in the spacing was most important in determining the in-plane modulus (E_1). The modulus E_2, which theoretically should be equivalent to E_1, was primarily dependent on the volume fractions (specifically, the void volume fraction). The discrepancy is due to the fact that in a generalized plane strain model, equivalent materials also have equivalent stresses. Therefore, the modulus is related to the quantity of each material. The out-of-plane modulus (E_3) is most strongly dependent on tow volume fraction. This is not to say that it is the only important factor, but rather with

the current modeling methodology it is shown to be the most impactful. As discussed later in the paper, it is hypothesized that the void size, shape, and alignment plays an even larger role than solely the volume fraction. Note that either tow volume fraction or void volume fraction can be used to determine the modulus, but not both, because they are dependent on one another. The shear moduli (G_{12}, G_{13}, and G_{23}) are dependent on the tow width, tow spacing, and tow volume fraction. This is likely due to the effects spacing and tow width has on the voids.

The response surfaces were then used to calculate the mechanical properties of 1000 artificial cross sections. The results from the response surfaces are presented in Table 3-7. The mean values agree well with the finite element results, and the standard deviations are slightly smaller. The difference in standard deviations is due to the fact that when fitting a polynomial response surface, noise is filtered, thereby decreasing the variability. It was found that the mechanical properties were normally distributed.

3.3.3 Comparison of Artificial Cross Sections and Real Cross Sections

The results from the RVEs were compared to finite element results of the cross sections presented in Table 3-6 from which the data was taken [1]. It is clear that there is significant variability in the out-of-plane modulus E_3, and it is not directly correlated to volume fractions. The comparison of the full cross sections to the current RVE analysis reveals that the variability in the RVE models is not capturing the variability exhibited in the full cross sections.

One variable that the present RVE analysis neglected was variation in ply shifting. A shifting of one tow offset was applied for each RVE, rather than allowing it to be variable. Previous work by Woo and Whitcomb [21] and Woo, Suh, and Whitcomb [61] showed that tow offset (a bi-product of ply shifting) has a significant effect on some

mechanical properties. In order to determine if neglecting ply shifting was a cause of the smaller variability in the RVEs as compared to the full cross sections, one RVE was used and assigned four different tow offsets. The magnitude of the tow offset is defined by assuming initial perfectly aligned tows or unit cells, then prescribing one unit cell to be offset by a certain fraction of a tow width. The results are summarized in Table 3-8. Note that there are small changes in volume fraction due to a small allowance of tow overlap in order to maintain a constant ply thickness. The variation in the shifting affects the out-of-plane modulus drastically. The standard deviation in the out-of-plane modulus for one cross section with ply shifting variation is 15% of the mean, as opposed to a standard deviation of approximately 5% of the mean for all architectural variability. The variability in ply shifting also decreases the average computed value of the modulus.

A visual assessment of the voids in Figure 3-10 provides insight into the increased variability in the moduli due to shifting. The RVE with the tow offset of one tow has one void with a large aspect ratio, and several that are square in shape. The RVE in Figure 3-11with a tow offset of 4.5 has three voids with an aspect ratio of the same order as the RVE in Figure 3-10. The cross section in Figure 12 has several voids with large aspect ratios distributed throughout the composite. This phenomenon is represented in the RVE in Figure 3-11.

It can be concluded that accounting for variability in ply shifting will likely may capture the variability exhibited by the full cross sections in a more accurate manner than varying the tow width, tow spacing, and tow height alone. However, since the void volume fraction is also varying in the shifted cross sections examined, it cannot be said that the shifting alone is the cause of the variability. Future work will investigate the

effects of ply shifting and attempt to precisely quantify the effect of void distribution and architecture on the mechanical properties.

3.3.4 Summary

The goal of this work was to select an RVE with architectural parameters that could be varied to effectively represent the variation in the thermo-mechanical properties of SiC/SiC composite, while also gaining an understanding of which architectural parameters were influential in determining the variability in mechanical properties. The method of artificially generating cross sections in 2D by using statistical information from the micrographs of actual composite cross sections works well. The statistics of the architectural parameters of the real and artificially generated cross sections are in agreement.

The RVE was characterized by varying tow widths, heights, and spacing, resulting in variability of 2-6% of the mean for normal moduli and 4-17% of the mean for shear moduli. A negligible amount of variability was found for the CTE, due to a lack of CTE mismatch in the constituents. The variability was highest for the out-of-plane tensile modulus (E_3), out-of-plane shear modulus (G_{13}), and in-plane shear modulus (G_{12}). The variability in mechanical properties was predominantly due to tow width, tow spacing, and volume fractions. This type of information may be useful if it is desired to model thermo-mechanical property variability in homogenized models at larger scales. If it is known that certain architectural features exist in part of a component, mechanical properties can be altered in that region to reflect the effects of those features.

FEA analysis of real composite cross sections revealed that there is more variability present than the variability predicted by the RVE with uniform ply shifting chosen. This indicates that modeling the variability in tow width, tow height, and tow

spacing is not sufficient for modeling the variability in the cross sections. Preliminary analysis that examined ply shifting indicated that the voids play a significant role in determination of the transverse stiffness and the voids should not be neglected. The following chapter provides insight into how the voids can be included to determine the stiffness.

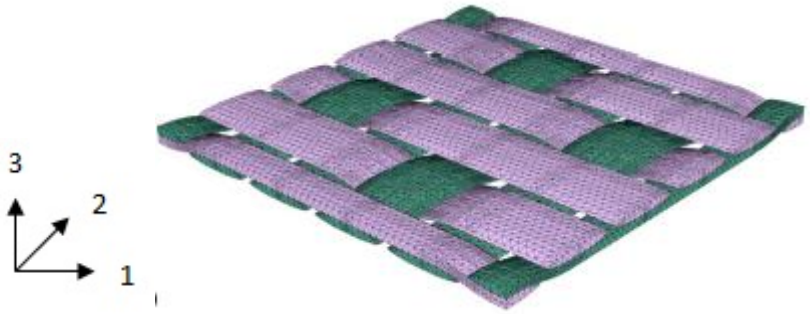

Figure 3-1. 3D finite element model of 5 harness satin weave

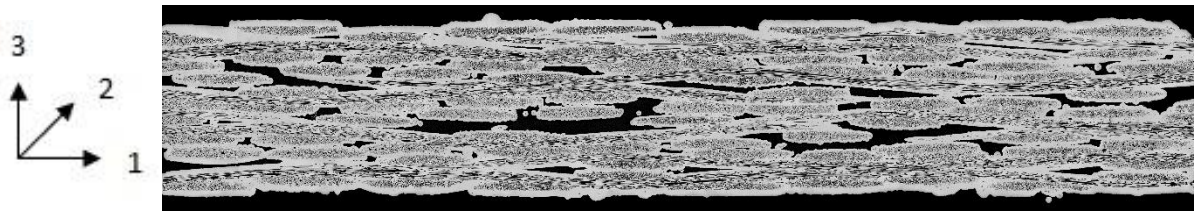

Figure 3-2. 2D cross section of the SiC/SiC composite microstructure where the black interior represents voids. The black area at the top and bottom is blank space around the composite specimen.

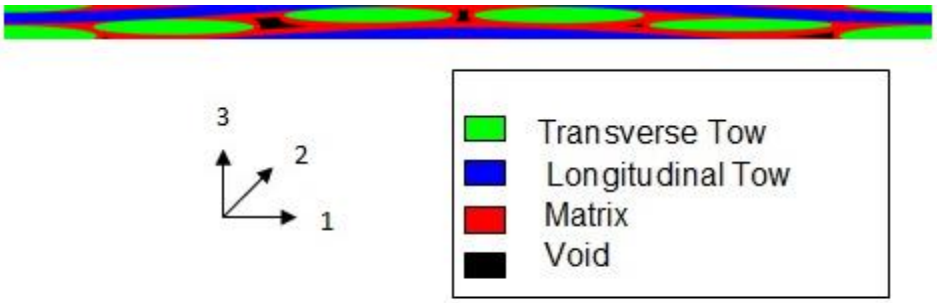

Figure 3-3. 2D Unit cell of 5 harness satin composite

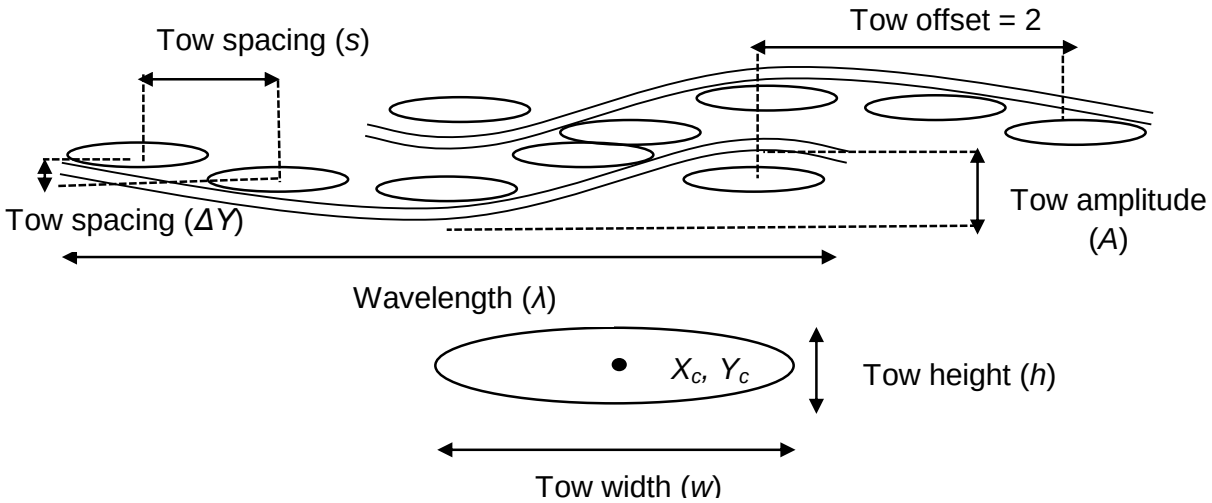

Figure 3-4. Geometry of unit cell

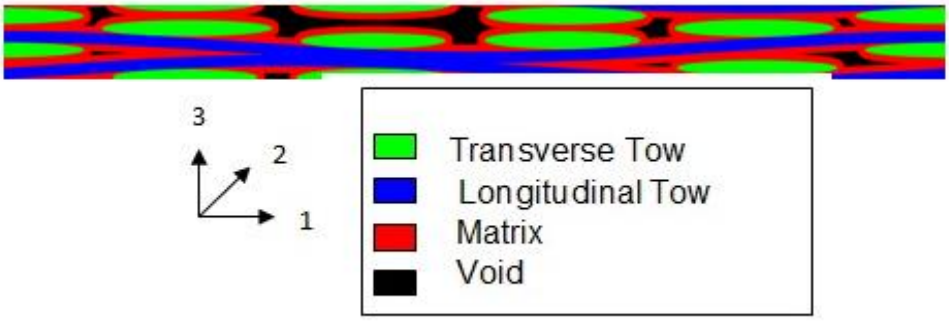

Figure 3-5. Example of a randomly generated representative volume element

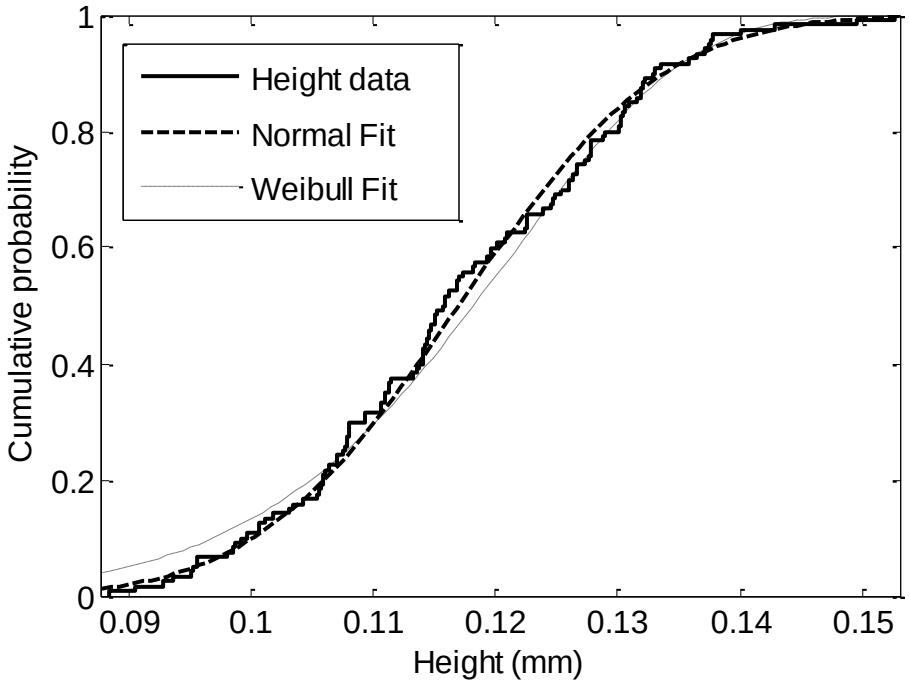

Figure 3-6. Empirical and normal cumulative distribution function plot for tow width

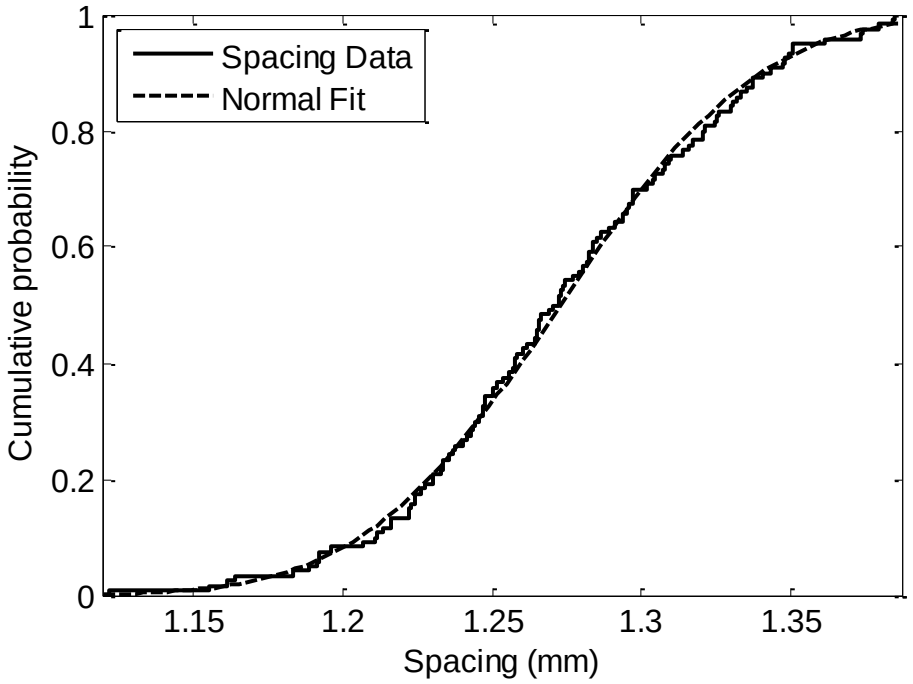

Figure 3-7. Empirical and normal cumulative distribution function plot for tow spacing

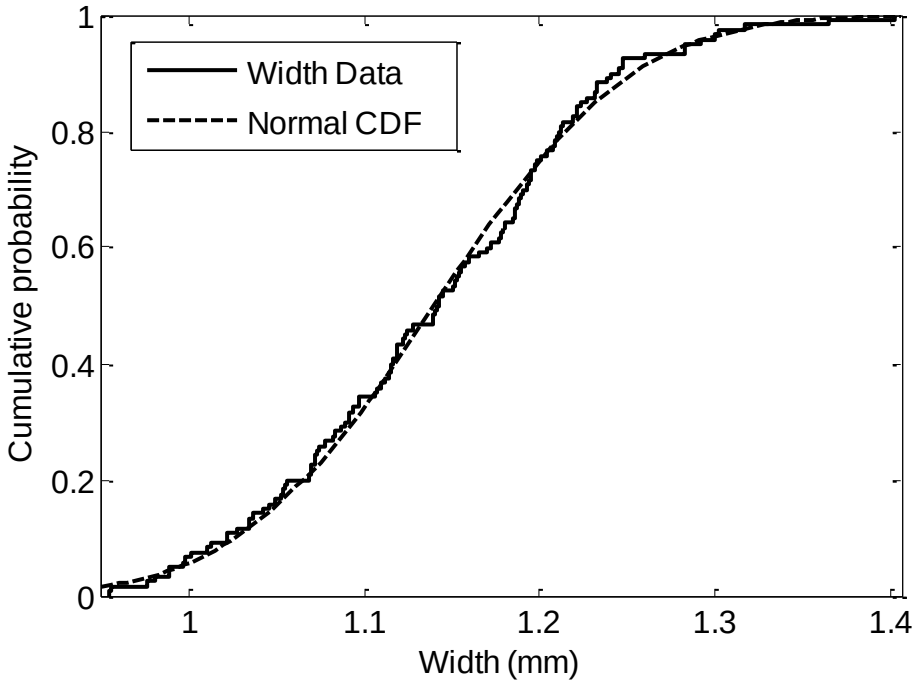

Figure 3-8. Empirical and normal cumulative distribution function plot for tow height

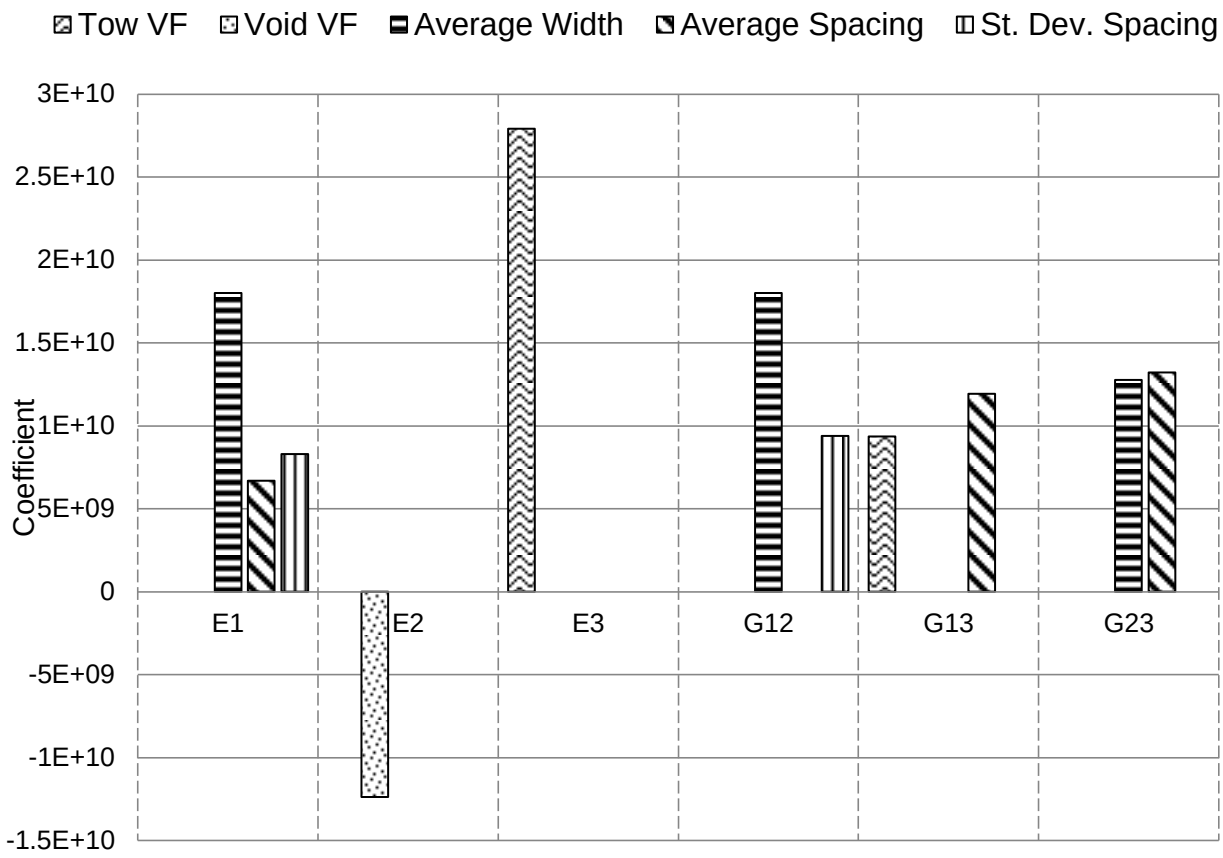

Figure 3-9. Dependencies of moduli on architectural variability and volume fractions. The 1-2 directions are in-plane properties and the 3-direction is an out of plane property.

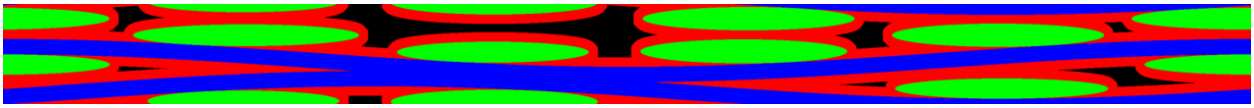

Figure 3-10. Representative volume element with tow offset equal to 1.0

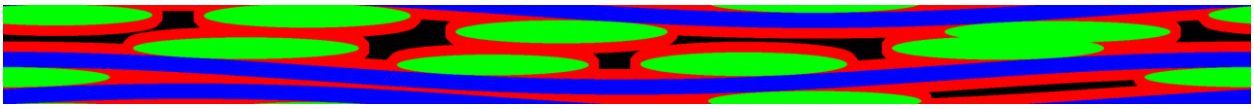

Figure 3-11. Representative volume element with tow offset equal to 4.5

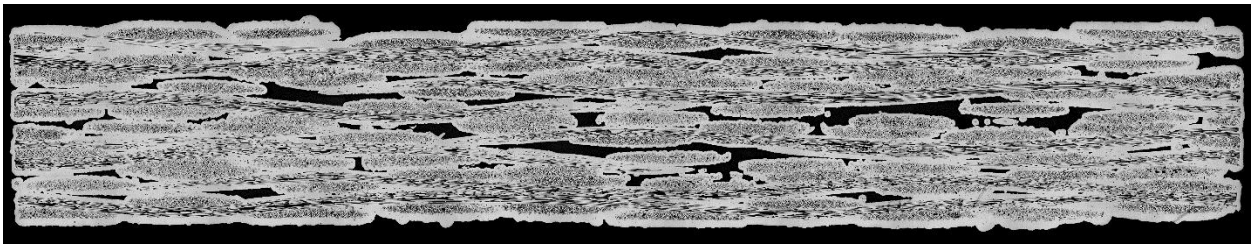

Figure 3-12. Real cross section to be compared to artificial RVE in Figure 3-10 and Figure 3-11.

Table 3-1. Summary of volume fractions and geometric characteristics (tow width, spacing, height) for 3 real sample cross sections. For the cases in which there are values in parentheses, the value in in parentheses is the standard deviation and the other value is the average for the specific cross section listed.

	% Void	% Matrix	% Tow	*w* (mm)	*s* (mm)	*h* (mm)
Cross section 1	3.2	33.8	63.0	1.14 (0.08)	1.27 (0.05)	0.12 (0.01)
Cross section 2	4.8	32.4	62.8	1.15 (0.08)	1.27 (0.06)	0.12 (0.01)
Cross section 3	3.5	32.6	63.9	1.14 (0.08)	1.27 (0.05)	0.12 (0.01)
Mean	3.8	32.9	63.2	1.14	1.27	0.12
SD	0.9	0.8	0.6	0.08	0.05	0.01

Table 3-2. Summary of volume fractions and geometric characteristics (tow width, spacing, height) for 38 artificial cross sections

	% Void	% Matrix	% Tow	*w* (mm)	*s* (mm)	*h* (mm)
Mean	4.2	32.9	62.9	1.15	1.27	0.12
SD	0.7	0.5	0.9	0.09	0.05	0.01

Table 3-3. Summary of volume fractions and geometric characteristics (tow width, spacing, height) for 1000 artificial cross sections

	% Void	% Matrix	% Tow	*w* (mm)	*s* (mm)	*h* (mm)
Mean	4.2	32.8	63.0	1.14	1.27	0.12
SD	0.7	0.5	0.8	0.09	0.05	0.01

Table 3-4. Comparison of correlation coefficients for real cross sections (first value) and artificial cross sections (second value). The value in parentheses is the statistical significance.

	Spacing 3	Spacing 4	Spacing 5	Width 3	Width 5
Spacing 1	-0.47, -0.44 (0.02)				
Spacing 2	-0.42, -0.41 (0.05)				0.41, 0.45 (0.05)
Spacing 3		0.45, 0.42 (0.05)			
Spacing 4			0.60, 0.58 (0.01)		
Width 1				0.56, 0.58 (0.01)	0.41, 0.43 (0.05)
Width 3					0.44, 0.46 (0.05)

Table 3-5. Constituent material properties

	Transverse Tow	Longitudinal Tow	Matrix
E_1 (GPa)	106.0	259.0	420.0
E_2 (GPa)	259.0	106.0	420.0
E_3 (GPa)	106.0	106.0	420.0
v_{12}	0.21	0.21	0.17
v_{13}	0.21	0.18	0.17
v_{23}	0.18	0.21	0.17
G_{12} (GPa)	41.4	41.4	179.5
G_{13} (GPa)	41.4	42.5	179.5
G_{23} (GPa)	42.5	41.4	179.5
α_1 (10^{-6}/°C)	4.6	4.6	4.7
α_2 (10^{-6}/°C)	4.6	4.6	4.7
α_3 (10^{-6}/°C)	4.6	4.6	4.7

Table 3-6. FEA results of full cross sections

	% Void	%Tow	% Matrix	E_1 (GPa)	E_3 (GPa)
Cross section 1	3.2	63.0	33.8	237.0	103.0
Cross section 2	4.8	62.8	32.4	227.0	77.0
Cross section 3	3.5	63.9	32.6	234.0	51.0

Table 3-7. Summary of FEA and response surface results

	Finite Element Analysis Results		Response Surface Results	
	Mean	SD	Mean	SD
E_1 (GPa)	231.0	5.0	230.4	3.6
E_2 (GPa)	259.9	1.9	260.0	1.9
E_3 (GPa)	105.8	6.2	106.2	4.4
v_{12}	0.174	0.005	0.174	0.003
v_{13}	0.202	0.004	0.201	0.003
v_{23}	0.123	0.006	0.123	0.005
G_{12} (GPa)	74.5	5.2	74.1	3.1
G_{13} (GPa)	20.6	3.6	20.4	2.3
G_{23} (GPa)	44.8	1.7	44.9	0.9
α_1 (10^{-6}/°C)	4.65	0.001	---	---
α_2 (10^{-6}/°C)	4.65	0.001	---	---
α_3 (10^{-6}/°C)	4.62	0.001	---	---

Table 3-8. Results due to shifting variation

Shifting (tow offset)	% Void	% Tow	% Matrix	E_1 (GPa)	E_3 (GPa)
1.00 (current RVE)	4.4	63.1	32.6	224	106
0.75	4.8	62.6	32.6	221	92
2.50	5.5	61.6	32.9	231	82
3.25	4.3	62.9	32.8	234	89
4.50	5.9	61.6	32.6	218	70

CHAPTER 4
3D MODELING OF VOIDS IN CERAMIC MATRIX COMPOSITES

The work in the previous chapter found that variation in tow size and tow spacing alone does not explain all of the variability found in the stiffness of the ceramic matrix composite system under investigation. Instead, it is hypothesized that the variable size and spacing of the voids plays a larger role in determining the composite properties than the tow size and tow spacing. The effects of voids have been studied in the past with a variety of methods and goals. There is a large body of work in which the results are related mostly to void volume fraction [31–34]. The relationships found may be relevant for some applications, but as will be shown later, the volume fraction of the voids is not the only thing that must be considered in the woven ceramic matrix composite under consideration in this work. The voids considered here are unevenly distributed and many have large aspect ratios. Huang and Talreja [6] demonstrated that the void shape and size was an important factor to consider, especially for transverse and shear stiffness of a unidirectional composite. They also observed that long, flat voids are most detrimental to the transverse stiffness. This agrees well with preliminary analysis on the woven CVI SiC/SiC composite where void volume fraction is not the sole mechanism of stiffness degradation [1]. Uniform distribution of voids was assumed for the analysis which was shown to compare well for experimental data in unidirectional composites. However, woven composites appear to have significantly greater variability in void size and distribution as compared to unidirectional composites. Therefore it would be beneficial to determine the degree of complexity that should be included in the model.

The goal of the work in this chapter is not to develop analytical equations that allow for accurate prediction of stiffness based on characteristics of the voids. Instead, the voids in the 5HS SiC/SiC composite are characterized such that they can be used as an example for which characteristics of voids are critical to model and which properties are most influenced by the types of voids observed. In addition, suggestions are made for how the complex voids can be modeled in a simplified manner.

4.1 Observations of Three Dimensional of Voids in Woven SiC/SiC Composites

The computed tomography completed by Bonacuse [23] yielded a 3D map of the composite microstructure. The voids can be isolated from the rest of the composite microstructure in order to easily view their shape and distribution. One small sample of the 3D rendering is provided in Figure 4-1. The voids appear as a white/light grey color. It is difficult to visualize the 3D voids on a 2D image, but a few characteristics were observed when exploring the 3D model. The voids are generally long and flat (square-like when projected onto the 1-2 plane and rectangular with a large aspect ratio when projecting the void on the 1-3 and 2-3 planes), lying in what appears to be seven interply layers. This can be visualized by looking at the three real cross sections of the 1-3 plane, presented in Appendix A. The 3 direction is through the thickness and the 1 direction and 2 direction are in-plane. The major voids in the interply regions are sometimes connected through the thickness by small, thin, void sections.

It is clear that the network of voids would be difficult to model exactly as seen, especially if attempting to create an appropriate finite element mesh. Therefore, a major goal of this work is to determine an effective and efficient way to model the complex voids, while still capturing their effect on the stiffness. While it would be difficult to verify that the assumed void structure and layout described in this chapter is a perfect

representation of reality, some careful studies can reveal which approximations are reasonable.

The preliminary qualitative observations stated above guided the type of voids that would be modeled and studied. Section 4.2 and Section 4.3 describe the effects that the types of voids observed have on the composite and offers some physical explanations as to why the voids have the effects that they do. In Section 4.4 the 3D voids in the composite are then characterized in such a way that they can be used to make a simplified finite element model. In addition guidance on how the voids would best be simplified and modeled is provided.

4.2 Preliminary Evaluation of the Importance of Void Characteristics in Determining Material Stiffness

As discussed in Section 3.3.3, with each new ply shifting applied, the key architectural changes are the size and location of the voids. The microstructure of the 5HS SiC/SiC composite is very complicated. In order to develop an understanding of the effects of voids, without the results being convoluted by other aspects of the material geometry, the preliminary analysis was completed on an isotropic material with a Young's modulus of 100 GPa and a Poisson's ratio of 0.3. Note that the stiffness is reported as a "percent retained stiffness" referring to the percent of stiffness remaining in the material due to the presence of the voids. For all isotropic models the void volume fraction was 4%. The aim of the following analysis was to determine which void characteristics were most important to model in order to understand how the voids affect the transverse stiffness. These characteristics include size, aspect ratio, and position or alignment in various directions. Since the voids in the 5HS SiC/SiC

composite were found to be oriented in the same direction as the planes of the composite, the effect of orientation was not studied.

4.2.1 Finite Element Model

Previous analysis of the effects of tow variability was completed in 2D for simplicity. This is not the best way to model the woven composite, but it gives reasonable estimates in regard to determining how to model the variability. Since modeling the variability in the tow size and tow spacing led to relatively small variability in the stiffness, it may be possible to capture the variability of stiffness in the composite specimens by modeling only the voids, and not the other details of the microstructure. At the least, studying the effects of voids in a homogeneous isotropic (and later, orthotropic) material will provide valuable preliminary insight into the physical effects of voids on the composite. This also simplifies the problem so that the effects of voids can be studied in 3D, eliminating some of the shortcomings of a 2D approximation, especially when considering the shear stiffness.

Finite element analysis was completed using Abaqus [54] with 4-node tetrahedron elements. Periodic boundary conditions were applied using the same methodology as described in Chapter 3. The illustration of the geometry used for the finite element model depicted in Figure 4-2 is a cuboid of equivalent length and width. The aspect ratio (ratio of the length to the height) is 4 to 1, similar to that of the composite cross sections that were available. The voids were modeled as cuboids. The sharp corners do not affect the stiffness results; however they should be avoided if a similar model were used for examining the effects of voids on strength. The length and width of a given void are also equivalent. Since the composite's weave is balanced, it is safe to assume that if the voids are of a given length when scanning from the 1-3 plane,

they will be similar when scanning from the 2-3 plane. The voids can occur anywhere in the 1-2 plane. However, they generally occur in layers, around where each individual ply lies. A more complete description of the voids in the actual composite is given in Section 4.4. The descriptions of the specific void sizes and locations studied are given in the following section.

4.2.2 Description of Void Cases

The variables for this study are the number of voids, the longitudinal aspect ratio, and the position of the voids. The longitudinal aspect ratio (AR) is defined by the width (1-direction) divided by the height (3-direction). The length (2-direction) is equal to the width. The size (8 mm x 8 mm x 2 mm) and isotropic material properties of the specimen will remain constant, in addition to the total void volume fraction of 4%. The specimen itself has an aspect ratio of 4. The initial exploratory results encompass 20 cases summarized pictorially in Figure 4-3 and in a list below. Some positions are not surveyed due to symmetry. Additional 1-void cases in which the length did not equal the width were analyzed for the shear stiffness analysis. The results of the 20 cases and the additional shear stiffness results can be found in Appendix B.

- Cases 1-4, Figure 4-3 A: 1 void; Centered; Aspect ratio (AR) = 3, AR = 5, AR = 8, AR = 10
- Cases 5-8, Figure 4-3 B: 2 voids; Centered and aligned in “1” direction; s_1 constant; AR = 3, AR = 5, AR = 8, AR = 10
- Cases 9-12, Figure 4-3 B: 2 voids; AR = 8; Aligned in “1” direction; s_1 = 0.15 mm, s_1 = .57 mm, s_1 = 1 mm, s_1 = 1.6 mm
- Cases 13, alignment s_1 pictured in Figure 4-3 B: 2 voids; AR = 8; Aligned in “1” direction; s_1 constant; s_2 – maximum possible distance apart (one void on bottom, one void on top)

- Case 14, Figure 4-3 C: 2 voids; AR = 8; NOT aligned in “1” direction (located in opposite corners); s_1 constant; s_2 – maximum possible distance apart (one void on bottom, one void on top);
- Cases 15-18, Figure 4-3 D: 3 voids; Centered and aligned in “1” direction; s_1 constant; AR = 3, AR = 5, AR = 8, AR = 10
- Case 19, Figure 4-3 E: 3 voids; AR = 10; Voids diagonal, but in same plane
- Case 20, Figure 4-3 F: 3 voids; AR = 10; Voids diagonal, but in different planes;

4.2.3 Results and Analysis

After analyzing 20 exploratory void cases, a few trends became obvious. Table 4-1 summarizes the mean and standard deviations of the stiffness loss based on these 20 cases. The longitudinal stiffness (E_1 and $E_{2)}$ and in-plane shear stiffness (G_{12}) were not significantly affected by changes in the void aspect ratio and location. However, the transverse stiffness and out-of-plane shear stiffness were significantly affected. For a constant void volume fraction of 4.0%, the loss in stiffness averaged up to 18%. This is significant in that many models accounting for voids rely on void volume fraction alone. For the particular composite studied here, there are other factors besides volume fraction that must be significant and important to consider. The average loss of stiffness and the respective standard deviation of the 20 cases are displayed in Table 4-1. When considering the effects of placing the voids in various locations with respect to one another, the stiffness is minimally impacted. Table 4-2 provides a comparison between the effect that varying aspect ratio has on the transverse stiffness versus the effect that varying the void position has on the stiffness. For the case of two voids, varying the aspect ratio between 3 and 10 results in a standard deviation of stiffness of 5.5%, while varying the position results in a standard deviation of 0.1%.

The key feature of the void that is changing as the aspect ratio increases is the projected area of the void on the 1-2 plane. Throughout this work the projected area may also be referred to as area fraction. It became clear that the projected area of the voids in the transverse direction (or the area of the void in the 1-2 plane) was important to determining the stiffness. The plot in Figure 4-4 plots the transverse stiffness (percent retained stiffness, or stiffness remaining as result of void being present) as a function of the area fraction, $\bar{a}_3$, which can be define as the ratio of the projected void area, a_3, to the total area of the 1-2 plane, A_3, and written as

$$\bar{a}_3 = \frac{a_3}{A_3} \tag{4.1}$$

Note that the void cases included in this plot only include the cases in which aspect ratio and number of voids varied because the spacing did not affect the stiffness. A strong linear relationship is found between the projected area of the voids and the resulting stiffness. The equation of the line is

$$E_3 = -0.68\bar{a}_3 + .99 \tag{4.2}$$

and the coefficient of determination, R^2, is 0.98.

In order to verify that the void height did not have as large of an influence as the projected area, another study was added in which for a given area fraction, the height was varied three times (note that this changes the void volume fraction). The height was randomly chosen, and applied to all voids for that particular case. This was repeated for several different areas, and included cases that included two voids and three voids. The data can be found in Table B-4. Figure 4-5 and Figure 4-6 show the variation in transverse stiffness for varying height fraction and varying area fraction, respectively. In

Figure 4-6 one can see the projected area fraction and stiffness are linearly related. It is also worth noting that for each area fraction there are three data points. This corresponds to the three different heights that were tested for that given area fraction. The figure effectively shows that varying the height only caused small, local perturbations in the stiffness. From Figure 4-5, it is clear that there is no discernible relationship between the height fraction and transverse stiffness. This does not imply that the height has no influence. However, it can be shown from that data while the area is kept constant, and the height is varied by 18%, the transverse stiffness only varies by 1.4%. In contrast, if the height is held constant, and the area is varied by approximately 5%, the transverse stiffness changed by 5% as well.

Another set of cases were studied in which voids of equal area were aligned with one another in the 3-direction (through the thickness) in order to determine whether or not the overlap in voids had any effect on the stiffness. Table 4-3 summarizes the results of 1 void, that is then split into 2 overlapping voids (aligned in the 3-direction), illustrated in Figure 4-7. The change in stiffness for the various cases is less than 2%, which like the height, has some impact on the transverse stiffness, but it is very small compared to that of the projected area. The relationship of the projected area to the transverse stiffness provided in Equation 4.2 may be useful, but it does not provide any physical understanding about the effects of voids. Therefore, a study of the voids in Section 4.3 will focus more on the effects of void size, rather than position, and include a larger range of area fractions.

The transverse shear stiffness G_{13} and G_{23} are also affected by the projected area of the voids, with position having minimal influence. A graph of the

transverse shear stiffness versus the projected area fraction is found in Figure 4-8. G_{13} and G_{23} are not equal when the transverse aspect ratio (ℓ_1/ℓ_2) is not one. Table B-3 contains all of the data. For a fixed aspect ratio, the relationship between the projected area and shear stiffness is linear. The transverse aspect ratio has a greater influence on the transverse shear stiffness than on the normal transverse stiffness because of the strong directionality dependence of G_{13} and G_{23}. Therefore, if voids were unevenly distributed, there is the potential for a large variation in transverse shear stiffness based on the orientation of the voids. As was discussed in Section 4.1, the voids in the 5HS SiC/SiC composite have some degree of symmetry within the composite due to the balanced weave of the composite.

4.2.4 Preliminary Conclusions

After completing finite element analysis on several cases of void size and spacing while the void volume fraction remained constant, it was clear that the voids affect the transverse stiffness and the out-of-plane shear stiffness the most (up to 18% stiffness degradation on average for a void volume fraction of 4%). In an attempt to determine the driving factors of the reduction in stiffness, we found that for the transverse stiffness, the projected area of the voids onto the 1-2 plane had a significant impact. A strong linear relationship was found between the area and the resulting stiffness. Similarly, it was found that the transverse shear stiffness is also related to the projected area of the voids onto the 1-2 plane. Analysis in Section 4.3 will provide a physical explanation for the observations that have been described.

4.3 Modeling Three Dimensional Voids of a Woven SiC/SiC Composite

The previous analysis was completed on an isotropic material. Since the 5HS SiC/SiC composite has orthotropic properties, follow-up analysis was completed on the

same finite element model, but with the idealized (matrix fully densified with no voids) orthotropic composite properties presented in Table 4-4. These properties came from analysis similar to that in Chapter 3 in which periodic boundary conditions were applied to a composite cross section. The cross section did not contain any voids, however. Note that stiffnesses are still reported as “percent stiffness retained” rather than the resultant stiffness in order to make the data easily interpretable.

4.3.1 Effect of Number of Voids on Stiffness

The analysis in Section 4.2 only focused on the effects of a small number of voids (1-3 voids). The area fraction was found to be very important in modeling transverse stiffness properties, but what was not studied thoroughly was whether or not the number of voids modeled would affect the results. For example, in the composite a complicated network of voids are observed in each plane that needs to be approximated. The simplest method would be to model the network of voids as one void of equivalent area. However, it is important to discern the implications of modeling all of the voids as one large equivalent void, or as several individual voids more like those physically present.

In order to determine the effects that the number of voids modeled has on the stiffness, models were produced that varied both the number of voids and the projected area fraction (projected area of the voids on the 1-2 plane divided by the total area, as defined in Equation 4.1). The void volume fraction remained at a constant value of 5% (the actual void volume fraction of the composite sample being analyzed). This implies that as the projected area in the transverse direction increases, the height, or thickness, of the void will become smaller. Voids were modeled in a square, symmetric array and were equally spaced throughout the specimen’s area on one plane. For example, 9

voids were modeled as a 3x3 array of cuboid voids. Therefore, the number of voids modeled was 1, 9, 16, 25, 36, 49, and 64. The void area fraction varied from 15% to 90% in increments of 15%. In other words, for each area fraction (15%, 30%, etc.), models with 1, 9, 16, 25, 36, 49, and 64 voids was run. The area fraction of the voids will vary throughout the composite. Varying the area fraction will allow us to look at a large range of potential area fractions and number of modeled voids. A void area smaller than 15% could not be modeled with a proper mesh, due to mesh refinement limitations. However, it can be said that if the projected area of the voids is at least 15% of the total area of the composite under investigation, the projected area will have an impact on the stiffness results (rather than only the volume fraction). A summary of results is displayed in Figure 4-9 and Figure 4-10, and are discussed individually in the following sections. The in-plane properties were not significantly affected by variation in void number and area. The results are summarized in Appendix B for reference.

4.3.1.1 Effect of number of voids and projected area on transverse stiffness E_3

Figure 4-9 demonstrates how the stiffness changes with both a varying number of voids, and with varying area fraction. Based on the study from Section 4.2, the large effect that the projected area has on the stiffness is not surprising. What is now clear though is that modeling only one void could be an extreme representation of the influence of void area if there is more than 1 cuboid void present. For all areas, as the void number increases, the stiffness also increases. It appears that, depending on the area, the number of voids modeled can change the resulting stiffness significantly (on the order of 20-30%). Therefore, modeling a complex network of voids as one void of equivalent area would be an extreme representation of reduction in stiffness due to the voids. Further discussion on how to choose the number of voids that should be modeled

is found in Section 4.4. In Figure 4-9, another trend to point out is that the variability in stiffness as the number of voids varies increases with increasing area fraction. This and the asymptotes in the figure are best explained after examining the following analysis.

It is interesting to look at a plot of the projected area versus the stiffness for the two extreme cases of modeling only one void, versus 64 voids. In Figure 4-11, the stiffness varies linearly with the projected area if only one void is being modeled. This was also found in the preliminary study of the isotropic models. The equation of this line in Figure 4-11 is

$$E_3 = -0.91\bar{a}_3 + 1.01$$

However, as the number of voids increase, their variation with area becomes quadratic. Note that the other void cases not plotted would be between the two extreme cases shown. This plot and other analysis that has been discussed lead us to question if there is an explanation as to why the number of voids influences the stiffness. To address this problem, we can look at a simplified example.

In order to arrive at a physical explanation we can examine a problem in which we have two materials stacked in series as shown in Figure 4-12. The materials are isotropic and the bottom material has a void. The displacement of the material can be written as

$$\Delta_3 = \frac{F(L_3 - l_3)}{A_3 E_3} + \frac{Fl_3}{(A_3 - a_3)E_3} = \frac{FL_3}{A_3 E_3'} \tag{4.3}$$

where F is a force applied to the material, A_3 is the area of the material, a_3 is the area of the void in the bottom part of the material, L_3 is the total length of the orthotropic material in the 3-direction, l_3 is the length of the void, E_3 is the material's nominal

stiffness, and E_3' is the resultant stiffness due to the void. A 3-dimensional image defining the variables is provided in Figure 4-13. Equation 4.3 simplifies to

$$\frac{1}{1-\frac{\Delta E_3}{E_3}} = 1 + V_v \frac{1}{(1-\bar{a}_3)} \tag{4.4}$$

where V_v is the void volume fraction, ΔE_3 is the change in trasverse stiffness due to the voids, and $\bar{a}_3$ was defined in Equation 4.1 and is referred to as the area fraction. Equation 4.4 can be written as

$$\frac{\Delta E_3}{E_3} = 1 - \frac{1}{1 + V_v \frac{1}{(1-\bar{a}_3)}} \tag{4.5}$$

This relationship poorly predicts the FEA results, with an RMS error of 37 GPa for the 1-void models and an RMS error of 13 GPa for the 64-void models. The analytical equation (Equation 4.5) is plotted with two of the FEA results to demonstrate the difference in the analytical prediction and FEA results in Figure 4-14. It was hypothesized that the height of the void, l_3, has an effect on the stiffness that extends beyond the nominal height, meaning the voids act taller than they physically are. The volume fraction in Equation 4.5 can be written in terms of area and length of the void such that Equation 4.5 can then be rewritten as

$$\frac{\Delta E_3}{E_3} = 1 - \frac{1}{1 + (\bar{l}_3 + \xi)(\bar{a}_3) \frac{1}{(1-\bar{a}_3)}} \tag{4.6}$$

where ξ is a correction factor to the height fraction of the void and $\bar{l}_3$ is the height fraction of the void

$$\bar{l}_3 = \frac{l_3}{L_3} \tag{4.7}$$

The height fraction may be referred to as the length fraction, also. In order to determine what the correction factor should be, the results from the basic approximation given by Equation 4.5 and the FEA results can be used to solve for ξ with the equation as derived below.

$$\frac{\Delta E_3}{E_3}^{FEA} - \frac{\Delta E_3}{E_3}^{Analytical} = \left(1 - \frac{1}{1+(\bar{l}_3+\xi)(\bar{a}_3)\frac{1}{(1-\bar{a}_3)}}\right) - \left(1 - \frac{1}{1+V_v\frac{1}{(1-\bar{a}_3)}}\right) \tag{4.8}$$

Note that this expression does not explicitly include the number of voids modeled. To simplify we can define new variables

$$\Delta E = \frac{\Delta E_3}{E_3}^{FEA} - \frac{\Delta E_3}{E_3}^{Analytical}$$

and effective length fraction

$$\rho = \bar{l}_3 + \xi$$

Then Equation 4.8 can be solved for the effective length fraction (corrected height), ρ as

$$\rho = \frac{\dfrac{1}{\Delta E - \dfrac{1}{1+V_v}\dfrac{1}{(1-\bar{a}_3)}} + 1}{-\bar{a}_3\dfrac{1}{(1-\bar{a}_3)}}$$

The effective length fraction is plotted against the original length fraction, $\bar{l}_3$, in Figure 4-15. The difference in results between the 1-void case and 64-void case is interesting. It reveals that the 1-void case needs a larger correction, than the 64-void case. The necessary correction decreases for larger original length fractions though because physically it would not make sense for the length to be corrected beyond the

boundary of the model. This is better illustrated in Figure 4-16 where we can see that the corrected length for 1-void is plateauing near 1. In essence, this correction in the void's height shows that the void's influence extends beyond its boundaries, and acts taller than it actually is. The necessary length correction decreases as the number of voids modeled increases.

As the number of voids increases, the individual voids also get smaller. The stress is zero at the boundary of the voids, but this does not happen abruptly. The small stresses begin to develop at some distance away from the voids. When the void is smaller, the region in which the small stresses begin to develop becomes smaller as well. This is illustrated by a 2D visualization of the stress field around 1 void, 3 voids, and 8 voids in Figure 4-17, Figure 4-18, and Figure 4-19. The case in which there is one large void, you can see that small stresses extend to the boundary. Whereas the region that the lower stresses extends begins to shrink as the number of voids are increase. From this analysis it is understood that the void's effect on the load bearing volume extends further than the space that the void physically occupies, which offers some explanation of why relationships based solely on volume fraction may not be sufficient for all cases.

The above analysis also explains the variability in stiffness as the number of voids varies increases with increasing area fraction. As one void increases in size, the stiffness linearly decreases more drastically than when more voids are modeled because of the effects of void height discussed. In Figure 4-14, we see that as the number of voids increases, the result is approaching that of the analytical relationship in Equation 4.5. The asymptotes in Figure 4-9 are approaching the value predicted by the

analytical equation in which less height correction is necessary. The analytical equation therefore predicts results for small voids with small aspect ratios, which is essentially what happens when many voids are modeled for a given area fraction.

4.3.1.2 Effect of number of voids and projected area on transverse stiffness G_{13} and G_{23}

The transverse shear stiffness properties, like the transverse normal stiffness properties, are predominantly affected by the projected area of the voids, and that the resulting stiffness does depend on how the voids are modeled (one equivalent void, or many voids). The graph in Figure 4-20 demonstrates the dependence on area fraction. As was the case for the transverse stiffness, the relationship is linear if only 1 void is being modeled but becomes quadratic if more voids are modeled. Note that only one graph is generated for both G_{13} and G_{23}. For the cases studied here, the voids were arranged symmetrically. However, G_{13} and G_{23} are dependent on the orientation or transverse aspect ratio of the voids, as was demonstrated in Section 4.2. Since G_{13} and G_{23} are dependent on the orientation, any type of correction factor to an analytical approximation would need to be dependent on the aspect ratio and orientation of the voids. The goal of the work is not to establish accurate predictions of the stiffness based on void characteristics, but rather understand which characteristics are important to model, and for which properties. Therefore, there is no added value in developing the correction factor. Instead, it is appropriate to note that when modeling the transverse shear stiffness, it is important that the projected area and orientation or shape of the voids is considered.

4.3.2 Neglecting Small Voids

Section 4.4 will contain more detailed information about examining the voids of the actual composite, but before going into the details of modeling those voids, it is necessary to determine if absolutely all voids must be modeled. If not all voids need to be modeled, it is important to determine if the neglected voids still need to be accounted for in some way. Figure 4-21 is a 2D projection of the 3D voids in one ply of the composite. There are many small voids that would be difficult to model in detail.

In order to determine the effect of neglecting any small voids (small relative to the other voids), a problem was set up such that a 3x3 square array of voids with a 30% area fraction was modeled, with the addition of nine more voids, each 25% the size of one of the voids in the main 3x3 structure, as illustrated in Figure 4-22. This increased the void area fraction to 37.5% (the void volume fraction is still 5%). In order to add an additional check (to determine the influence of the change in area by 7.5%), another 3x3 model was analyzed with a total void area of 37.5%). The data points are plotted in Figure 4-23, which are the same results from Figure 4-9 with a few additional data points described here. The case for which 9 large voids and 9 small voids are modeled lies somewhere in between the cases of neglecting the 9 smaller voids completely, and including them in the total area, but only modeling 9 voids rather than all 18. The result is slightly closer to the case in which the voids are neglected completely. It is also important to note that as the extra voids get even smaller, they will have even less impact on the overall stiffness.

Given that there is not necessarily one answer that is more correct than another, it would be up to the analyst to choose which situation is most appropriate. For this application, most of the voids are significantly smaller than 25% of the largest void

present (as demonstrated in Figure 4-21). Therefore, for the analysis presented in Section 4.4 it was decided that voids that were less than 25% the size of the largest void could be neglected in terms of area fraction. However, their presence would be preserved with respect to their volume fraction. In other words, rather than modeling their projected area, their volume fraction would be included in the total volume fraction by including it in the thickness of the voids.

4.4 Three Dimensional Characterization of Voids in Woven SiC/SiC Composites

In order to demonstrate the potential applicability of what was learned by the studies in the previous sections, the voids in the 5 HS SiC/SiC composite are characterized and modeled using some of the assumptions discussed. From preliminary studies described in Section 4.2, it is known that the area of the voids has a large impact on the transverse stiffness properties. The large variability in stiffness for a constant volume fraction demonstrated that the volume fraction is not the key factor driving the behavior. There was not a lot of variability in the in-plane stiffness properties, and the resultant properties corresponded to volume fraction predictions (5% voids results in 5% reduction of stiffness). Therefore, the composite's image was divided into 8 layers, and void data was collected in each of those layers, such that the voids in a given layer are projected on to a 2D surface in the 1-2 plane, like that illustrated previously in Figure 4-21. There will be some area through the thickness of one layer where there is overlap in the voids (given that the voids have a thickness to them). Every void in a given layer will be prescribed an equivalent thickness. The thickness will be determined by the total volume fraction of voids found in that ply of the actual composite. This will allow for conservation of a 4.9% volume fraction in the entire specimen. This will also allow local volume fractions to be maintained.

It was observed, as was described in Section 4.3.2, that small voids (relative to the other voids) do not significantly impact the stiffness. Therefore, these relatively small voids were also removed, and are accounted for in volume fraction by being included in the thickness of the significantly sized voids. A small void was considered any void smaller than 25% the size of the largest void. MATLAB's regionprops() function was used in order to quantitatively discretize the voids and their size [62]. The function interprets the black and white space as zeros and ones, respectively. Each group of ones (defined as a group when the ones are surrounded by zeros) is recorded and can then be analyzed in terms of area or other properties of interest (aspect ratio, compactness, etc.).

Since the voids are being analyzed on a projected 2D surface, the thickness included in that projection must be considered. The composite is made up of 8 woven plies. Therefore, the composite image was broken up into eight equal layers in the through-thickness direction. The top and bottom ply were found to not contain any voids of significant size (the voids appeared as barely discernible flecks). The 6 plies in the middle, however, had large complex voids. Images of each of these plies can be found in Appendix C. Others will be shown for reference in the following discussion.

As previously mentioned, the number of voids used to approximate the actual voids can have a large effect on the results. A potential method of determining this was evaluated. First, a section was taken from the 3D composite to be analyzed and its 2D void projection is shown in Figure 4-24. In the finite element program Abaqus, the void projection was set as a background so that the voids could be roughly sketched as illustrated in Figure 4-25. Exact details are difficult to capture in this manner, but the

general sketch of the voids which is likely more important than the minute details is obtained. The final voids sketched for the finite element analysis is shown in Figure 4-26. Knowing that the area fraction is important in determining stiffness, the area fraction of the real voids and the simulated voids were recorded. The simulated voids had an area fraction of 0.38 while the voids in the real image had an area fraction of 0.40. The simulated voids were analyzed using finite element analysis.

A summary of results for the simulated voids, as well as the results from equivalent square array models are shown in Table 4-5. The data point is also visualized on the graph that demonstrates variation in stiffness with respect to varying void number and area fraction in Figure 4-26. A few things can be ascertained from this Figure. The circle represents the actual data point with respect to the finite element result and the number of voids modeled (twelve). The straight line is at 78% stiffness. If this line is followed to the point of 4x4 arrays, you can see that with 38% void area (about half way between 30% area and 45% area) you would obtain the result that we did (77% stiffness). However, in the finite element model of the sketched voids, there are 12 voids (not 16). It appears that if you have complex shapes, the effects on stiffness are smaller than when voids are perfect solid cuboids. The results indicate that it is also possible that when voids have complex shapes and narrow connection between larger sections, there are acting like several voids, rather than one.

From this demonstration we learned that it would be difficult to determine the how many voids in a square array are appropriate without trial and error. By inspection of the original image, different designers may describe it anywhere between a 3x3 array and a 6x6 array. It would be helpful if in future work, methods are developed in which the

complex shape can be quantified in some way that would allow for a more measurable explanation for how the voids should be modeled. Currently, the analyst would have to use a simple guess and check method. Quantitative measures of the shapes or topology of the voids would be especially useful when the voids are not generally symmetric in nature. As mentioned previously, since the 5HS SiC/SiC composite has a symmetric pattern, the voids also look relatively symmetrical. This would not be true for all composite layups, and this lack of symmetry would affect the transverse shear stiffness.

Since there is not an exact method of determining which square void approximation is best for each layer, the voids were sketched for each of the six plies modeled (the top and bottom plies did not have large voids). For each sketch in the finite element model, the area fraction between the original and sketched model was compared. The difference in area fraction never exceeded 2%. As previously mentioned, the thickness of each layer of voids was determined by the void volume fraction in that ply. Once the void area was determined, the thickness was chosen such that the local void volume fraction would be preserved. The void area and void volume fraction in each ply is summarized in Table 4-6. The sketched images used in the finite element model can be found in Appendix C with the original void images. The results of the finite element analysis are found in Table 4-7.

One feature worth noting about the void volume fracture in each ply is that the void volume fraction is largest in the middle of the composite, and decreases as you approach the outer ply. This was also observed qualitatively when inspecting the 2D cross sections of the composite. This phenomenon is caused by the manufacturing

process. The matrix particles are deposited on to the surface of the tows and are built up around the tows. At some point, matrix particles in neighboring sections will meet with one another and may close off an area that has not yet been filled by the matrix. There is then no way for the matrix to continue depositing in that section. The area in the middle becomes closed off first, and loses its ability to become further densified with the matrix. This information highlights importance of potential improvements in the manufacturing process. Since the area fraction of the voids impacts the transverse stiffness, and the area fraction of the voids is largest at the center, there may be some value in improving the process such that the middle of the composite has a higher matrix density.

The stiffness results are not surprising. Since the voids are flat and thin, the in-plane stiffness properties $E_{1,}$ $E_{2,}$ and G_{12} were reduced by 5%, the approximate void volume fraction. However the transverse stiffness properties were significantly impacted by the presence of the voids, beyond the effects that would be computed if only the void volume fraction were used. As previously mentioned, since there are no experimental results available for this material it is not possible to know if this solution is correct. At best, there is an experimental result reported on a similar, but different material with lower void volume fraction in which the transverse stiffness was reported as almost 50% of the ideal value [28]. However, the purpose of this model was not to obtain an accurate value, but rather demonstrate a potential simplified method of modeling the voids. Given the dependence of stiffness on projected area fraction, the results found may not be unreasonable.

4.5 Conclusions

It is very common for the effects of voids to be accounted for by their volume fraction. For example, if there is a 5% void volume fraction in the matrix of the composite, the properties would be degraded by approximately 5%. When voids are relatively small and evenly distributed this is not necessarily a bad approach. However, this work provides insight into why this may not always be correct. The goal of the work in this chapter was to determine which characteristics of the complex voids in a 5HS SiC/SiC composite were most influential on the stiffness of the composite, and provide suggestions for how these voids could be modeled in a simplified manner. It was found that the spacing and alignment of voids were not critical to model. However there are other characteristics of the voids that were found to be very important to consider. Below is a summary of what should be considered when determining the stiffness of the composite material with voids.

The influence of the voids' projected area has been discussed several times. The projected area becomes important when that area is of a certain size relative to the area being observed. In this work, we found that if the projected area of the void is at least 15% of the total area, the stiffness in that direction will be influenced by that area (rather than only the volume fraction). This is why for the 5HS SiC/SiC composite with thin, flat voids, the voids' effect on in-plane stiffness is benign (and related to the volume fraction). Areas less than 15% were not studied due to mesh refinement issues, so it cannot be said with certainty whether or not areas smaller than that will affect the stiffness.

In regard to void size, we also established that larger voids will have a larger influence on the stiffness than the smaller voids around it. For example, while a void's

area may be 15% of the total area of the composite, if there is another much larger void, the influence of the smaller void can be considered negligible. For this work, it was decided that any void 25% smaller than the largest void would not be modeled explicitly, and instead would be included as part of the total volume fraction by contributing to the thickness of the void.

The area of the voids was not the only characteristic of the void that impacted the stiffness. The number of voids and the aspect ratio impacted the stiffness results also. This was explained analytically when we found that it was necessary to correct the height of the void used in the calculation. The stress will become zero on the boundary of the void. However, the stress will not become zero suddenly. For one void of large aspect ratio, the stress around the void becomes smaller at a larger distance away from the void. When the voids have space between them (and smaller aspect ratios) the stress does not have to become small at as large of a distance as when the aspect ratio was larger. This is why, for a larger number of voids, the correction to the height was smaller for a larger number of voids

While we learned that the number of voids modeled had an influence on the results, it was not clearly defined how to determine what number of voids should be used. For example, when examining one 2D projection of the voids in the composite, there was not a precise way to determine if the voids should be modeled in a 3x3 array, a 4x4 array, or something else entirely. What was learned is that if the voids have complex shapes with large areas connected by smaller ones, it is possible that 1 complex void could be behaving as two or more voids as approximated by the model with square voids. Therefore, the analyst would have to decide how they would want to

approximate the voids (either by sketching as was done in Section 4.4) or by visually approximating what kind of square array would be best. Future work should consider how to quantitatively approximate the complex voids into a simpler model, as the current method used could prove to be time consuming.

In summary, the projected area onto the 1-2 plane of the 5HS SiC/SiC composite had a large influence on the transverse stiffness properties (both normal and shear). Using a volume fraction estimate alone could result in significant over-prediction of the stiffness. It was found that accounting for this area appropriately and the number of voids modeled is critical, while some aspects such as modeling the accurate spacing between the voids would not be as important.

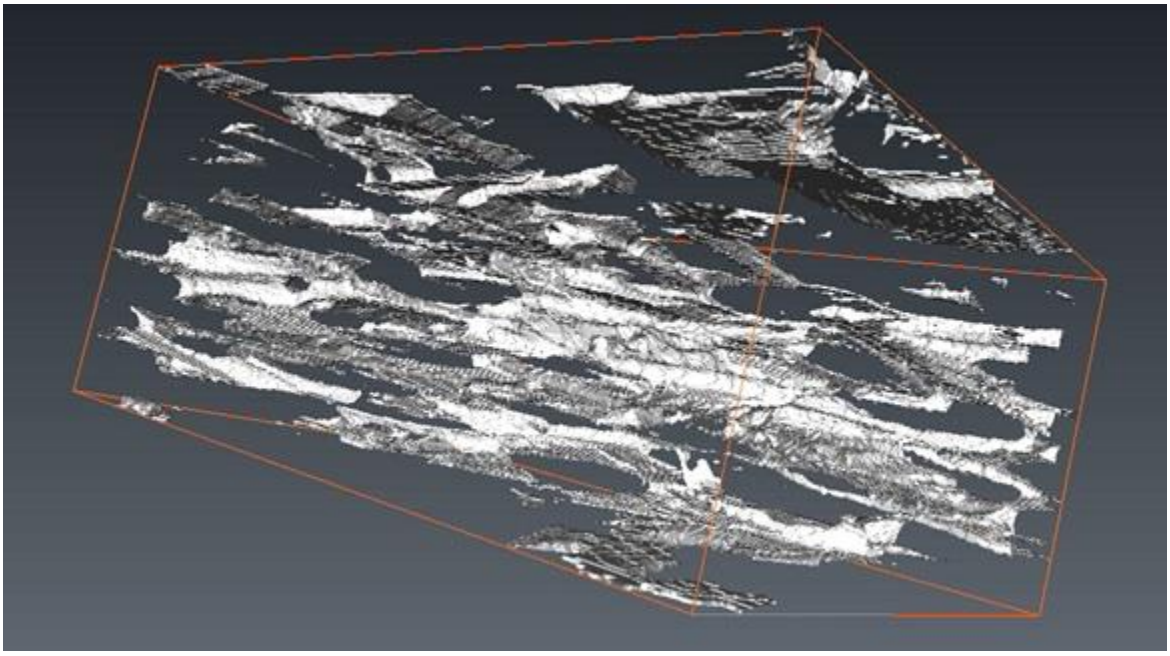

Figure 4-1. Small section of the 3D rendition of the voids where the white and light gray areas are the voids

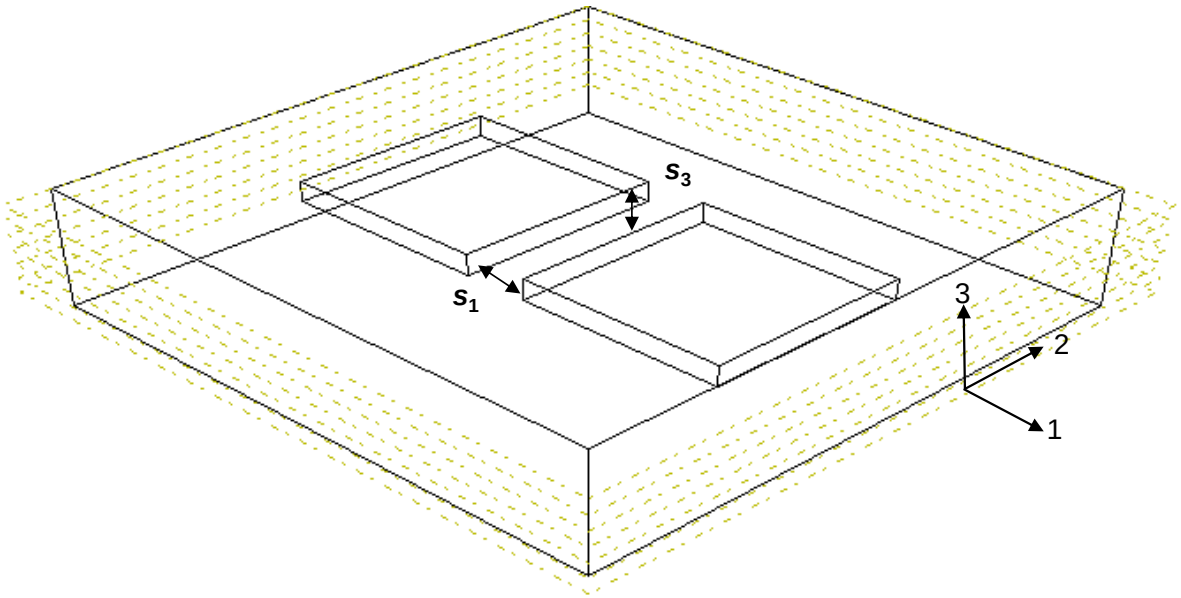

Figure 4-2. 3D model with 2 cuboid voids, illustrating spacing s_1 and s_3

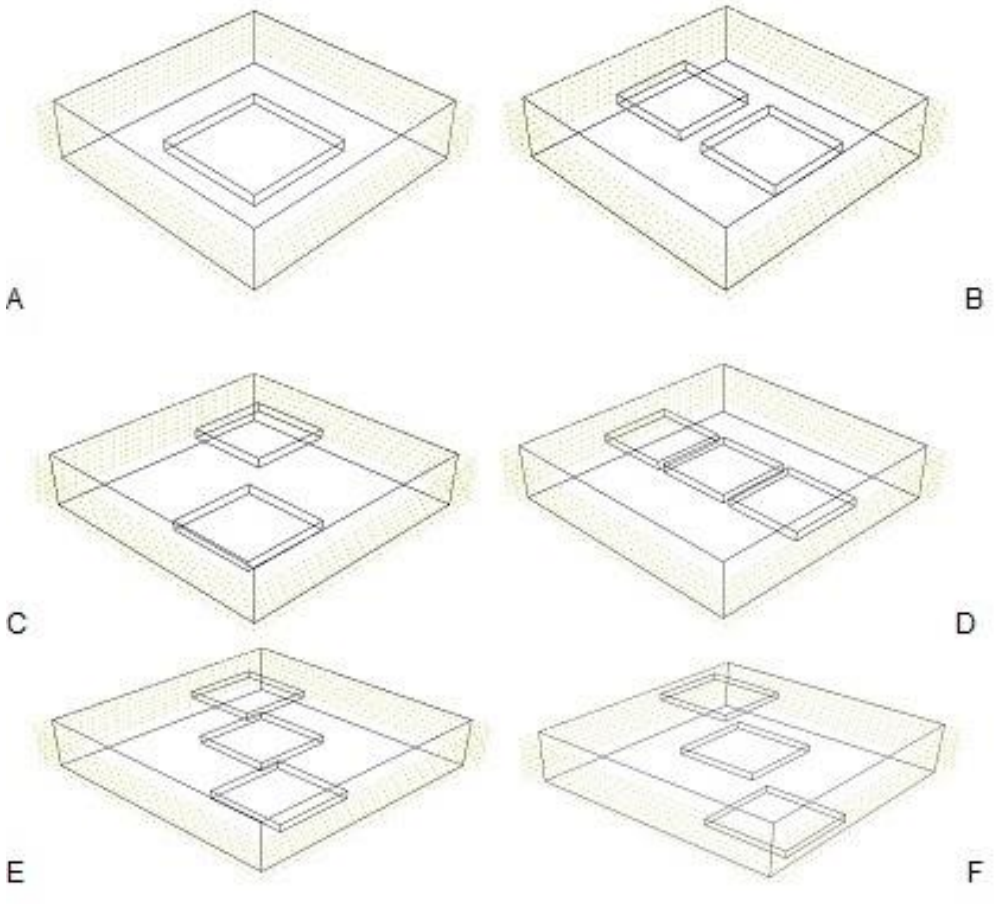

Figure 4-3. Illustrations of various exploratory void cases. A) Cases 1-4: 1 Void; centered; varying AR, B) Cases 5-13: 2 Voids; Centered along 1-axis; vary AR, s_1, and s_2. C) Case 14: 2 Voids; AR = 8; Voids in opposite corner. D) Cases 15-18: Voids; Centered; Varying AR. E) Case 19: 3 Voids; Arranged diagonally on one plane. F) Case 20: 3 Voids; Arranged diagonally on multiple planes.

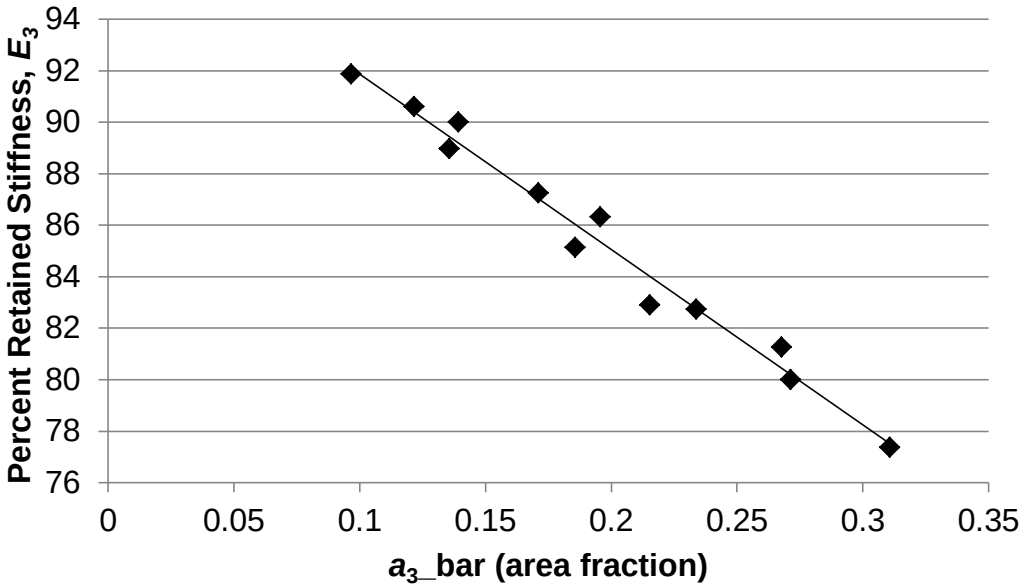

Figure 4-4. Plot of area ratio versus percent retained transverse stiffness for 12 different void cases (one void with four aspect ratios, two voids with four aspect ratios, and three voids with four aspect ratios)

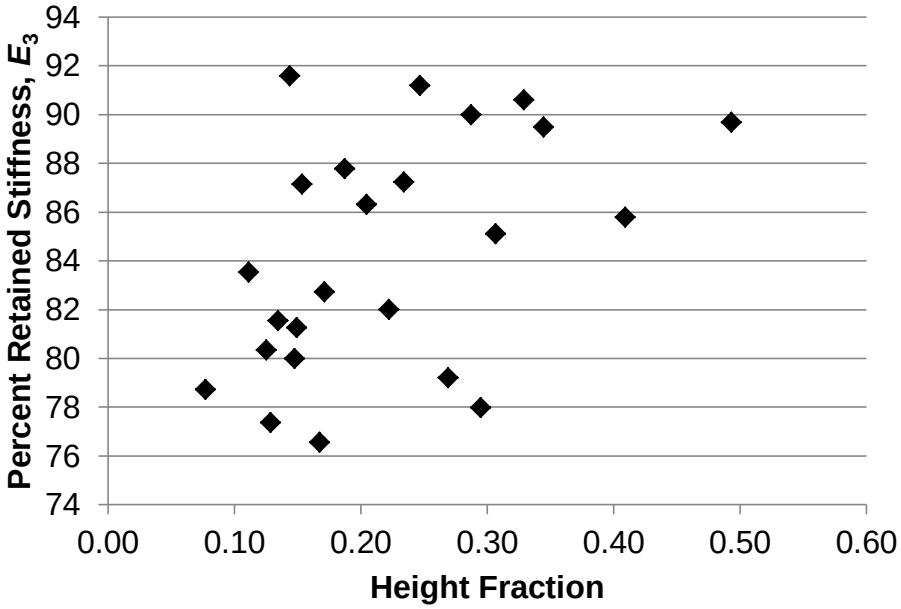

Figure 4-5. Plot of height fraction versus transverse stiffness for cases in which three different random void heights were used for several constant area fractions.

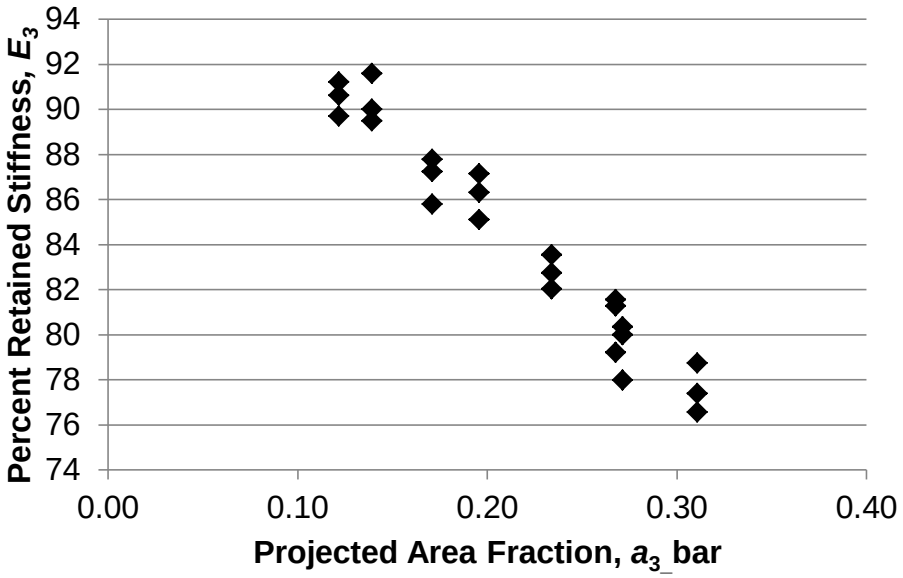

Figure 4-6. Plot of projected area versus transverse stiffness for cases in which for a given area fraction and either 1, 2, or 3 voids, three random heights are tested. One vertical set of diamonds corresponds to one area fraction and a fixed number of voids, with results due to varying the height.

Figure 4-7. 1 Void (left) being split into two overlapping voids (right). The height of the original void is equal to the combined height of the two voids.

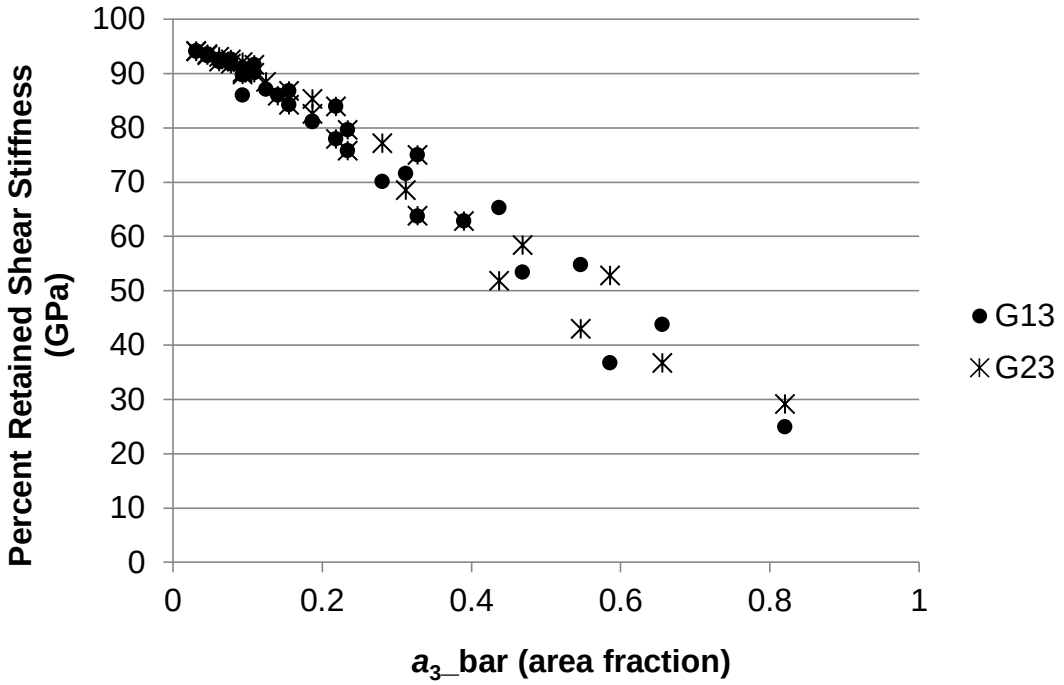

Figure 4-8. Shear stiffness versus projected area fraction. Note that the aspect ratio varies also, which is why G_{13} is not equal to G_{23} at all points.

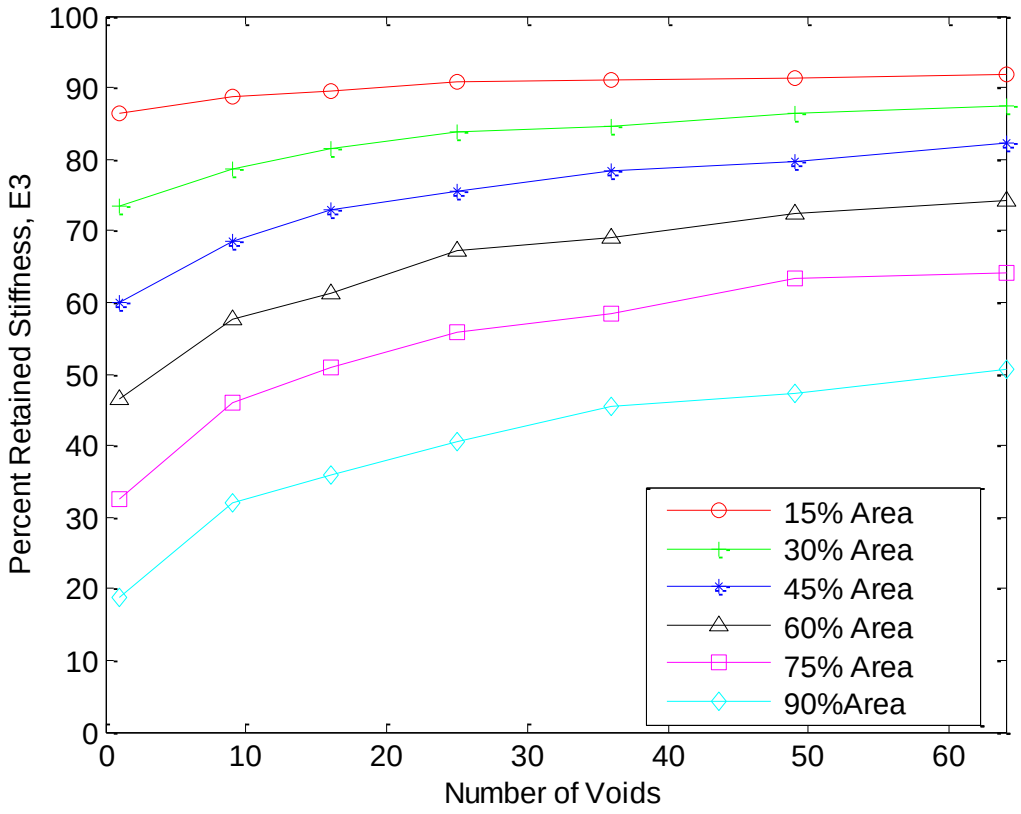

Figure 4-9. Percent stiffness in the transverse direction (E_3) for varying projected area and number of voids modeled

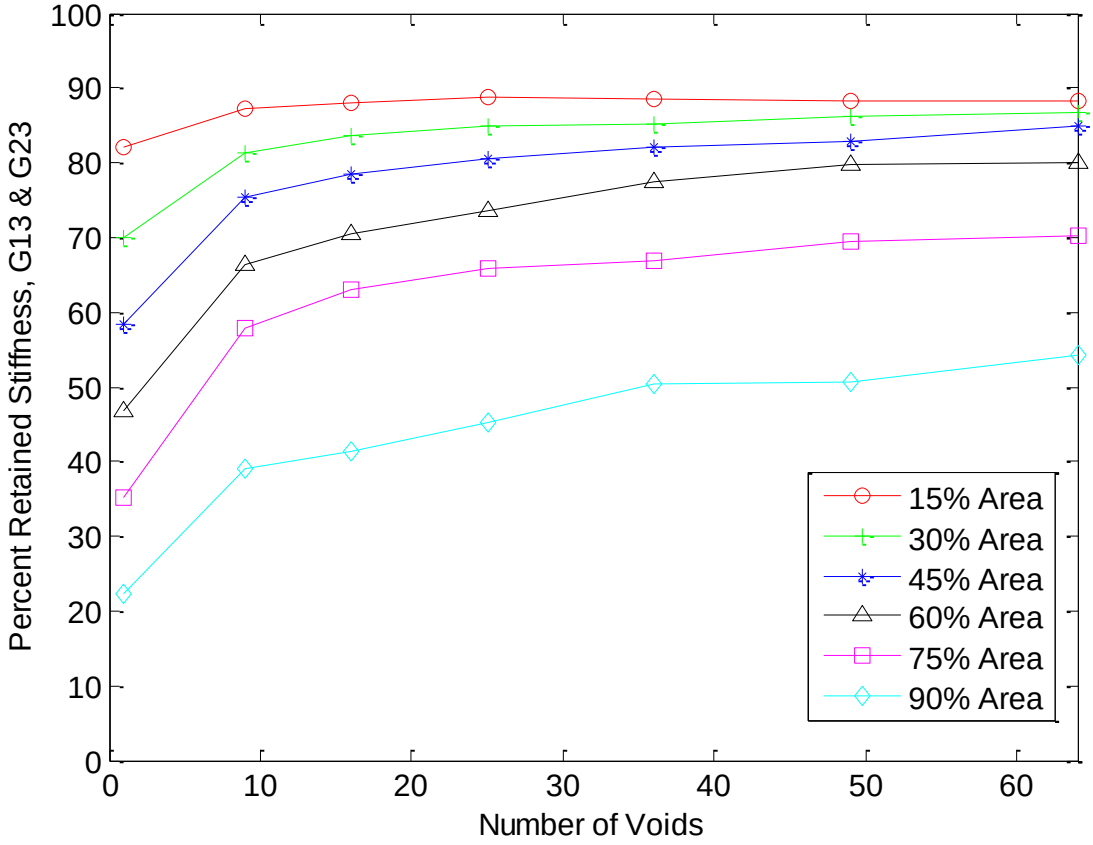

Figure 4-10. Percent transverse shear stiffness retained (G_{13} and G_{23}) for varying projected area and number of voids modeled

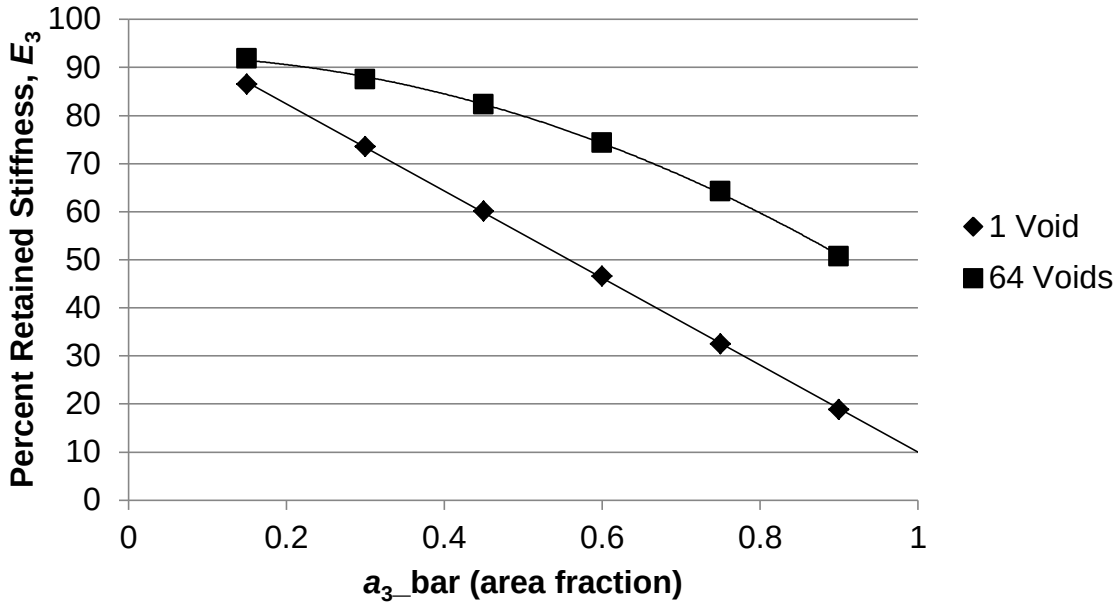

Figure 4-11. Effect of area fraction on transverse stiffness when using a different number of voids to model the same area.

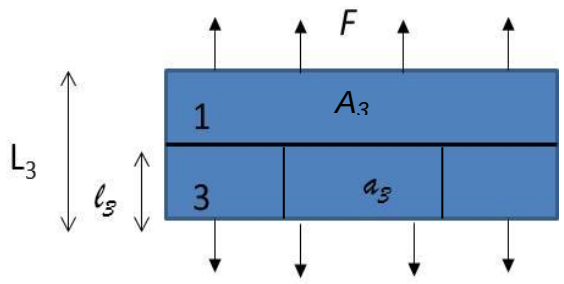

Figure 4-12. Illustration of example problem. F is a force applied to the material, A_3 is the area of the top material 1 and the bottom material 3, a_3 is the area of the void in the bottom part of the material (material 3) bounded by the black lines in the center, L_3 is the total length of the orthotropic material in the 3-direction, l_3 is the length of the void,

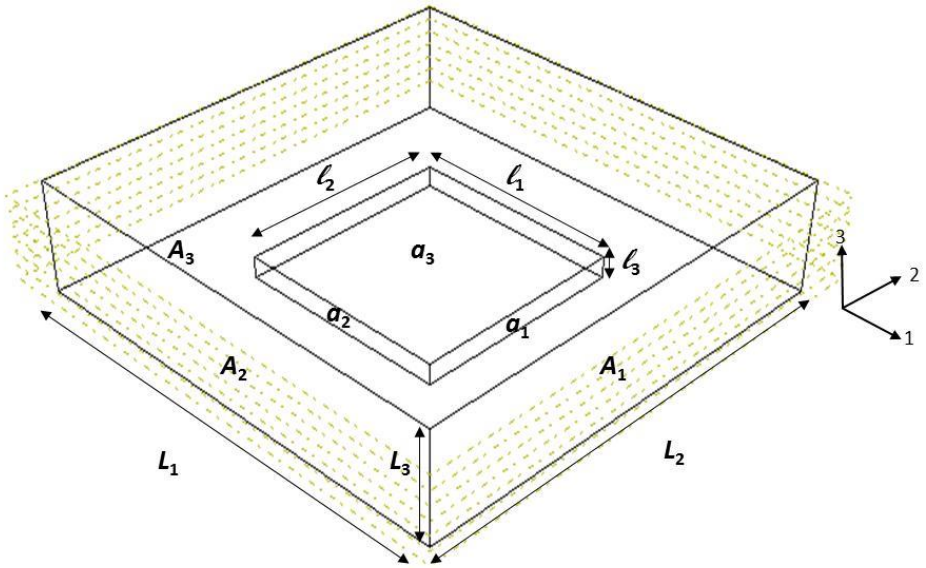

Figure 4-13. Definition of geometry for example problem

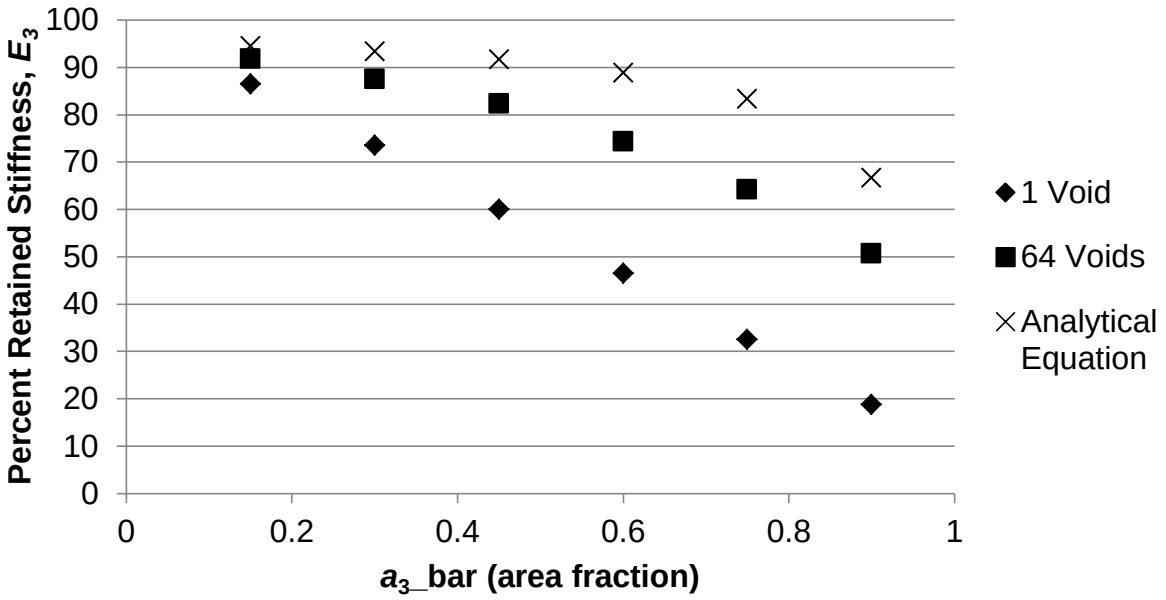

Figure 4-14. Analytical prediction of stiffness versus FEA results of stiffness modeled with 1 void and 64 voids.

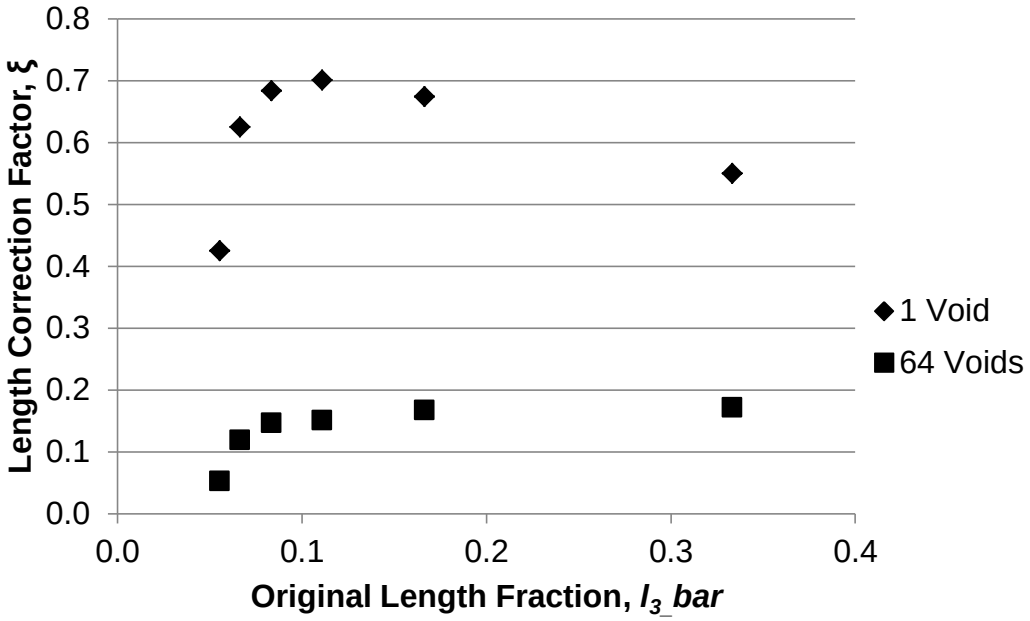

Figure 4-15. Length correction factor for the 1-void and 64-void cases

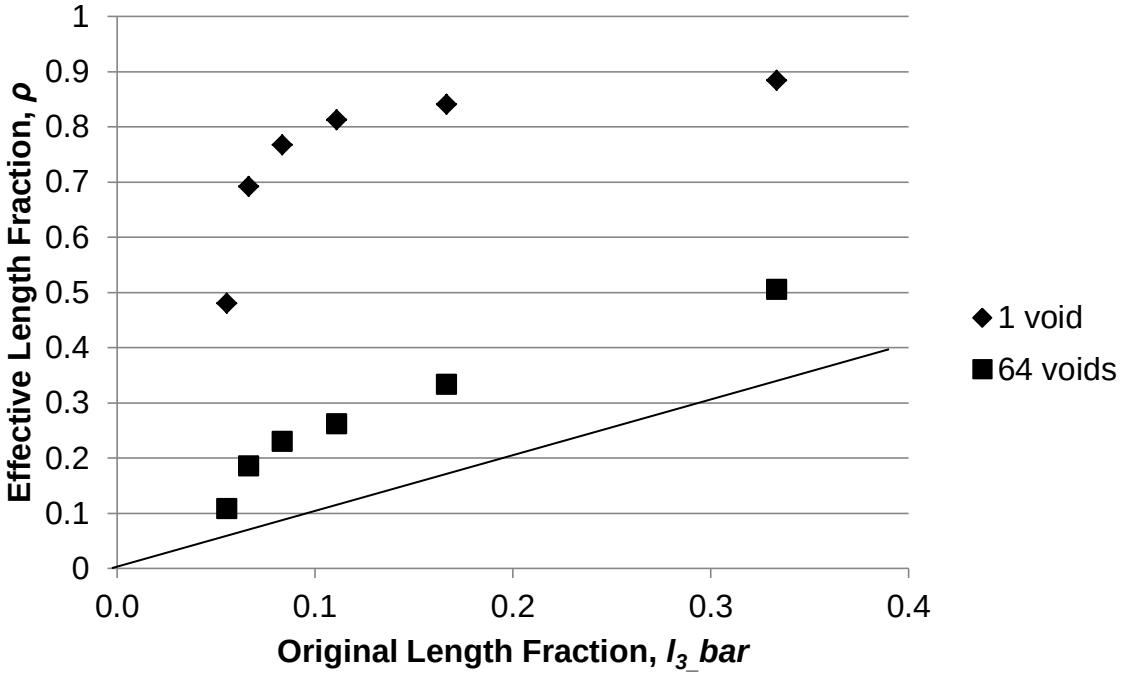

Figure 4-16. Effective length fraction for 1-void and 64-void models. The 45° line assists in illustrating the difference between the original length fraction and the corrected value.

Figure 4-17. Stress field in the transverse direction for one void. Note that the small stresses extend to the upper and lower boundaries. (Blue: low stress, Red: high stress, Green: stress in between stresses corresponding to blue and red)

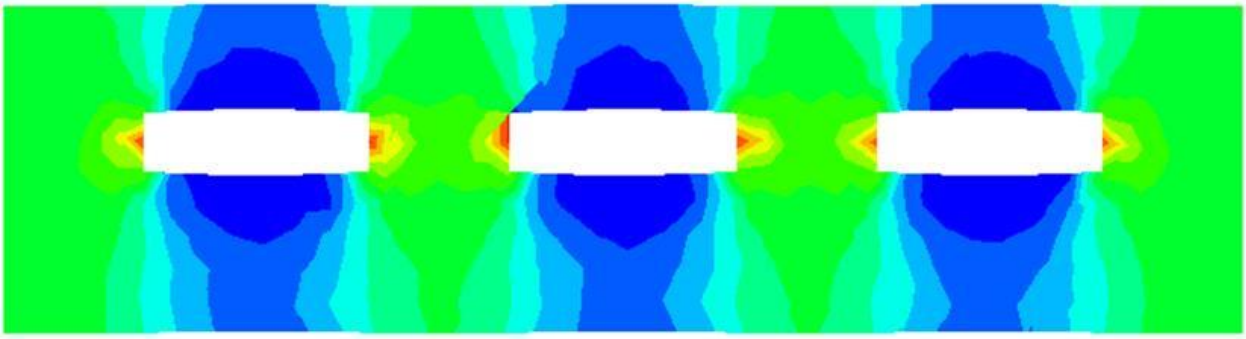

Figure 4-18. Stress field in the transverse direction for three voids. Note that the small stresses do not extend as far in the transverse direction as they do for case shown in Figure 4-17, but further than what is shown in Figure 4-19. (Blue: low stress, Red: high stress, Green: stress in between stresses corresponding to blue and red)

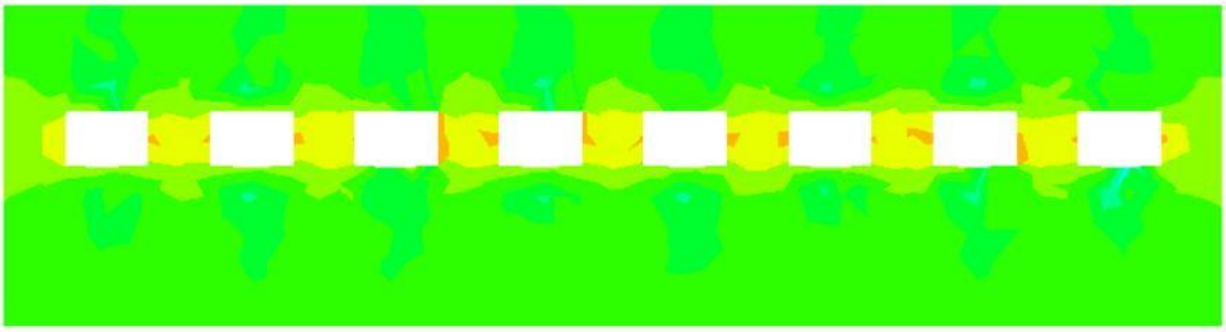

Figure 4-19. Stress field in the transverse direction for eight voids. (Blue: low stress, Red: high stress, Green: stress in between stresses corresponding to blue and red)

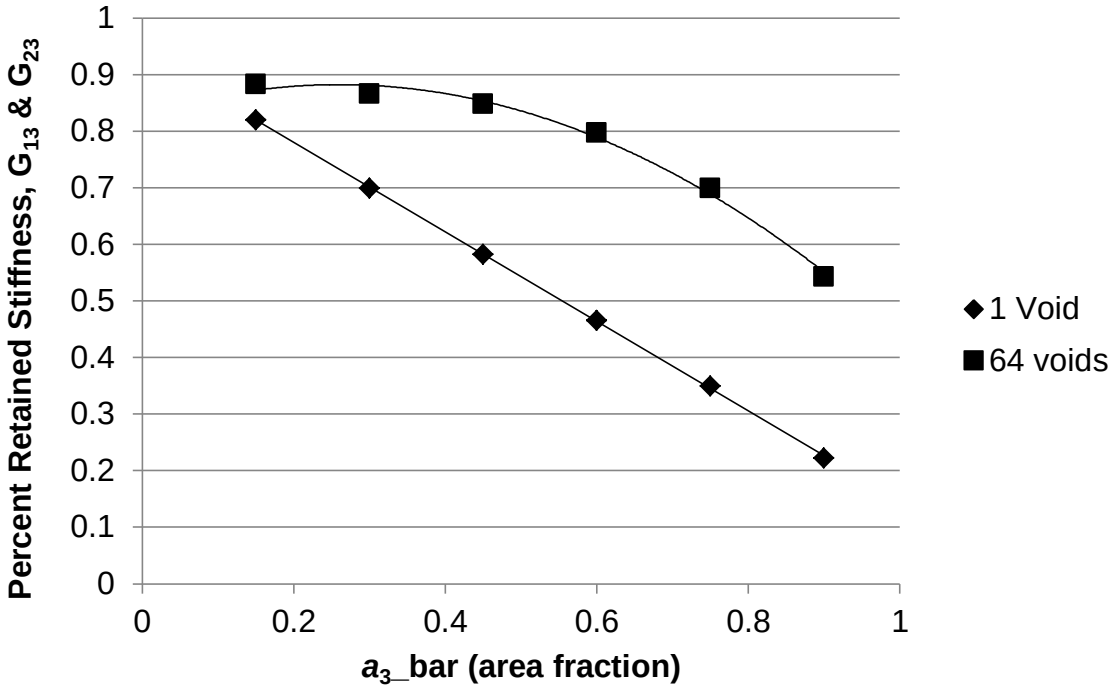

Figure 4-20. The resulting transverse shear stiffness for varying area fraction and number of voids

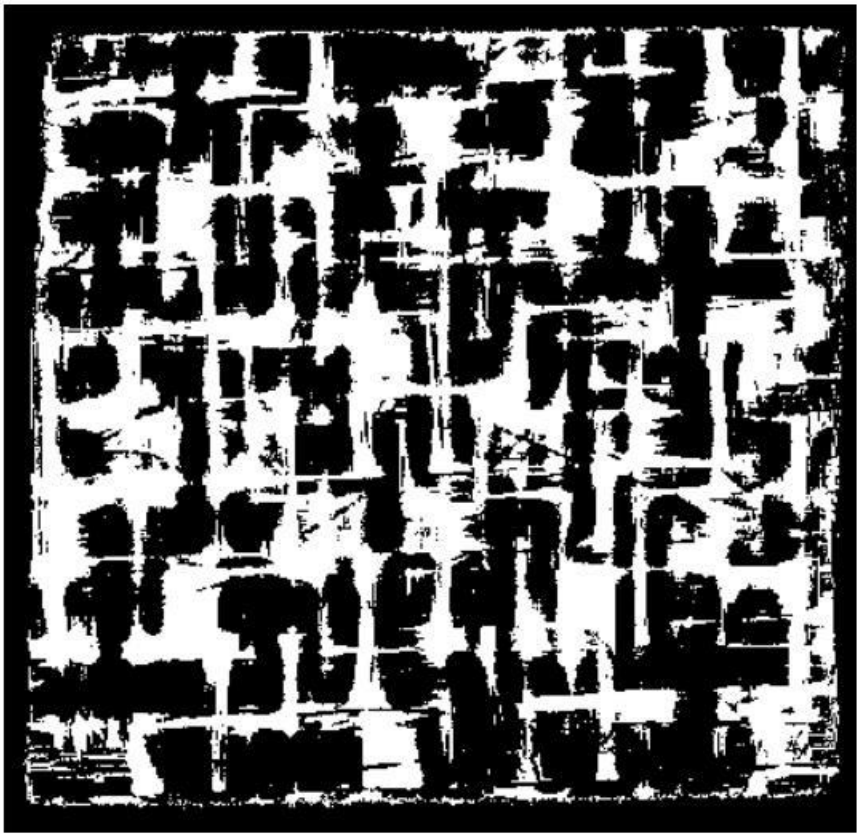

Figure 4-21. 2D projection of the voids in one 3D ply (the white represents the voids)

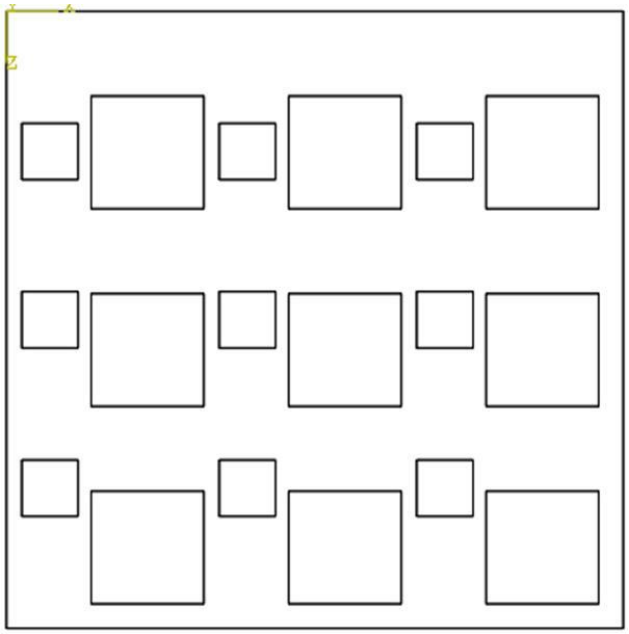

Figure 4-22. Illustration of test case to determine how to account for small voids

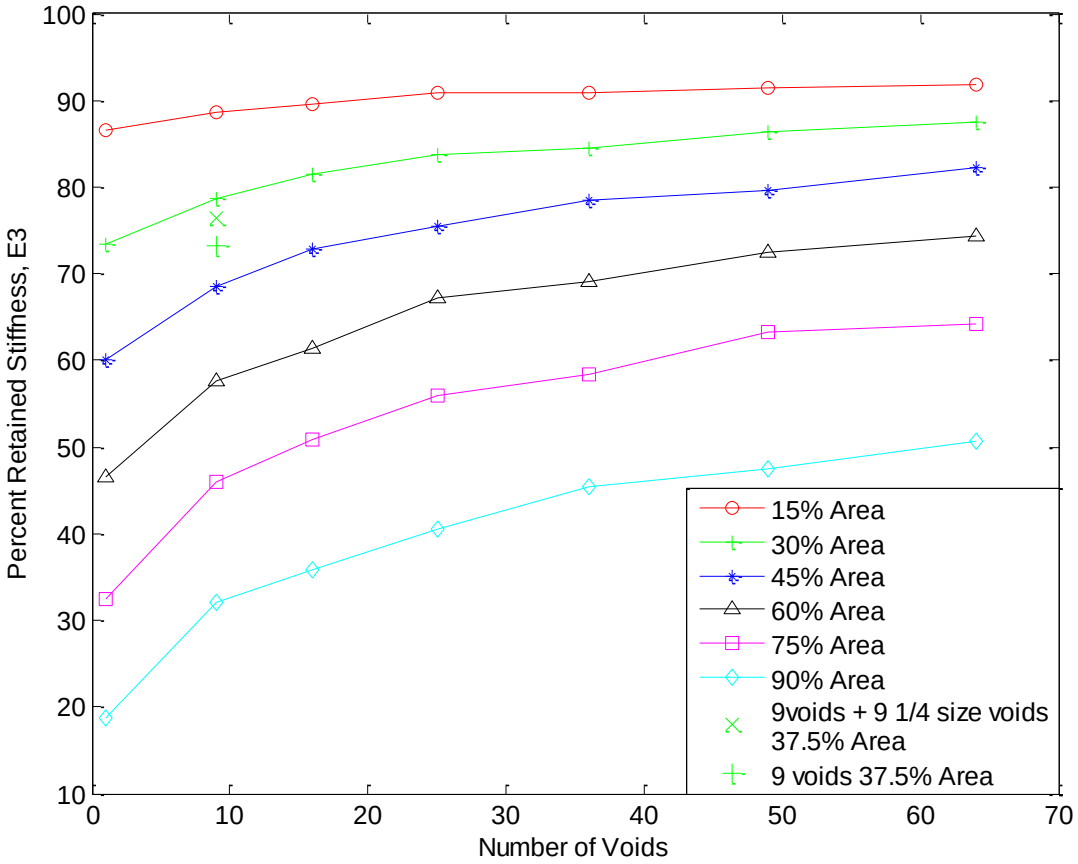

Figure 4-23. Results for cases used to determine effects of small voids

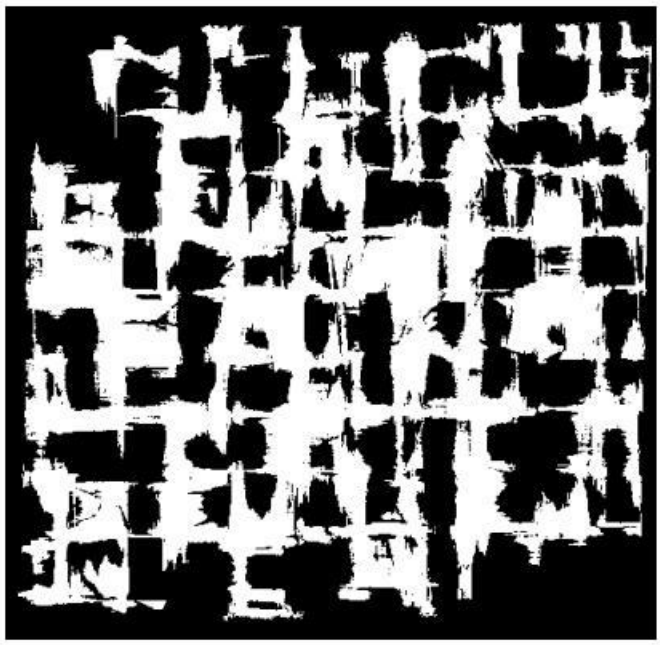

Figure 4-24. Example of a 2D void projection for the square array analysis

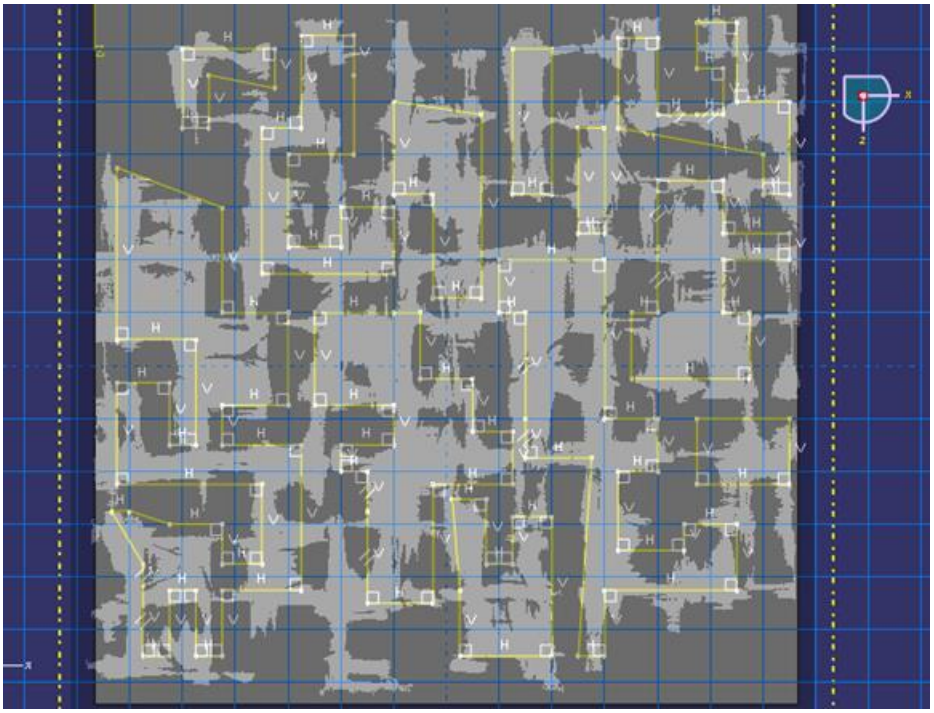

Figure 4-25. Screenshot of voids being sketched over the image of the projected voids of Figure 4-24.

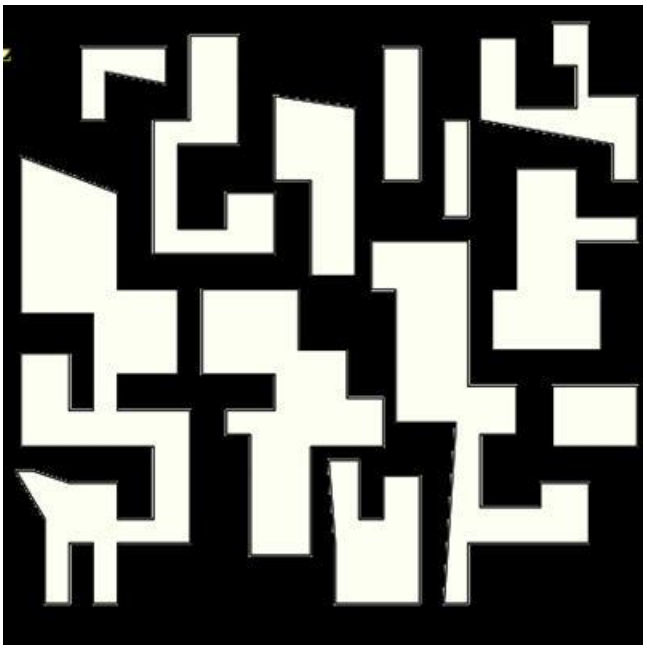

Figure 4-26. Final sketch of the voids modeled in Abaqus for finite element analysis

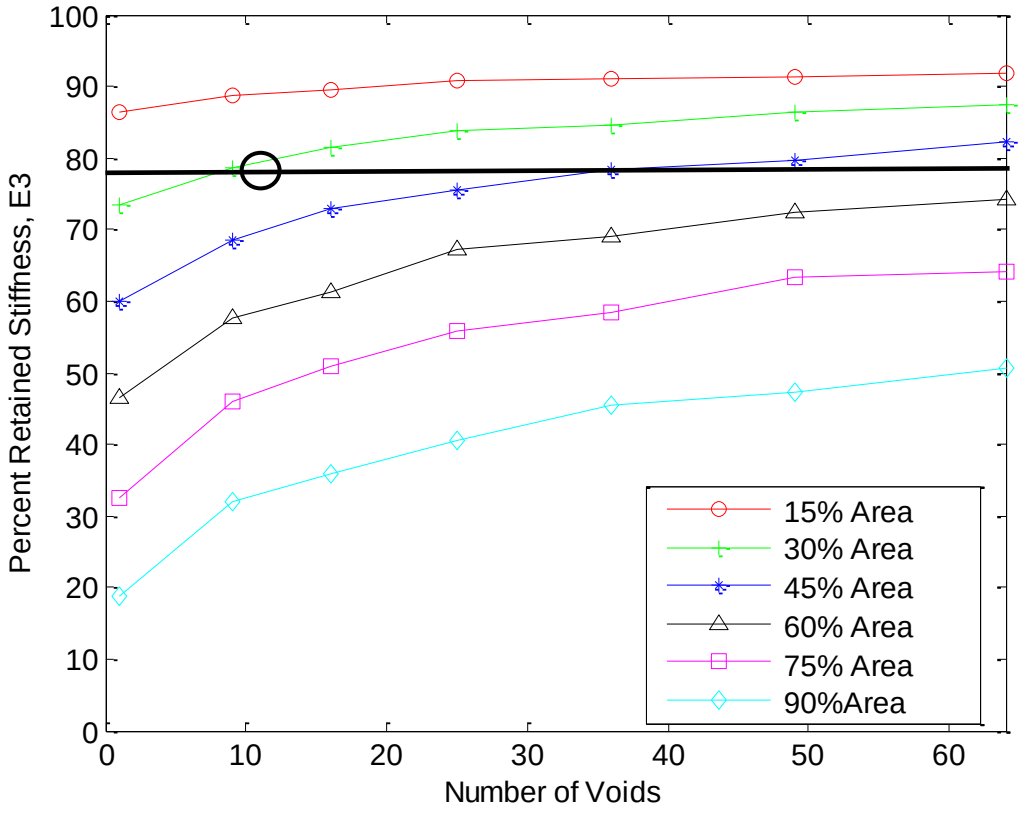

Figure 4-27. Finite element analysis result plotted with effects of void area and number of voids on the transverse stiffness with points added to show results when modeling sketched void indicated by the black circle.

Table 4-1. Loss of stiffness based on 20 void cases with a constant volume fraction of 4.0%, described in 4.2.2 and 4.2.3

	E_1	E_2	E_3	G_{12}	G_{13}	G_{23}
Average % loss of stiffness	4.7	5.0	16.0	5.1	15.9	18.3
Standard Deviation	0.5	0.5	4.1	0.7	3.1	4.4

Table 4-2. Resulting stiffness comparisons between varying aspect ratio and varying void position. s_1 and s_3 are the spacing between the voids in the 1-direction and 3-direction, labeled in Figure 4-2.

# Voids	AR	Spacing	E_3 (GPa)	Mean (GPa)	Std. Dev. (GPa)
2	3	Uniform	90.5		
2	5	Uniform	87.3		
2	8	Uniform	82.7		
2	10	Uniform	79.9	85.1	4.7
2	8	s_1 = 0.16 mm	82.6		
2	8	s_1 = 0.57 mm	82.8		
2	8	s_1 = 1 mm	82.8		
2	8	s_1 = 1.6 mm	82.8		
2	8	s_3 = max (voids in top most and bottom most layers)	82.6		
2	8	Opposite Corners	82.7	82.7	0.1

Table 4-3. Effect of aligning voids in the 3-direction, where s_3 is defined as the center to center distance between each void

# Voids	s_3 (mm)	E_3 (GPa)
1		80.7
2	0.50	79.9
2	1.25	79.7
6	0.25	79.0

Table 4-4. Idealized (fully densified matrix with no voids) material properties of 5HS SiC/SiC composite

E_1 (GPa)	E_2 (GPa)	E_3 (GPa)	G_{12} (GPa)	G_{13} (GPa)	G_{23} (GPa)	v_{12}	v_{13}	v_{23}
262.0	262.0	153.0	37.0	60.4	60.4	0.20	0.20	0.18

Table 4-5. Transverse stiffness retained as a result of different methods of modeling voids in a ply

	Simulated Voids	1 Void	3x3 array	4x4 Array
E_3	0.78	0.66	0.73	0.77

Table 4-6. Void volume fraction and void area fraction for each ply

Ply	Void Volume Fraction (%)	Void Area Fraction (%)
2	0.45	14.2
3	0.73	31.9
4	1.06	42.8
5	1.18	49.7
6	0.94	38.8
7	0.57	15.6
TOTAL	4.93%	

Table 4-7. Stiffness results from finite element analysis of sketched voids

	% Retained Stiffness
E_1	95
E_2	95
E_3	43
G_{12}	95
G_{13}	64
G_{23}	61

CHAPTER 5
IN-PLANE DAMAGE INTITIATION AND PROPAGATION

In Chapter 3 and Chapter 4, we learned that modeling the voids is important when determining the transverse stiffness. The in-plane stiffness properties were not as sensitive to changes in the architecture and were generally related to the void volume fraction. The goal of the work described in this chapter is to first asses the amount of variability in the in-plane tensile strength measured by a 0.02% yield offset (further explained in Section 5.1) for three cross sections of different architecture. Then, this amount of variability is compared to the effects of using random strength in the constituents (a more common variable to randomize). This is done with a progressive damage model so that when an element in the finite element analysis reaches its maximum allowable strength, its load-bearing capabilities gradually degrade to zero.

5.1 Definition of Failure

Engineers frequently refer to the stress-strain curve produced by experiments on a material coupon to predict when and how a component will fail. Failure may be defined differently, depending on what the engineer's design criteria are. Four common points of failure which can be defined on a stress-strain curve labeled in Figure 5-1 are the yield strength (the stress at which the stress-strain curve becomes non-linear and plastic or inelastic deformation begins), the ultimate strength (the maximum tensile stress reached in a tension test), a breaking strength (stress at which catastrophic failure occurs), and a 0.2% offset yield strength. The 0.2% offset is used as a simpler method of defining yield stress because it is not always clear at which point the stress-strain curve becomes nonlinear and it is considered to still be within a tolerable yielding range.

While these definitions of material failure are commonly used for ductile materials such as metals, similar definitions can be applied to composites which often behave in a ductile manner, despite the behavior of the individual constituents. In the case of ceramic matrix composites, the individual constituents fail in a brittle manner, but due to fiber reinforcements, the global behavior will mimic a ductile response. For this work, the composite strength in a uniaxial displacement-controlled simulation is found by using the yield offset method with a yield offset of 0.02%. A smaller (or larger) strain offset can be used, but similar results will be obtained when comparing strengths relative to one another. As previously mentioned, a 0.2% offset is used for ductile materials. Brittle materials, even in the woven ceramic matrix composite form do not yield this much. Using a 0.02% offset allows for the same concept of the 0.2% offset to be used, but still be meaningful for a ceramic matrix composite. The composite can still sustain substantial loads after this point, but the failure requires inclusion of damage mechanisms beyond the scope of this work, like environmental effects.

5.2 Details of Finite Element Model and Progressive Damage

It was desired to find a readily available material model which could be used, along with appropriate assumptions, to evaluate the importance of modeling the varying architecture and the varying strength of the constituents. There are several types of damage initiation and evolution models in commercial FE software, e.g. Abaqus [54]. The majority of them are applicable to metals in which the post-peak softening behavior is ductile rather than brittle. However, there are a few models which allow the simulation of brittle behavior. One of them is the Brittle Cracking Model for Concrete which uses Rankine (maximum stress) failure criteria and degradation of material properties using concepts derived from fracture mechanics which determines the post-peak softening

behavior based on the energy required to open a crack [55]. The model was initially developed for concrete, but is applicable to some other brittle materials as well.

Since we are only interested in the yield strength, and not the ultimate tensile strength, failure and damage in the longitudinal tows are not modeled. Several researchers have shown experimentally that in the region of the stress-strain curve that lead up to yield strength, damage occurs predominantly in the inter-tow matrix and in the matrix of the tows. Lamon [63] outlines the failure process in a plain woven CMC as follows. First, cracks initiate at inter-tow pores (macropores) at strains between 0.025% and 0.12%. Then cracks begin to form in the transverse tows between strains of 0.12% and 0.2%. Lastly, cracks are seen in the longitudinal tows for strains larger than 0.2%. The strains at which these failure modes occur in the 5HS SiC/SiC composite are different, due to the different weave and manufacturing process, but the general evolution of damage is the same. This is validated by the work of Morscher [64] in which damage was detected using acoustic emission (AE) techniques on a 5HS CVI SiC/SiC composite, almost identical to the one currently being studied. The first AE event occurred at small strains (less than 0.05%) and corresponded to formation of microcracks. The large AE event was related to large matrix cracking and crack bridging through the tows which occurred around a strain of 0.05%. These experimental observations indicate that if the yield strength is the strength of interest, modeling damage in matrix and transverse tows is sufficient.

5.2.1 Material Properties

5.2.1.1 Stiffness and deterministic strength

The Young's moduli, shear moduli, and Poisson's ratios of the matrix and longitudinal tows are the same that were prescribed for the stiffness analysis in Table 3-

5. However, the Brittle Cracking Model in Abaqus can only be used for isotropic materials. Since the transverse tow properties are transversely isotropic, and they are only being loaded in the transverse direction, the tows can be prescribed as an isotropic material with properties that are equivalent to those of the transverse direction (E = 106 GPa, v = 0.21).

Strength properties of the constituents are less straight-forward and are not widely found in the literature. However, the goal of the work is to determine which characteristics of the model need to be varied in order to capture variability. Therefore, determining reasonable properties based on experience and pertinent assumptions with the aid of limited experimental data is appropriate. Note that discussion of stochastic strength properties follows this discussion. The first assumption made is that the transverse tows fail because of matrix cracks. The fibers do not carry any significant load in the transverse tows when the load is in the longitudinal direction. Therefore, the strength of the tows can be found similarly to the matrix. Then, Morscher observed that in a 5HS CVI SiC/SiC composite, the large acoustic emission occurred at 0.05% strain [64]. At this time, there were significant cracks in the matrix and transverse tows. We can then make the assumption that if the local strain is approximately equal to the global strain, than the matrix may fail at a strain of approximate 0.05% also. We know that the local strain everywhere is not equivalent to the global strain, but it is not an unreasonable approximation. Figure 5-2 is a composite model at a global strain of 0.05%. The area marked in red corresponds to local strains of 0.04% to 0.06%. The blue elements (lower strains) and grey elements (higher strains) are the only ones

outside of this range. Therefore, to assume that the global failure strain can be related to the local strain is not unreasonable. Then we can use the relationship

$$\sigma_f = \varepsilon_f E = 0.0005E$$

to determine that the failure stress of the matrix is 252 MPa and the failure stress of the transverse tows is 53 MPa. The transverse tow strength may intuitively seem low. However, if one compares the value to that of the matrix strength, and considers that the fibers could have a weakening effect in the transverse direction, the value is not unreasonable. There are no experimental results to verify the strength, but work by Evans and Zok [65] also indicate that the result is reasonable. Evans and Zok cite a transverse tow strength of 10 MPa for another CMC, SiC/CAS (calcium aluminosilicate) [65]. A summary of the stiffness, strength, and fracture energy properties discussed here and continued below are found in Table 5-1.

5.2.1.2 Stochastic strength of the transverse tows and matrix

Ceramic failure is especially stochastic due to its sensitivity to flaws in the material. The strength of a ceramic is generally described by a two parameter Weibull distribution. The parameters are the scale parameter λ, and the shape parameter (frequently referred to as the Weibull modulus) m. These parameters can be used to determine the mean and standard deviation of the distributions using the equations

$$\mu = \lambda\Gamma(1+\frac{1}{m}) \tag{5.1}$$

$$\sigma = \sqrt{\lambda^2\Gamma(1+\frac{2}{m}) - \mu^2} \tag{5.2}$$

where Γ is the gamma function. Estimations of the Weibull parameters for the inter-tow matrix and transverse tow matrix were made by Lamon et.al. [66], using finite element

analysis that included probabilistic information about the constituents. The scale parameter and shape parameter for the matrix were found to be 291 MPa and 4.9, respectively. The scale parameter and shape parameter for the transverse tow matrix were 120 MPa and 4.9, respectively. The scale parameter has a large influence on the calculated mean (mean found as a result of the distribution), whereas the shape parameter has a large influence on the calculated standard deviation or amount of variability. The purpose of using Lamon's estimates is to obtain an approximation for the variability of the composite's constituents. The mean strength has already been decided by previous deductions described in the previous section (Section 5.2.1.1). Therefore, the shape parameter *m* from the work cited (*m* = 4.9) will be used in combination with our previously determined mean strength. Using Equation 5.1 and Equation 5.2, the corresponding scale parameter of the Weibull distribution, and standard deviation can be determined. A summary of the Weibull parameters, mean, and standard deviation is given in Table 5-2. In addition, a plot of the cumulative distribution function and probability distribution function are given in Figure 5-3 and Figure 5-4 to provide a visual representation of the variability in strength.

5.2.1.3 Damage evolution and fracture energy

This section will explain the physics of the damage evolution after an element reaches its maximum allowable stress and explain how the fracture energy of the constituents was selected. The Brittle Cracking Model for Concrete available in Abaqus combines finite element analysis with fracture mechanics concepts [54,55]. Abaqus uses a smeared crack approach which means that cracks are not explicitly modeled, but their effects enter the calculations by the way cracks affect the stress of the element. The crack is formed perpendicular to the direction of the maximum principal stress.

Hillerborg's model is illustrated in Figure 5-5 and described as follows. The crack propagates when the principal stress at the crack tip is equal to the failure stress of the constituent (σ_f) that was discussed in Section 5.2.1.1. The stress in the element then begins to decrease with increasing crack opening u_c, as illustrated in Figure 5-6. When $u = u_u$, the stress is zero and the element can no longer carry any load. The area under the stress-displacement curve corresponds to a microcrack zone where there is stress to be overcome by opening the crack. The energy required to open the crack, or fracture energy, can then be used to describe how the stress changes with crack opening displacement, after the failure stress has been reached. The fracture energy can be written as

$$G = \int_0^{u_u} \sigma du \tag{5.3}$$

The shape of the stress-displacement curve is not limited to that of Figure 5-6. A curve generated experimentally can be used, or a different assumed post-peak softening behavior, depending on what is appropriate for the application. Since ideally a brittle material will fail rapidly (almost no deformation after the maximum stress is reached), a simple linear degradation is appropriate and Equation 5.3 can be simplified to

$$G = \frac{1}{2}\sigma_f u_u \tag{5.4}$$

In addition to minimal experimental data being available for strength values, information about the fracture energy is not readily available either. Given the relationship of fracture energy to fracture toughness for plane stress and knowing that the typical fracture toughness for SiC is between 3-5 $\mathrm{MPa}\sqrt{\mathrm{m}}$ [67] we can estimate the fracture energy to be approximately

$$G = \frac{K_I^2}{E} = \frac{\left(3\times10^6\right)^2}{420\times10^9} = 21\frac{\text{J}}{\text{m}^2} \tag{5.5}$$

Fracture energy values of 15-25 J/m^2 have been cited by NIST (National Institute of Standards and Technology) for SiC, so the above approximation falls within a reasonable range [68]. The properties cited above are related to a SiC matrix. Similar properties were not available for the tows. Since the transverse tows fail due to matrix damage, the same fracture energy was assumed for the tows. Due to the failure stress of the tows being lower than that of the matrix, the slope of the post-peak softening behavior will be shallower, implying a larger displacement or strain to failure. However, the strain to failure is still small.

5.2.2 Loads and Boundary Conditions

The analysis being considered in this study is a uniaxial displacement-controlled tensile test in the longitudinal direction. The boundary conditions are illustrated in Figure 5-7. The right side of the composite (perpendicular to the loading direction) is prescribed a displacement. The left side is on rollers, free to move in the 3-direction, but remains straight with respect to the 1-direction. The boundary conditions on the edges parallel to the loading direction are free. The model then simulates a repeating RVE (representative volume element) in the loading direction.

The displacement increments were not uniform for the entire analysis because of the computational expense. Instead, the first three steps (steps in which damage typically does not begin), and last five (steps that occur after onset of non-linearity) were in increments of 0.5 μm and 0.75 μm, respectively. The 23 steps in between were incremented by 0.15 μm. The final total strain of the composite was approximately 1%. Beyond this strain it becomes important to model damage in the longitudinal tows.

Additionally, it is likely that environmental effects would start to play a major role as cracks have typically formed on the matrix surface.

5.2.3 Elements

The elements used for the strength analysis are a mix of 4-node plane stress quadrilateral elements and 3-node plane stress triangular elements. The plane stress elements allow the uniaxial tensile test to be simulated (no stress in the 2-direction). However, it does imply that the material is thin. The specimen has 3D geometrical variation, and the geometry in the 2-direction is not accounted for by using plane stress elements. However, since the goal is to determine relative effects of varying architecture and varying constituent strength, the 2D approximation allows us to make general observations in a relatively small amount of time. A more complete understanding of the effects of architecture should be obtained by using 3D models in future work.

5.3 Description of Damage Analysis Cases and Results

5.3.1 Effects of Varying Architecture on Strength

The first goal was to assess the impact of varying architecture on the strength of three different cross sections of the 5HS CVI SiC/SiC composite. The cross sections are taken from micrographs of the composite that were described in Chapter 3. The micrographs can be found in Figure A-1. The stress-strain curve based on the finite element results is shown in Figure 5-8 along with an experimental result on a similar, but slightly different material (different ends per inch used in manufacturing and different fiber volume fraction) from Morscher et.al. [64]. Therefore the stiffness is higher, but the failure characteristics are the same in terms of when damage is observed, and the region in which the stress-strain relationship becomes nonlinear is also the same. Damage initiates in areas of high stress concentration in the matrix (near the voids, and

between the tows on the surface, shown in Figure 5-9, and labeled as Point 1 in Figure 5-8). This point would likely correlate to the first acoustic emissions (AE) event discussed by Morscher, which was an AE event that signaled some degree of damage, but occurred before an onset of non-linearity in the stress-strain curve [64]. The onset of non-linearity in the stress strain curve begins around a strain of approximately 0.04%. At this point, damage has initiated in much of the matrix and the tows, shown in Figure 5-10 and labeled as Point 2 in Figure 5-8. Then, at the 0.02% offset, a significant amount of damage has occurred and many elements have completely failed, shown in Figure 5-11 and labeled in Figure 5-8 with the 0.02% offset line. Note that the longitudinal tows will always appear undamaged since damage is not being modeled in those elements. The observations made regarding when and where failure occurred was similar to those found by Mital et.al. [69]. They also observed failure initiating near tows and voids. However, they did not observe variability in the strength. This is likely because progressive failure was not considered and instead the behavior after failure was perfectly plastic. As the constituents fail, the load-bearing capabilities decrease, and this plays an important role in the strength of the composite.

Using a 0.02% yield offset method as discussed previously, the variability in strength between the three cross sections is approximately 20 MPA or 17%. The variability in stiffness was approximately 5%. Damage is more dependent on local phenomena and areas of high stress concentrations can decrease the strength significantly, especially when the elements lose load-bearing capabilities; whereas the stiffness involves averaging the stresses which effectively smears the effects of local phenomena. It is not clear exactly what aspects of the architecture cause the variability

in strength. For all cases, damage initiates near voids and in between tows that are close together on the surface.

5.3.2 Effects of Varying Constituent Strength on Composite Strength

After varying the architecture, a varying constituent strength was applied. The strengths were chosen based on the Weibull distributions discussed in Section 5.2. Computational limitations prevented each element from having a unique strength. Instead, each strength was assigned to 75 elements (with 7500 elements, this would imply 100 different strengths applied to groups of 75 elements). The elements in the group of 75 were distributed randomly so that 75 elements of the same strength were not bordering each other. Three different sets of strengths were tested (distribution of strengths drawn three separate times).

When generating random strengths, the mean of the distribution can vary (it will not always be 252 MPa for example). In order to ensure that variability in the mean strength of the distributions did not contribute to strength of the composite, the mean strength of the constituents did not exceed ±3% of the intended mean strength (252 MPa for the matrix and 53 MPa for the transverse tows). Two additional deterministic analyses with the strength of the matrix increased by one standard deviation and decreased by one standard deviation were completed in order to determine how much of the variability in strength found was due to the change in the mean or actually due to the variable strength. A 23% change in the deterministic strength resulted in a 9% change in 0.02% offset strength. The change in offset strength due to the mean is found by linear interpolation. Table 5-3 summarizes the expected change in strength due to the different mean strength of the distribution, compared to the actual change in strength.

For each of the three varying strength distributions in the three architectural models, there was almost no variability in the offset yield strength (less than 0.5%). The results are plotted in Figure 5-12, Figure 5-13, and Figure 5-14. With the exception of cross section number 3, the yield strength did not change with respect to using a deterministic strength either. As indicated by Table 5-3, cross section 3 is the only cross section that indicated variability in strength due to the variable distribution (the expected change in strength due to the mean is smaller than the change in strength found). In all of the models there are areas of high stress concentration due to the voids. Failure begins near these points, and eventually occurs, at least to some degree, in most other areas of the composite. The initiation of damage may happen at a lower global strain due to an area of lower strength, but when the strain becomes large enough, a significant amount of failure is going to occur everywhere. It is not yet clear what causes cross section 3 to have a variation in strength. The variation is low (4%), but it is still higher than the other models. One hypothesis is that aspects of the architecture lead to more areas with large stress risers and this may increase the chance that weak elements and high stress concentrations will occur together as compared to the case in which the strength is deterministic. However, it is difficult to discern precisely which aspects of the architecture yield higher stress concentrations. Generally it appears that damage occurs near voids, and when tows are close together on the surface. Since it is difficult to visualize the concept close to the yield offset, it is illustrated at a smaller strain. Figure 5-15 shows cross section 1 with a deterministic strength and the randomly distributed strength. The areas in which damage initially evolves in the deterministic model are very similar to those in the randomly distributed strength model, with the

exception of 2 spots highlighted in red. In cross section 3, the areas in which damage evolves are more numerous than at the equivalent strain in the deterministic model shown in Figure 5-16. The areas circled in red highlight areas in which elements have completely failed (or come very close to doing so) in the random model, but not the deterministic model.

Instead of the strengths being completely randomly distributed, it is also possible that the local strength manifests in clusters. There is no data to show whether this is the case or not, but if it does create some additional changes in the damage, it may be worth investigating. In order to test the effects of clusters, two models were used. The first one had 10 clusters of matrix strengths, and the variability in tows was the same as that applied in the initial models previously described. The second one had 10 clusters of tow strengths, with randomly varying matrix strength. The clusters were chosen such that they were layered through the thickness, numbered with cluster 1 at the bottom and cluster 10 at the top. Cluster 1 and cluster 5 of the matrix are highlighted in Figure 5-17. The strength of each cluster can be found in Table 5-4.

When the tows were clustered, the yield offset strength still did not change. However, when the matrix was clustered, the strength increased by approximately 4%. This is not large, but it is worth investigating why this may occur. If we observe the regions that have failed between the deterministic model, and the matrix clustered model, we see that for the same applied displacement, damage did not initiate in at least two major spots. In the deterministic model at the top of Figure 5-18, we see that damage occurred near a void at the top and bottom of the composite, and we can see approximately where a crack would occur through the thickness. In the clustered model

shown at the bottom of Figure 5-18, damage does not occur at the same time, or to the same degree. If we look at the strength of the matrix in those two regions in Table 5-4 (Cluster 2 and Cluster 9), we see that the strength is much higher than the deterministic strength of 252 MPa. If in this clustered model the points near the voids were especially weak, we can imagine that the amount of damage through the thickness would increase, resulting in a lower strength. The tows are not as sensitive to the local strength, likely because the failure of them is less dependent on the stress concentrations cause by the voids.

5.4 Conclusions

From these studies, a few valuable conclusions can be drawn. First, the variability in architecture causes a significant amount of variability in strength, especially as compared to the stiffness. Strength is more dependent on local effects than stiffness is, and the voids in the architecture can cause high local stress concentrations. It is not clear what causes the variation in strength between the three architectural models, but should be a topic of future study. What is clear is that variation in the architecture is important to consider.

When the strength is varied randomly, there is not a large effect when using the 0.02% offset yield strength. However, when the local strength is grouped into large clusters, more variability in the strength can occur. If there is a region of high stress concentration, met with a large region of relatively strong elements, the composite's strength will be larger than if that area had relatively weak elements. In summary, aspects of the architecture determine how impactful the given local strength will be on the final results. While the architecture causes a larger amount of variability than

random constituent strength, the architecture and local constituent strength play a synergistic role in determining the strength of the composite.

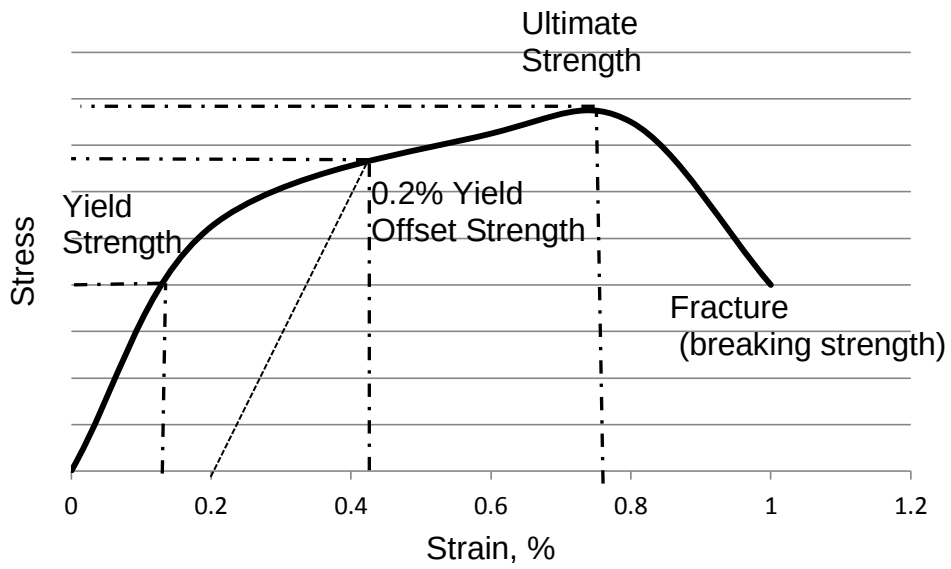

Figure 5-1. Typical measures of strength illustrated on a stress-strain curve

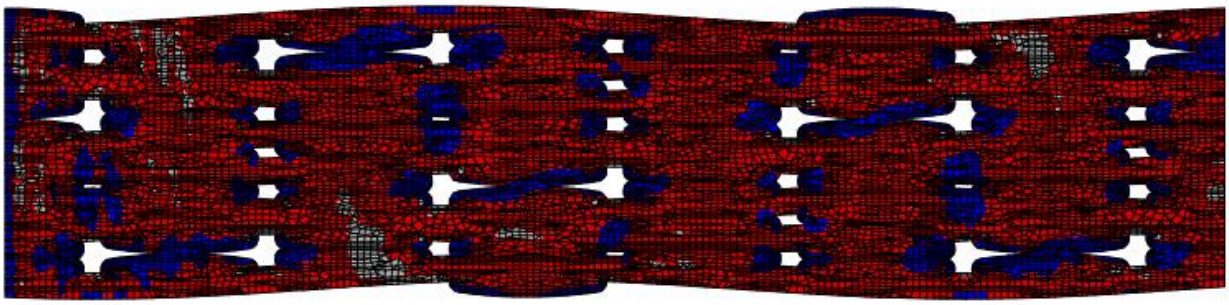

Figure 5-2. Finite element model at a global longitudinal strain of 0.05%. The red elements have a strain of 0.05 ±0.01%, while they blue elements and grey elements lie below and above this range, respectively.

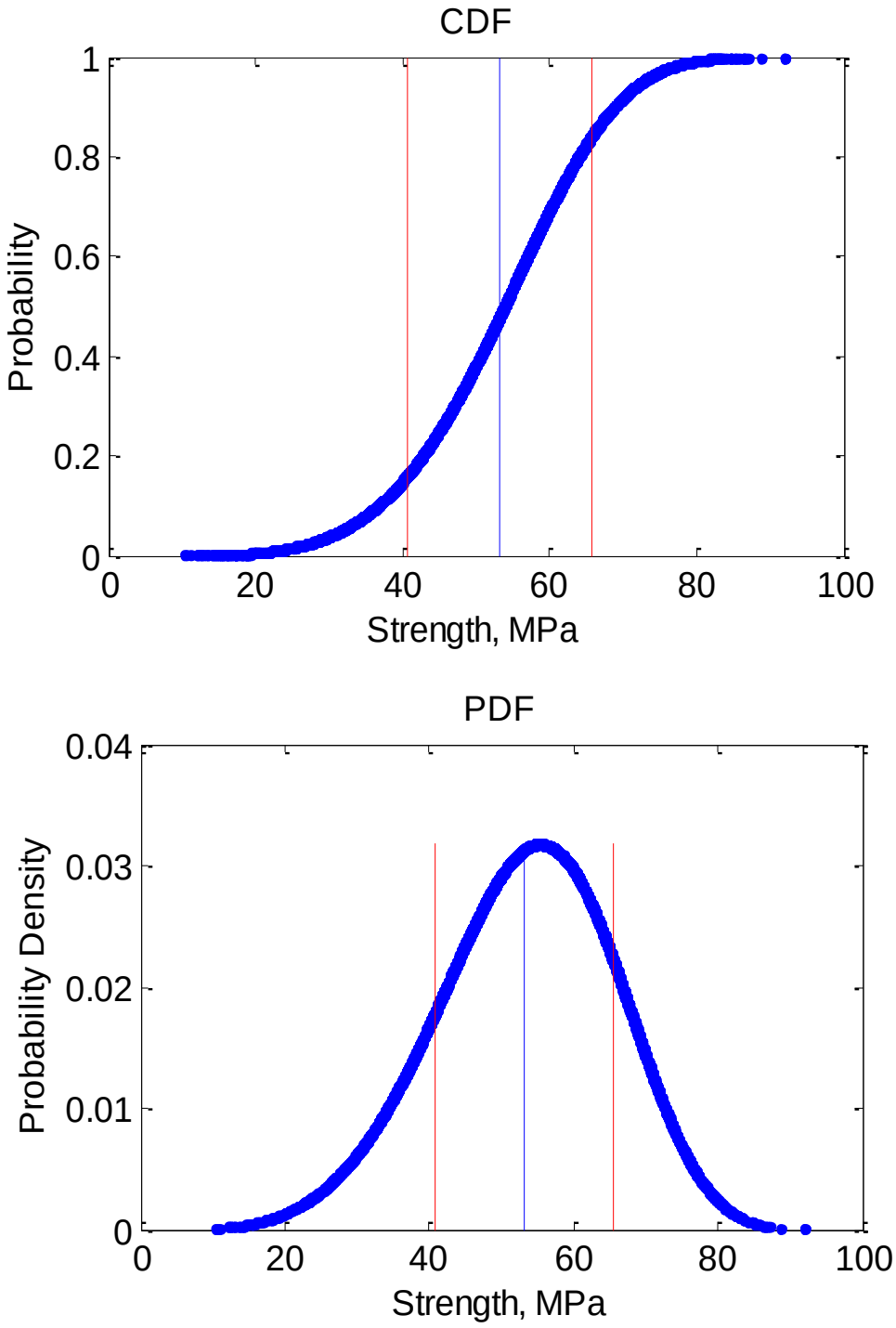

Figure 5-3. Cumulative distribution function and probability distribution function plots of the Weibull distribution of transverse tow strength. The straight blue line and 2 red lines mark the mean and one standard deviation from the mean, respectively.

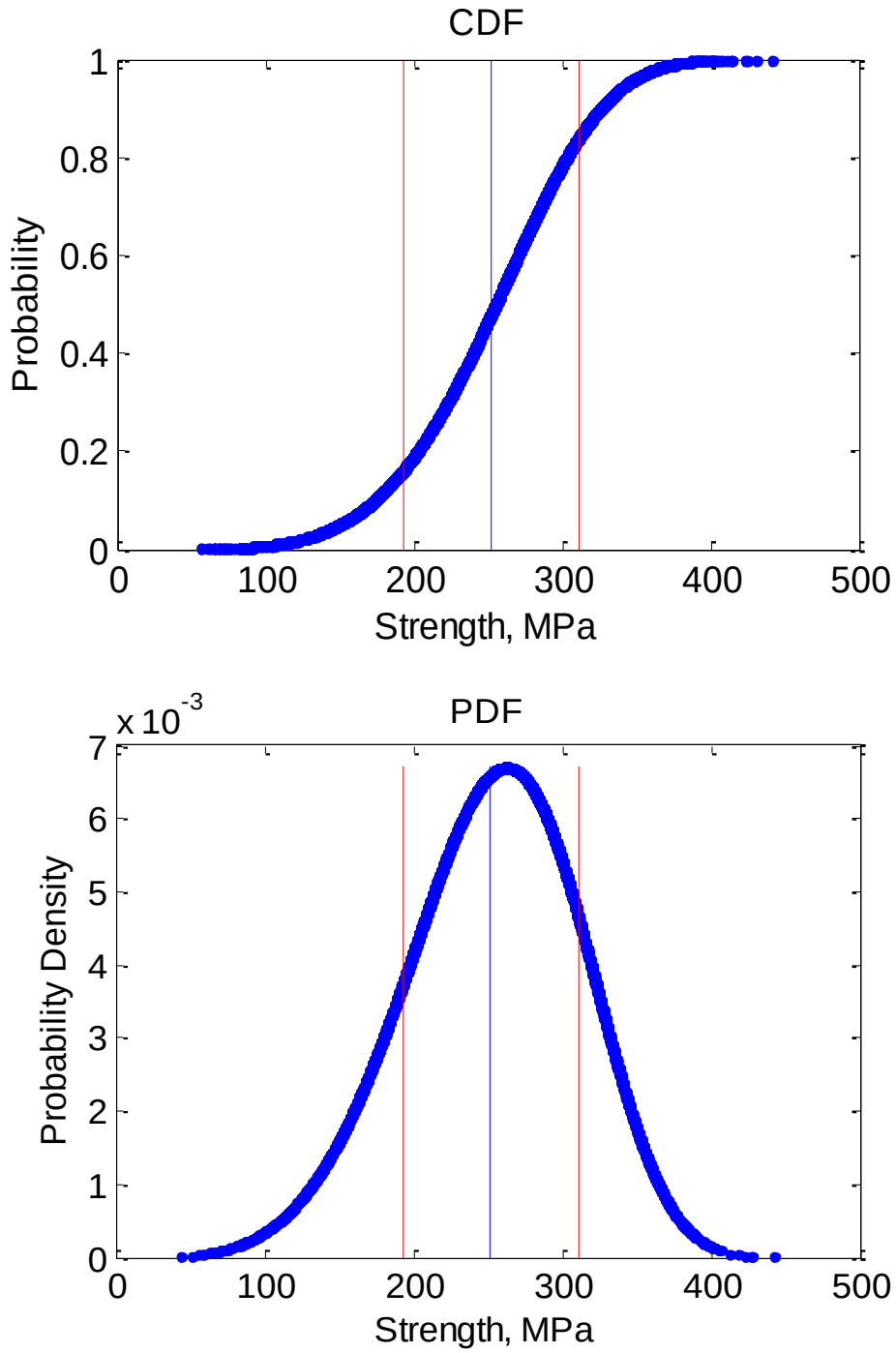

Figure 5-4. Cumulative distribution function and probability distribution function plots of the Weibull distribution matrix strength. The straight blue line and 2 red lines mark the mean and one standard deviation from the mean, respectively.

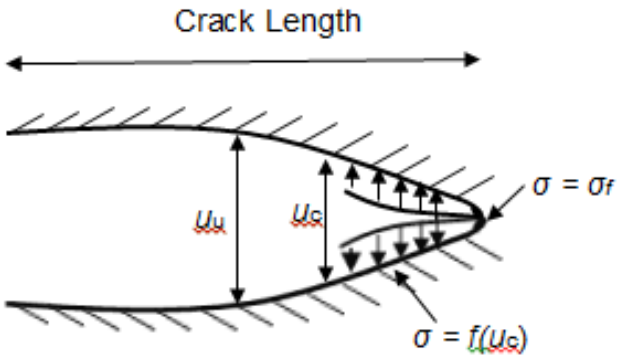

Figure 5-5. Illustration of variables used to describe damage evolution. σ_f is the maximum allowable stress, u_c is the crack opening displacement, and u_u is the crack opening displacement at failure.

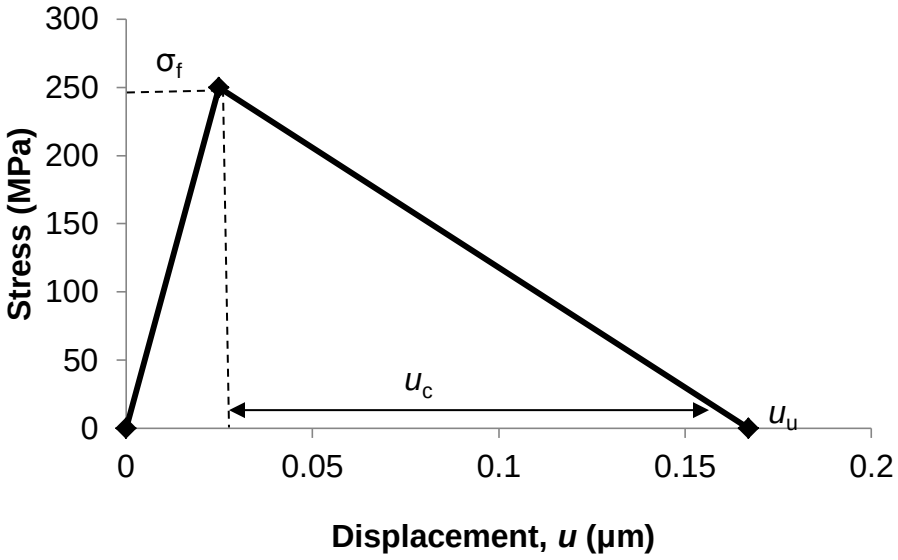

Figure 5-6. Sample stress-displacement curve illustrating the variables used to describe the damage evolution. Note that the area under the curve is the fracture energy.

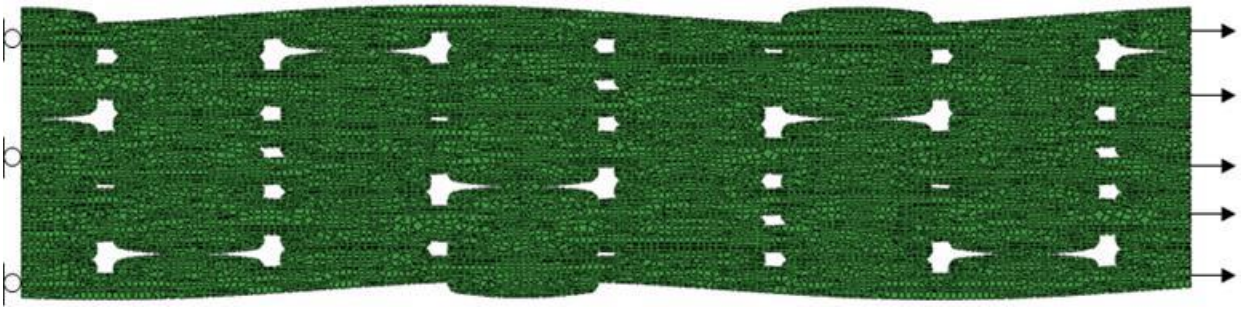

Figure 5-7. Boundary conditions for uniaxial tensile displacement-controlled loading

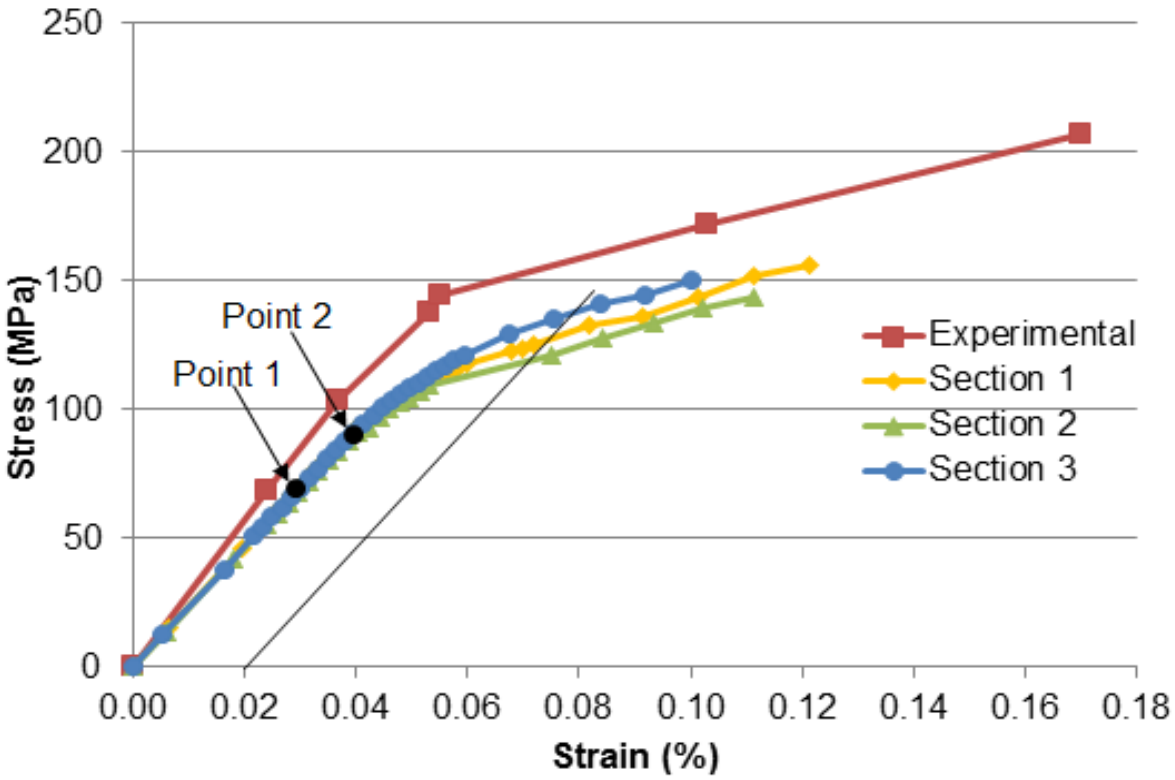

Figure 5-8. Stress-strain curve of three models with varying architecture compared to one experimental model of a similar, but different material. Point 1 corresponds to damage onset. Point 2 corresponds to approximate onset of non-linearity. The 0.02% offset is also labeled.

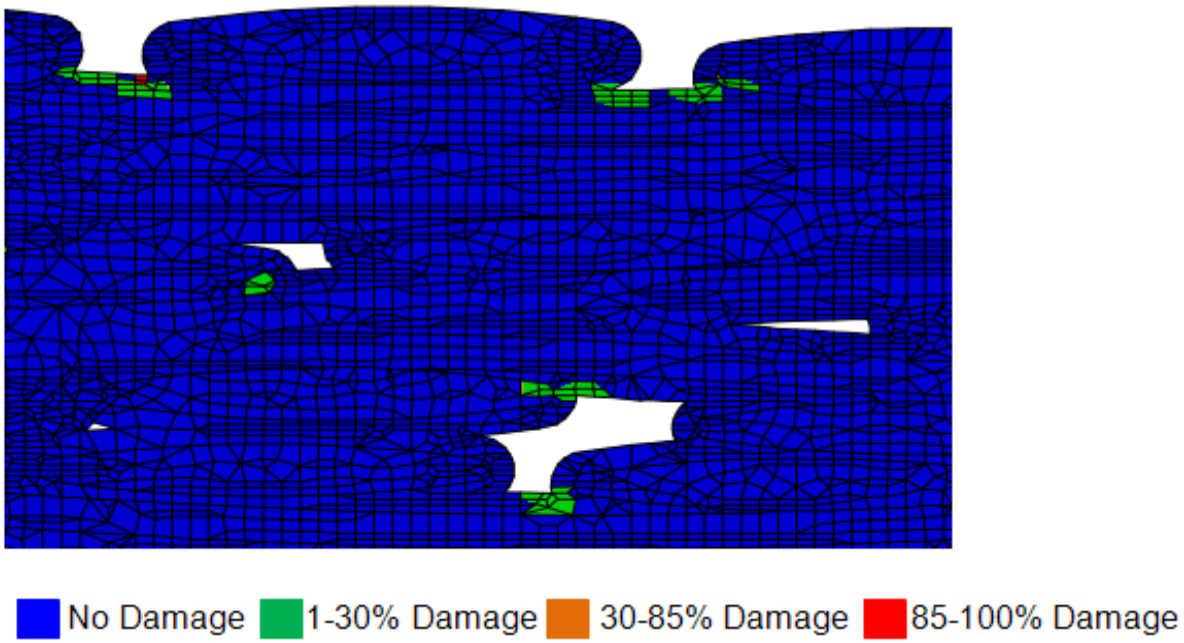

Figure 5-9. Zoomed in image of cross section 1 corresponding to damage onset labeled in Figure 5-8 as Point 1.

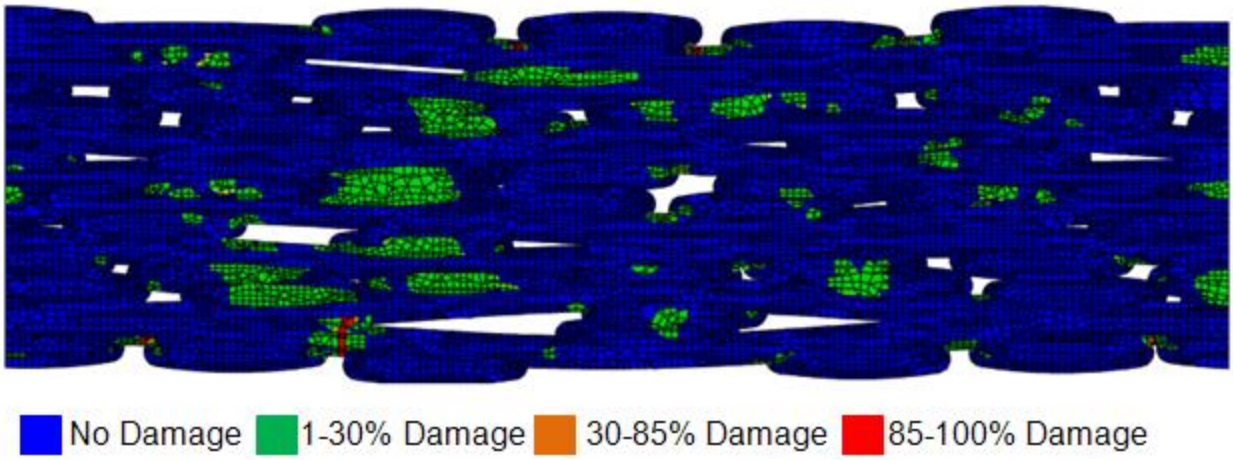

Figure 5-10. Image of cross section 1 corresponding to approximate onset of non-linearity labeled in Figure 5-8 as Point 2.

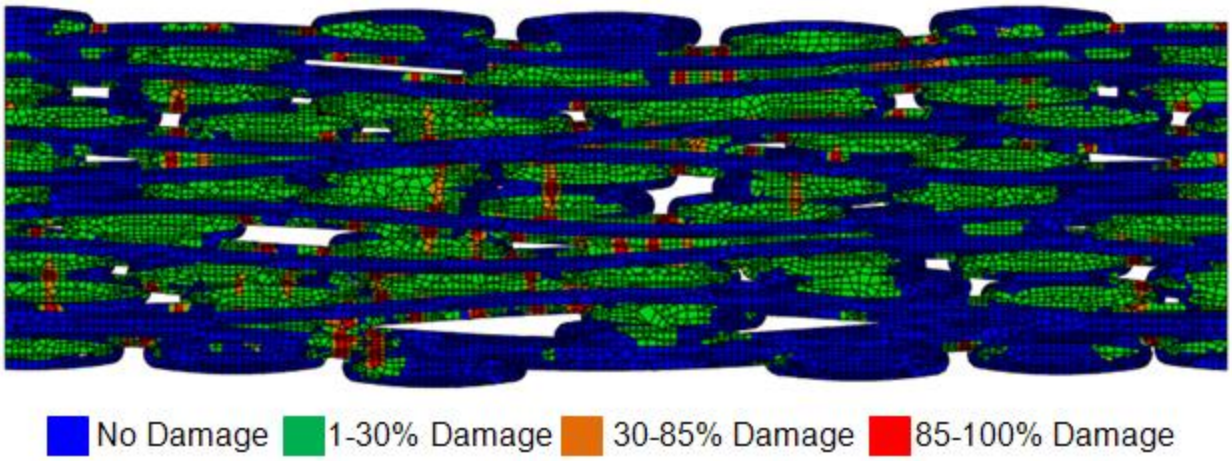

Figure 5-11. Image of cross section 1 corresponding to 0.02% yield offset labeled in Figure 5-8 with a black line

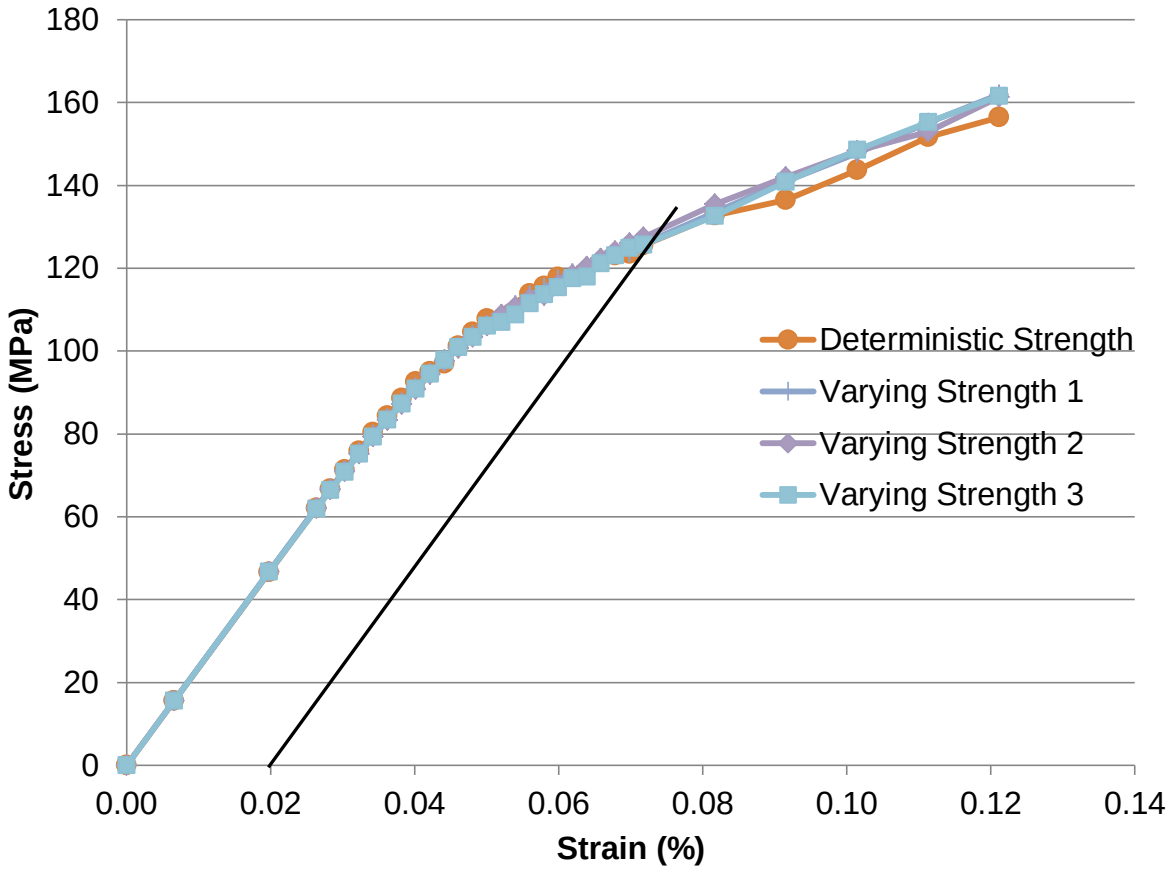

Figure 5-12. Stress-strain curves of cross section 1 with the deterministic strength and three different sets of strengths drawn from a Weibull distribution

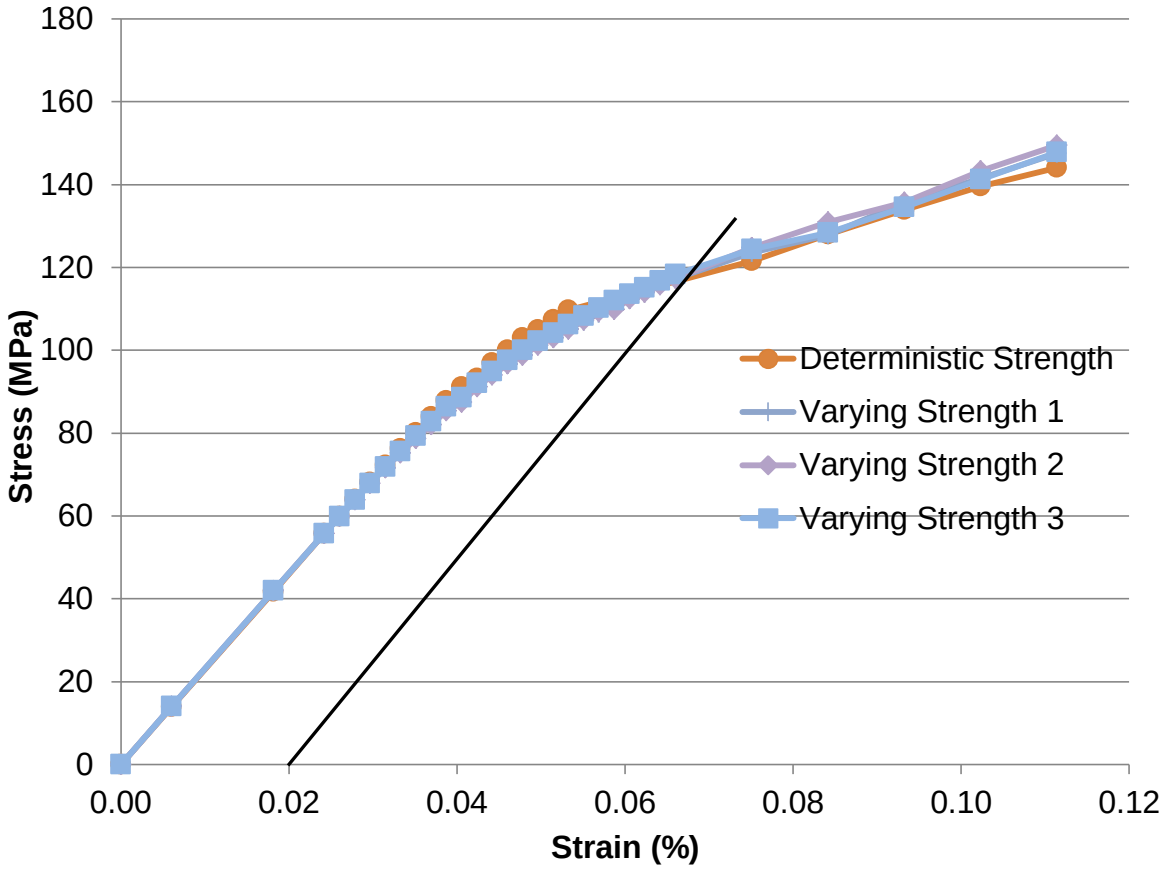

Figure 5-13. Stress-strain curves of cross section 2 with the deterministic strength and three different sets of strengths drawn from a Weibull distribution

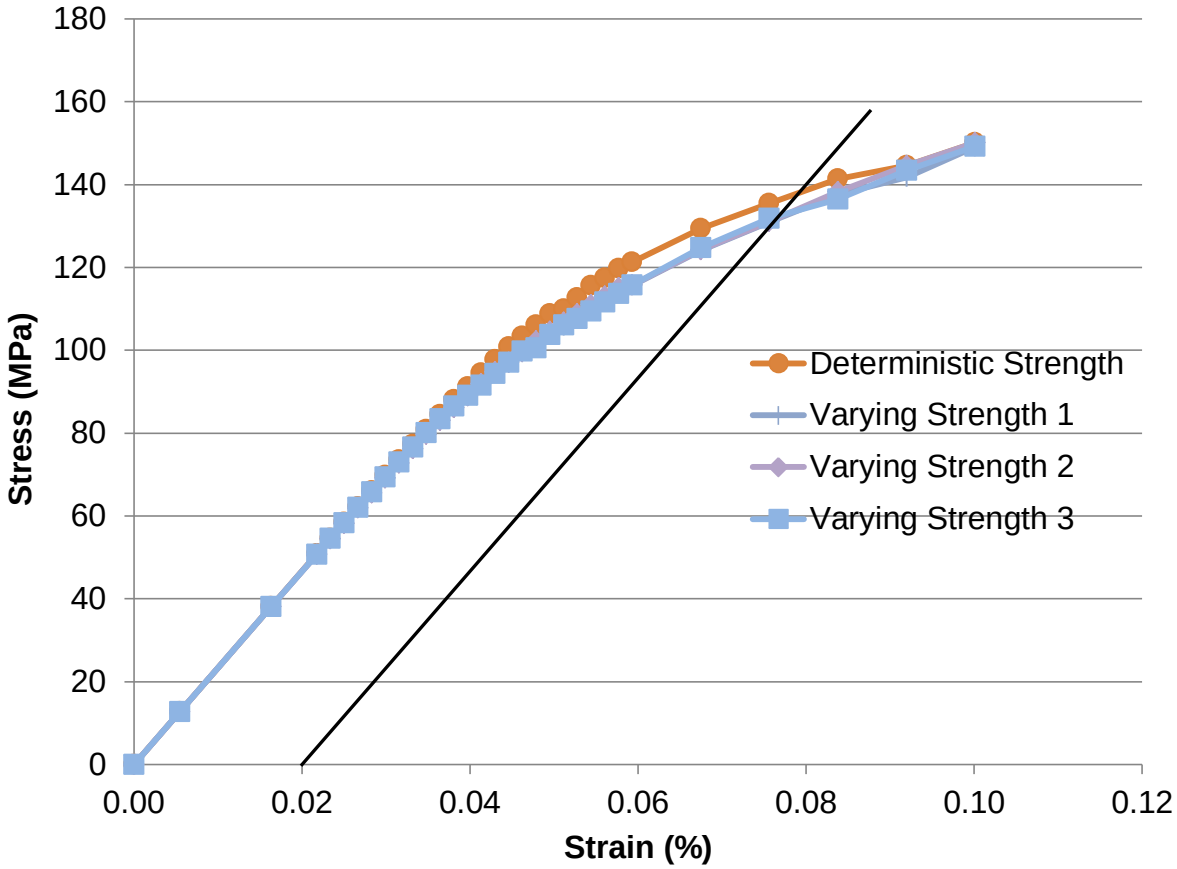

Figure 5-14. Stress-strain curves of cross section 3 with the deterministic strength and three different sets of strengths drawn from a Weibull distribution

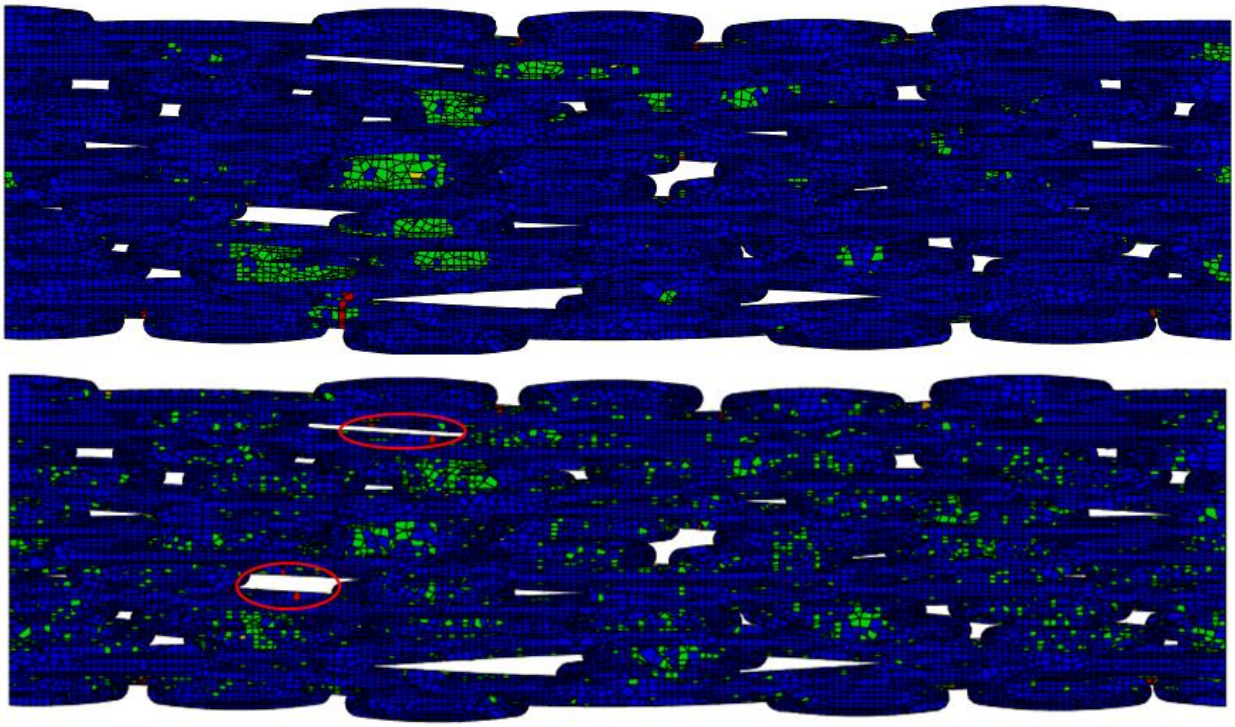

Figure 5-15. Comparison of damaged area in the deterministic and randomized models of cross section 1

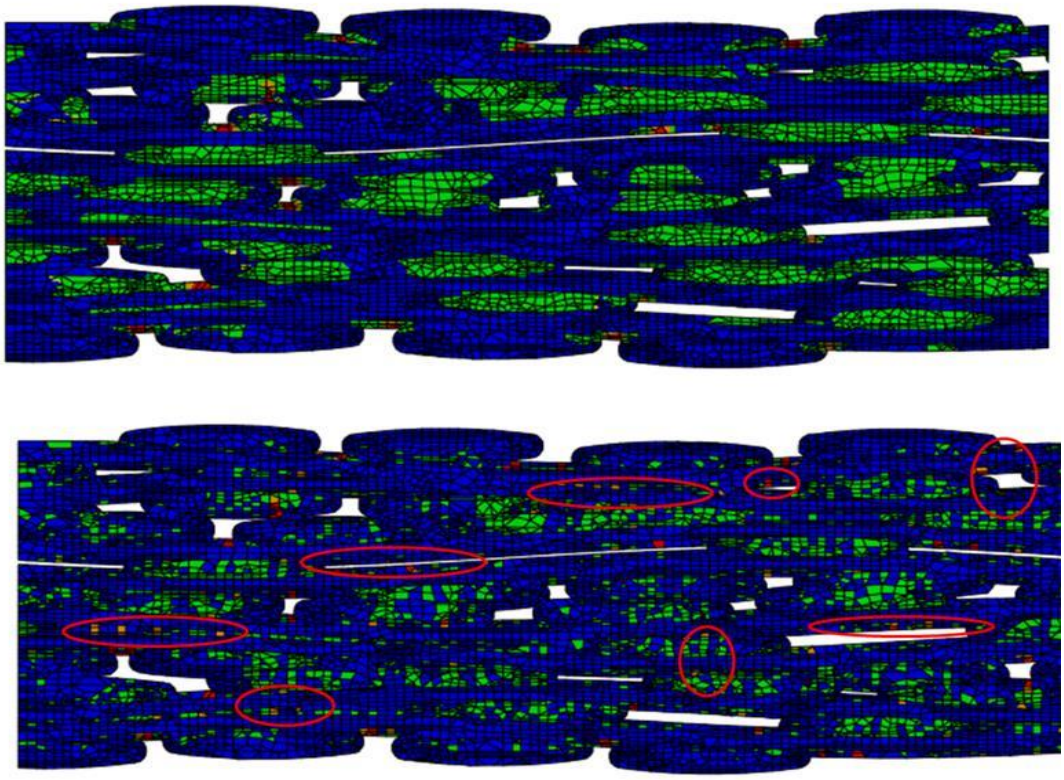

Figure 5-16. Comparison of damaged area in the deterministic and randomized models of cross section 3

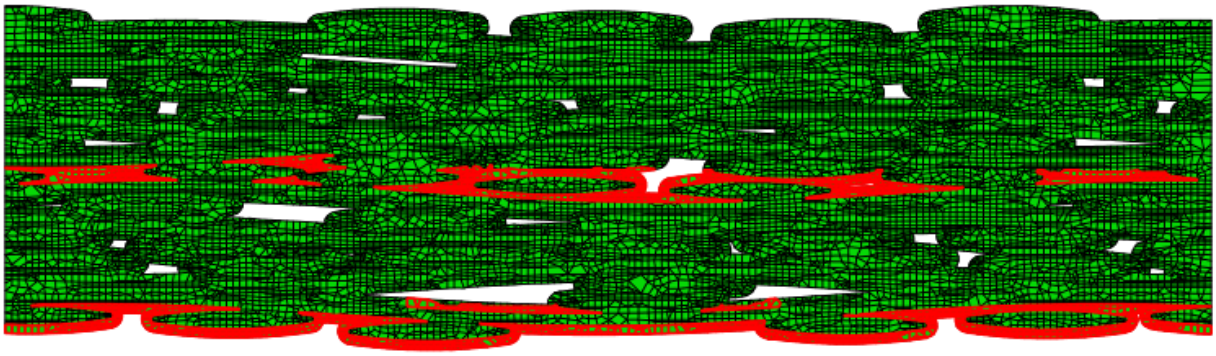

Figure 5-17. Model with matrix cluster 1 and matrix cluster 5 highlighted in red. The clusters are numbered bottom to top.

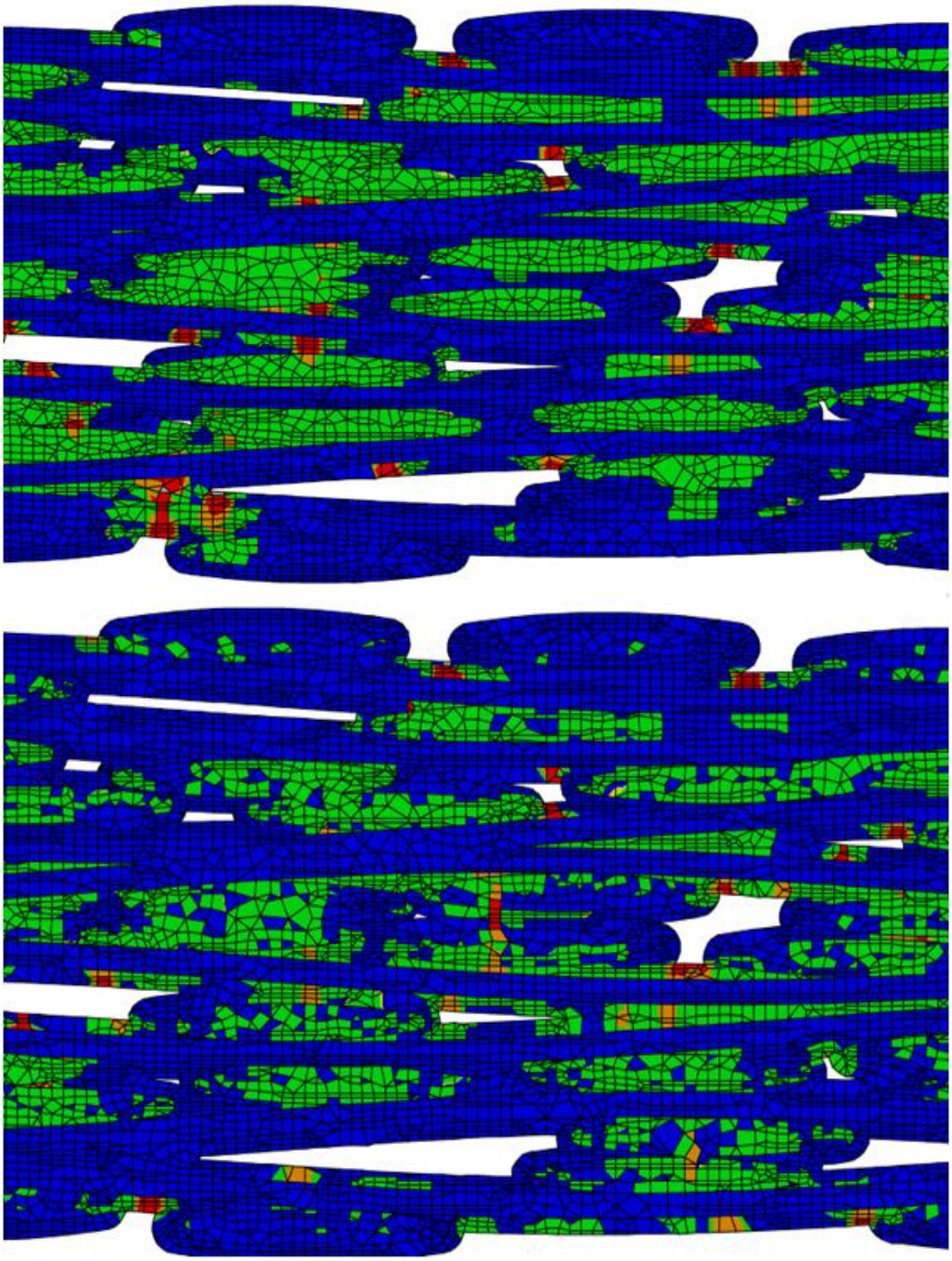

Figure 5-18. Comparison of randomized model (top) with clustered model (bottom) in which the clustered model does not fail near one large top void and one large bottom void due to a higher strength in that region

Table 5-1. Young's modulus, Poisson's ratio, strength, strain at maximum tensile stress, fracture energy, and displacement at failure for the transverse tows and matrix

	Transverse Tow	Matrix
E (GPa)	106.0	420.0
v	0.21	0.21
σ_f (MPa)	53.0	252.0
ε_f	0.05%	0.05%
G (N/m^2)	21.0	21.0
u_u (μm)	8.0	1.7

Table 5-2. Weibull parameters of two parameter Weibull distribution and the corresponding mean and standard deviation

	Transverse Tow	Matrix
Scale parameter, λ (MPa)	58.0	275.0
Shape parameter, m	4.9	4.9
Mean of distribution, μ (MPa)	53.0	252.0
Standard deviation, σ (MPa)	12.0	59.0

Table 5-3. Expected change in strength (Δσ) due to a change in mean, compared to the measured change in strength when variable strength used

Mean Matrix Strength (MPa)	Mean Tow Strength (MPa)	Expected Δσ due to mean (MPa)	Δσ Section 1 (MPa)	Δσ Section 2 (MPa)	Δσ Section 3 (MPa)
247	54.0	-1.0	0.5	1.0	-6.0
254	53.0	3.0	2.5	2.0	-6.0
252	53.0	0.0	0.0	1.0	-5.0

Table 5-4. Strength in the clusters for the matrix cluster model and tow cluster model. Note that the mean and standard deviation of the strength distributions are the same as that of the randomized model with many clusters

Cluster	Matrix Strength (MPa)	Tow Strength (MPa)
1	213	65
2	293	46
3	254	55
4	223	66
5	177	59
6	144	50
7	248	64
8	316	45
9	314	62
10	293	35
Mean	247	55
St.Dev.	58	10

CHAPTER 6
CONCLUSIONS

6.1 Summary of Research

In order to eventually reduce the number of tests required for implementation of advanced materials such as ceramic matrix composites, it is important that the variability in the properties can be evaluated with simulations. Architectural properties are proving to play an important role in the stiffness and strength of the material. It is necessary then, to be able to predict the variability in material properties based on the variability in the architecture. This poses a very complex problem as there are many types of variability that can be considered. The research set out to lay a foundation in which architectural variables could eventually be translated to material properties such as stiffness and strength.

The main contributions of this research are as follows:

1. The architectural variability was statistically quantified and applied to a 2D representative volume element (RVE) in order to evaluate which architectural variables are relevant in capturing the variability in stiffness of a few composite cross sections. **Tow width, tow spacing, and tow volume fraction were found to be important, but did not completely describe the variability. Ply shifting that causes change in void size and position was to contribute more to the variability.**
2. A methodology was developed in which complex 3D voids could be approximated in a simple manner (more complex than volume fraction relationships, but less complex than using a 3D image of the composite to generate an exact replica of the voids). **It was found that volume fraction is not always an appropriate parameter in determining voids' effects on stiffness and can result in over-prediction of stiffness. The area projected normal to the loading direction and the number of voids are key to the effect voids have on the transverse normal stiffness and transverse shear stiffness.**
3. **It was established that varying architecture for in-plane strength is important in capturing the variability, unlike the in-plane stiffness. When using a 0.02% yield offset method to define strength, completely random spatial distribution of strength properties can be ignored.**

An RVE was characterized by varying tow widths, heights, and spacing, resulting in variability of 2-6% of the mean for normal moduli and 4-17% of the mean for shear moduli. When considering the tow width height, and spacing, the variability was largest for the out-of-plane tensile modulus (E_3), out-of-plane shear modulus (G_{13}), and in-plane shear modulus (G_{12}) due to tow width, tow spacing, and tow volume fraction. FEA analysis of real composite cross sections revealed that there is more variability present than the variability predicted by the RVE with uniform ply shifting chosen. This indicates that modeling the variability in tow width, tow height, and tow spacing is not sufficient for modeling the variability in the cross sections. Analysis that examined ply shifting indicated that the voids play a significant role in determination of the transverse stiffness and the variation in size or positions of the voids should not be neglected. While the tow characteristics did not capture all of the variability in the actual cross sections, using the architectural description of the voids would be useful in generating realistic RVEs in which the tow characteristics will influence void formation when simulating the manufacturing process.

This study deemed it necessary to understand how to account for voids in modeling. It is very common for the effects of voids to be accounted for by their volume fraction. When voids are relatively small and evenly distributed this is a good approximation. However, this work provides insight into why this may not always be correct. The goal of the work was to determine which characteristics of the complex voids in a 5HS SiC/SiC composite were most influential on the stiffness of the composite, and provide suggestions for how these voids could be modeled in a simplified manner. It was found that the spacing and alignment of voids was not critical

to model. However, the projected area becomes important when that area is of a certain size relative to the area being observed. In this work, we found that if the area of the void projected normal to the loading direction is at least 15% of the total area, the stiffness in that direction will be influenced by that area (rather than only the volume fraction). The number of voids and the aspect ratio impacted the stiffness results also. In summary a simplified void model was used to establish which void characteristics are most important to model in order to capture its effects on stiffness. The projected area and number of voids are key to understanding their effect on the stiffness.

Lastly, from the strength studies we first learned that the variability in architecture results in variability in strength, especially as compared to the stiffness. Strength is more dependent on local effects than stiffness is, and the voids in the architecture can cause high local stress concentrations. It is not clear what causes the variation in strength between the three architectural models, but should be a topic of future study. What is clear is that variation in the architecture is important to consider because they determine how impactful the given local strength will be on the final results. The architecture and local constituent strength play a synergistic role in determining the strength of the composite. Using a 0.02% offset yield criterion allows the random spatial distribution of constituents' strengths to be ignored. However, it may be important to include them in future models that are concerned with failure beyond the yield strength.

6.2 Suggestions for Future Work

It was shown that statistical variation between RVEs is a viable option for determining variability in stiffness. While the statistics from the cross sections are used to generate the RVEs, the cross sections and RVEs are not necessarily statistically equivalent. Being statistically equivalent implies that the statistics of certain parameters

(like the effective material properties and the local architectural characteristics) are equivalent to the overall microstructure (within some tolerance) and independent of the location in microstructure being observed [70]. It would be useful to characterize the RVE such that it is statistically equivalent to a cross section. The concept is more commonly used at the microstructural level (fiber level). In order to determine what constitutes statistical equivalence at the ply or tow level, larger cross sections would be necessary.

While determining what characteristics of the voids needed to be modeled to capture their effects on stiffness, it was found that the number of voids modeled had some influence on the results. Future work would benefit from being able to quantify the images of the voids in such a way that the number of voids to be modeled can be determined in a more precise manner.

It was shown that the architectural variability impacts the variability in in-plane tensile strength. Future work should include a process similar to that used for the stiffness modeling. However, because the strength may be influenced by many local phenomena, a larger RVE would be necessary (possible even larger than the cross sections that are currently available). A statistically equivalent RVE would again be useful. Moreover, the stiffness and strength analysis would benefit from 3D models, especially if trying to accurately link the architectural variability to the mechanical properties. Several aspects of the composite are lost in 2D including the undulation of tows in the transverse direction and the fact that voids do not act as tunnels and rather close off at various points. 3D modeling may prove especially important for strength in

order to appropriately evaluate the architectural effects on the intended toughening mechanisms.

APPENDIX A
TOW DATA OF THREE CROSS SECTIONS

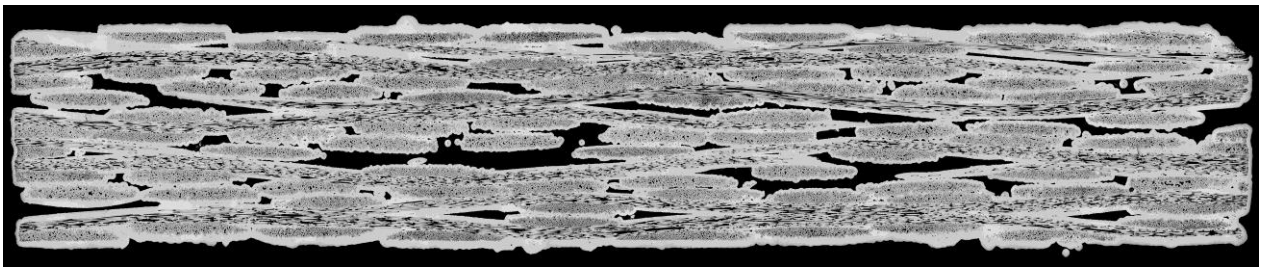

Cross Section 1

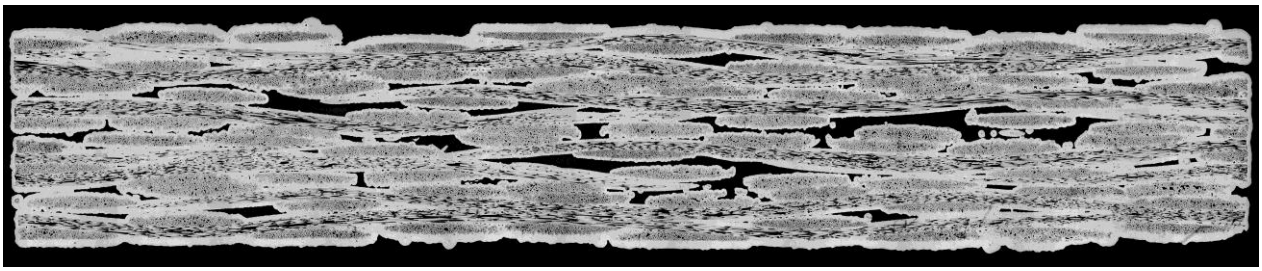

Cross Section 2

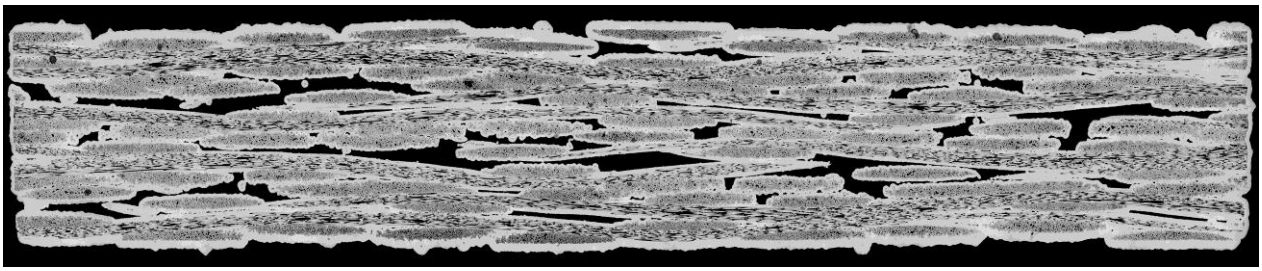

Cross Section 3

Figure A-1. Images of cross sections corresponding to tow data presented in Table A-1, Table A-2, Table A-3 [23]

Table A-1. Tow data of cross section 1

X center (mm)	Y center (mm)	Ellipse Major Axis (mm)	Ellipse Minor Axis (mm)
11.8259	0.3227	1.2724	0.1272
1.707	0.302	1.2446	0.1169
5.5081	0.3012	1.2829	0.1034
4.2141	0.3105	1.2603	0.1079
8.0973	0.301	1.1998	0.1033
10.5662	0.3139	1.2412	0.1185
6.7896	0.3908	1.1239	0.1246
2.8708	0.3899	1.0129	0.1078
9.2813	0.4199	1.2101	0.0979
5.4288	0.5473	1.1864	0.1017
11.7647	0.5862	1.0505	0.0983
9.273	0.6264	1.0987	0.1324
1.5695	0.6328	1.0556	0.1303
2.9538	0.6487	1.1451	0.114
7.9963	0.6573	1.1814	0.1174
6.7258	0.6995	1.0538	0.1303
4.2124	0.7307	1.0892	0.1328
5.9281	0.7468	0.9978	0.1496
10.4952	0.7435	1.1158	0.1192
12.2123	0.7657	1.0242	0.1363
2.1274	0.7828	1.0213	0.1319
8.4611	0.7805	1.2192	0.106
3.393	0.8182	0.9893	0.1319
9.6977	0.8328	1.0813	0.13
10.9007	0.8569	1.1876	0.0983
7.1886	0.8975	1.1832	0.1039
1.6526	1.0518	1.1426	0.1058
7.9405	1.0565	1.1337	0.1096
11.7268	1.0719	1.1314	0.1093
5.36	1.1069	1.0721	0.1114
4.1495	1.1589	1.0777	0.1323
10.5349	1.1694	1.0593	0.1109
9.2926	1.1932	1.0401	0.1409
2.894	1.2117	1.1113	0.126
6.734	1.2279	1.0715	0.1428
1.4715	1.2397	1.201	0.1043
7.8082	1.2495	1.1521	0.1234
10.3105	1.2746	1.1637	0.1195
3.8743	1.3058	1.1863	0.1276

Table A-1. Continued

X center (mm)	Y center (mm)	Ellipse Major Axis (mm)	Ellipse Minor Axis (mm)
11.6219	1.2997	1.1024	0.1149
2.6631	1.3823	1.143	0.1069
6.4875	1.3805	1.2191	0.0979
9.0767	1.4048	1.1021	0.113
8.2122	1.5661	1.0648	0.1226
4.3273	1.5685	1.2038	0.0928
10.8071	1.595	1.2012	0.0999
1.8417	1.6103	1.1152	0.1316
6.915	1.6617	1.1768	0.1193
12.0665	1.6784	1.0758	0.1411
5.678	1.7118	1.0546	0.1279
3.0996	1.7202	1.0683	0.1247
9.4525	1.7229	1.2495	0.1232
0.8017	1.7723	1.1075	0.1377
4.6011	1.7539	1.213	0.1143
10.9774	1.7563	1.2126	0.1063
2.0592	1.7788	1.1777	0.1266
7.2011	1.78	1.1483	0.1143
8.4149	1.8098	1.0323	0.1247
9.6585	1.82	1.1367	0.1055
3.3848	1.855	0.9812	0.1182
5.9103	1.9109	1.1502	0.1061
12.1905	1.9169	1.1501	0.1054
5.7456	2.0386	1.1151	0.1074
12.0948	2.0588	1.1453	0.099
1.892	2.1031	1.227	0.1202
9.5047	2.0991	1.1501	0.1051
3.1723	2.1341	1.2125	0.1071
8.332	2.1374	1.2167	0.1067
10.7982	2.1673	1.3097	0.1107
4.5194	2.1758	1.2211	0.1006
7.0596	2.1733	1.4017	0.0956

Table A-2. Tow data of cross section 2

X center (mm)	Y center (mm)	Ellipse Major Axis (mm)	Ellipse Minor Axis (mm)
1.6737	0.3078	1.1931	0.1309
2.8563	0.3002	1.0428	0.1144
5.5109	0.2891	1.3167	0.0884
8.1269	0.3147	1.1837	0.1122
11.7691	0.3091	1.3295	0.1063
9.2491	0.3383	1.2579	0.1156
10.5002	0.3956	1.1974	0.1134
4.1735	0.4021	1.1877	0.1011
6.7762	0.4092	1.1549	0.1151
1.5813	0.5732	1.0971	0.1149
8.0249	0.5927	1.1807	0.1013
11.7643	0.6195	1.093	0.0974
5.4169	0.6385	1.1514	0.1168
4.2555	0.6544	1.1166	0.1239
6.6895	0.7159	1.1798	0.1195
2.9604	0.7129	1.1418	0.1156
10.4979	0.7087	1.1687	0.1103
9.3024	0.7248	1.1165	0.1182
5.9884	0.771	1.0214	0.1526
3.4549	0.7851	1.0345	0.1254
0.9619	0.7724	1.0524	0.1133
9.7664	0.7982	1.0598	0.1227
7.2358	0.8146	1.1894	0.1117
8.4669	0.851	1.1468	0.1091
2.1509	0.861	1.0697	0.1183
4.7019	0.9113	1.1191	0.0984
10.9374	0.9342	1.1874	0.0903
4.1439	1.0525	1.2406	0.1077
7.9346	1.0863	1.1144	0.1179
10.5119	1.0842	1.0167	0.1056
1.6763	1.1041	1.1525	0.1226
11.7475	1.1656	1.1576	0.1179
6.7428	1.1744	1.0914	0.1377
5.4176	1.1728	1.0934	0.1077
2.9005	1.1907	1.0735	0.1031
9.3138	1.2192	1.076	0.1408
5.2177	1.2699	1.0742	0.1263
2.6152	1.2749	1.1569	0.1137
7.7985	1.2825	1.1331	0.1353
11.5737	1.2759	1.1456	0.1205

Table A-2. Continued

X center (mm)	Y center (mm)	Ellipse Major Axis (mm)	Ellipse Minor Axis (mm)
9.0871	1.3282	1.0743	0.1203
10.2911	1.3504	1.1425	0.1281
3.8687	1.373	1.2099	0.114
6.5027	1.4024	1.1788	0.0935
6.883	1.5846	1.1696	0.1152
10.7584	1.5835	1.1986	0.0976
4.2744	1.6093	1.1181	0.1209
3.0782	1.6295	0.997	0.1113
1.8117	1.6511	1.1907	0.1146
8.1621	1.6665	1.0585	0.1232
9.4087	1.6881	1.154	0.1169
2.0814	1.7385	1.1985	0.1248
5.6588	1.7127	1.0362	0.1058
12.0365	1.7327	1.0748	0.143
8.4016	1.7665	1.0517	0.1243
4.6415	1.7532	1.1721	0.114
11.012	1.756	1.17	0.1108
5.8253	1.8146	1.2915	0.1145
7.1626	1.8511	1.1049	0.1405
0.8041	1.8574	1.1056	0.1226
12.1823	1.8667	1.1579	0.1168
3.3912	1.8836	0.9892	0.1158
9.6518	1.902	1.1254	0.101
1.8619	2.0303	1.1873	0.1136
8.2869	2.0554	1.189	0.1055
12.0519	2.0997	1.1335	0.111
4.5172	2.1053	1.2071	0.1147
5.709	2.1082	1.1596	0.1093
10.7351	2.1522	1.1898	0.14
3.1927	2.1549	1.2469	0.1063
9.5059	2.1732	1.1993	0.107
6.9661	2.179	1.365	0.0952

Table A-3. Tow data of cross section 3

X center (mm)	Y center (mm)	Ellipse Major Axis (mm)	Ellipse Minor Axis (mm)
4.136	0.2752	1.195	0.1056
6.7315	0.2766	1.302	0.1059
9.2026	0.3046	1.2141	0.1148
2.8746	0.3154	1.0455	0.1158
10.4575	0.3316	1.2157	0.119
1.5912	0.3695	1.2384	0.1224
11.6915	0.389	1.2757	0.1164
7.996	0.3963	1.0791	0.1093
5.4379	0.3925	1.2207	0.0955
6.7242	0.5482	1.2331	0.1007
2.9898	0.6169	1.1655	0.111
10.5125	0.6193	1.0788	0.1174
4.2271	0.6373	1.1232	0.1289
9.3138	0.6872	1.0427	0.1362
5.5016	0.6979	0.9558	0.126
8.0722	0.7081	1.1068	0.1192
1.6283	0.7161	1.0343	0.1401
4.8013	0.7458	1.0692	0.1374
11.8099	0.7105	1.1051	0.1078
11.0198	0.7659	1.0282	0.1243
7.3291	0.7757	1.1562	0.1171
2.2665	0.7903	1.0912	0.1304
1.0165	0.7949	1.083	0.1278
8.5875	0.8162	1.1039	0.1179
9.8653	0.8518	1.1084	0.1153
3.5119	0.8743	1.1389	0.1053
6.0986	0.8921	1.1215	0.1287
2.8925	1.0433	1.1392	0.0904
9.2832	1.0743	1.1295	0.1085
6.7235	1.0918	1.1845	0.1196
5.4075	1.1553	0.9551	0.1335
10.4865	1.1619	0.9952	0.1332
11.7382	1.1657	1.194	0.1301
4.1748	1.1708	1.1401	0.1277
1.6704	1.1936	1.0817	0.1371
7.9635	1.2056	1.1713	0.1201
6.4832	1.2361	1.1941	0.108
9.0871	1.2556	1.107	0.1259
2.6413	1.2668	1.1536	0.1305
3.8634	1.2798	1.2106	0.1301

Table A-3. Continued

X center (mm)	Y center (mm)	Ellipse Major Axis (mm)	Ellipse Minor Axis (mm)
10.2675	1.3096	1.1818	0.1176
11.5756	1.334	1.0945	0.1131
1.4281	1.3465	1.2318	0.0991
5.2365	1.3835	1.1181	0.1113
7.748	1.3879	1.1634	0.1101
5.5429	1.5665	1.0873	0.1079
9.357	1.584	1.2127	0.1067
11.9784	1.5946	1.1746	0.1069
2.9439	1.6029	0.9763	0.117
1.7139	1.6274	1.1136	0.1358
6.786	1.7018	1.2993	0.1267
8.0514	1.6877	1.0943	0.1237
4.2128	1.7177	1.1098	0.1226
10.7531	1.7091	1.1275	0.1028
3.3673	1.7402	1.0276	0.1365
9.6981	1.7489	1.2375	0.1221
12.1786	1.735	1.0747	0.1315
0.7638	1.7668	1.0966	0.1272
5.8485	1.7775	1.0101	0.1321
7.1819	1.8233	1.1472	0.1211
8.3963	1.8478	1.0745	0.1119
2.046	1.8645	1.2086	0.1162
4.6151	1.9099	1.1971	0.0997
10.968	1.9004	1.1704	0.0925
10.727	2.0825	1.2386	0.1254
6.96	2.0731	1.233	0.095
3.1143	2.1121	1.2476	0.1109
9.4332	2.1263	1.1823	0.1091
4.4191	2.1504	1.1889	0.1173
8.2915	2.167	1.3278	0.0992
1.8788	2.1693	1.2828	0.1106
12.0206	2.1736	1.213	0.0994
5.6526	2.1987	1.1947	0.1094

APPENDIX B
VOID RESULTS

Table B-1 and Table B-2 summarize the results from 20 exploratory void cases that varied the aspect ratio, the number of voids, and the position of the voids. Table B-3 shows the results when the voids are not square. Note that for Table B-1and Table B-2 the void volume fraction was always 4%. For the rectangular voids, the height of the voids was the constant factor.

Table B-1. Stiffness as a result of varying the number of voids and aspect ratio of the voids

# Voids	AR	E_1 (GPa)	E_2 (GPa)	E_3 (GPa)	G_{12} (GPa)	G_{13} (GPa)	G_{23} (GPa)
1	3	94.1	94.1	91.9	35.9	34.0	34.0
1	5	94.8	94.8	89.0	36.3	33.0	33.0
1	8	95.1	95.1	85.2	36.5	31.6	31.6
1	10	95.4	95.4	82.8	36.6	30.7	30.7
2	3	94.6	94.2	90.5	36.0	34.4	33.9
2	5	95.1	94.8	87.3	36.3	33.5	32.7
2	8	95.5	95.3	82.7	36.6	32.3	31.0
2	10	95.6	95.4	79.9	36.7	31.3	29.8
3	3	95.0	94.3	90.0	36.0	34.6	33.7
3	5	95.4	94.8	86.3	36.4	33.4	32.3
3	8	95.8	95.3	81.3	36.6	31.9	30.0
3	10	95.9	95.4	77.0	36.7	30.4	27.6

Table B-2. Stiffness as a result of varying the position of the voids. s_1 and s_3 are the spacing between the voids in the 1-direction and 3-direction, labeled in Figure 4-2.

# Voids	Spacing Description	E_1 (GPa)	E_2 (GPa)	E_3 (GPa)	G_{12} (GPa)	G_{13} (GPa)
2	s_1 = 0.16 mm	95.6	95.3	82.6	36.6	31.7
2	s_1 = 0.57 mm	95.6	95.3	82.8	36.6	32.2
2	s_1 = 1 mm	95.5	95.3	82.8	36.6	32.3
2	s_1 = 1.6 mm	95.5	95.3	82.8	36.6	32.3
2	s_3 = max (voids in top most and bottom most layers)	95.5	95.3	82.6	36.6	32.4
2	Opposite corners	95.3	95.3	82.7	36.7	31.7
3	Diagonal; same plane	95.4	95.3	81.3	36.7	31.8
3	Diagonal; tiered planes	95.5	95.3	81.1	36.7	32.0

Table B-3. Stiffness as a result of using voids with a width to length aspect ratio different than 1, to show the effect on the transverse shear stiffness G_{13} and G_{23}. ℓ_1 and ℓ_2 are the lengths of the void in the 1-direction and 2-direction.

ℓ_1	ℓ_2	E_1 (GPa)	E_2 (GPa)	E_3 (GPa)	G_{12} (GPa)	G_{13} (GPa)	G_{23} (GPa)
0.001	0.001	99.6	99.6	99.2	38.3	38.2	38.2
0.001	0.002	99.2	99.3	98.2	38.2	37.9	37.9
0.001	0.003	98.8	99.0	97.2	38.1	37.5	37.6
0.001	0.004	98.3	98.7	96.3	37.9	37.1	37.3
0.001	0.005	98.0	98.5	95.2	37.7	36.6	37.0
0.001	0.006	97.6	98.2	94.2	37.5	36.2	36.6
0.001	0.007	97.1	97.9	93.3	37.4	35.8	36.3
0.002	0.001	99.3	99.2	98.2	38.2	37.9	37.9
0.002	0.002	98.5	98.5	95.8	37.9	36.9	36.9
0.002	0.003	97.9	98.0	93.3	37.6	35.7	35.9
0.002	0.004	97.1	97.4	90.8	37.3	34.4	35.0
0.002	0.005	96.4	96.8	88.3	37.1	33.1	34.1
0.002	0.006	95.7	96.3	85.8	36.8	31.8	33.3
0.002	0.007	94.9	95.8	83.3	36.6	30.2	32.6
0.003	0.001	99.0	98.8	97.2	38.1	37.6	37.5
0.003	0.002	98.0	97.9	93.4	37.6	34.2	35.7
0.003	0.003	96.9	96.9	89.3	37.2	33.9	33.9
0.003	0.004	96.0	96.0	85.3	36.9	31.7	32.2
0.003	0.005	94.9	95.3	81.4	36.4	29.4	30.8
0.003	0.006	93.8	94.4	77.4	36.0	26.9	29.6
0.003	0.007	92.8	93.6	73.4	35.7	24.2	28.5
0.005	0.001	98.5	98.0	95.3	37.7	37.0	36.6
0.005	0.002	96.8	96.4	88.3	37.1	34.1	33.1
0.005	0.003	95.3	94.9	81.4	36.4	30.8	29.4
0.005	0.004	93.7	93.5	74.3	35.8	27.3	26.1

Table B-4. Varying the void height (ℓ_3) for several sets of area to demonstrated the transverse stiffness dependence on the projected area fraction $\bar{a}_3$, and lack of dependence on the void height

# Voids	AR	$\bar{a}_3$	ℓ_3	E_1 (GPa)	E_2 (GPa)	E_3 (GPa)
2	3	0.12	0.33	94.6	94.2	90.6
2	4	0.12	0.25	96.2	96.0	91.2
2	2	0.12	0.49	91.3	90.2	89.7
2	5	0.17	0.23	95.1	94.8	87.2
2	6	0.17	0.19	96.3	96.2	87.8
2	3	0.17	0.41	90.8	89.6	85.8
2	8	0.23	0.17	95.6	95.4	82.7
2	12	0.23	0.11	97.2	97.1	83.5
2	6	0.23	0.22	93.9	93.5	82.0
2	10	0.27	0.15	95.7	95.5	80.0
2	12	0.27	0.13	96.3	96.2	80.3
2	5	0.27	0.29	90.7	89.6	78.0
3	3	0.14	0.29	95.0	94.3	90.0
3	6	0.14	0.14	97.7	97.6	91.6
3	3	0.14	0.34	93.9	92.7	89.5
3	5	0.20	0.20	95.4	94.8	86.3
3	7	0.20	0.15	96.7	96.4	87.1
3	3	0.20	0.31	93.0	91.5	85.1
3	8	0.27	0.15	95.8	95.3	81.3
3	9	0.27	0.13	96.3	95.8	81.5
3	4	0.27	0.27	92.3	90.3	79.2
3	10	0.31	0.13	95.9	95.4	77.4
3	17	0.31	0.08	97.6	97.4	78.7
3	8	0.31	0.17	94.7	93.8	76.6

The figures below show the results of the in-plane stiffness properties with respect to the height fraction. Note that for most cases, the variability in stiffness is very small (less than 1%). The heights for which the variability starts to increase are not void heights exhibited in the 5HS SiC/SiC composite, but were necessary to examine small area fractions while maintain a constant void volume fraction of 5%.

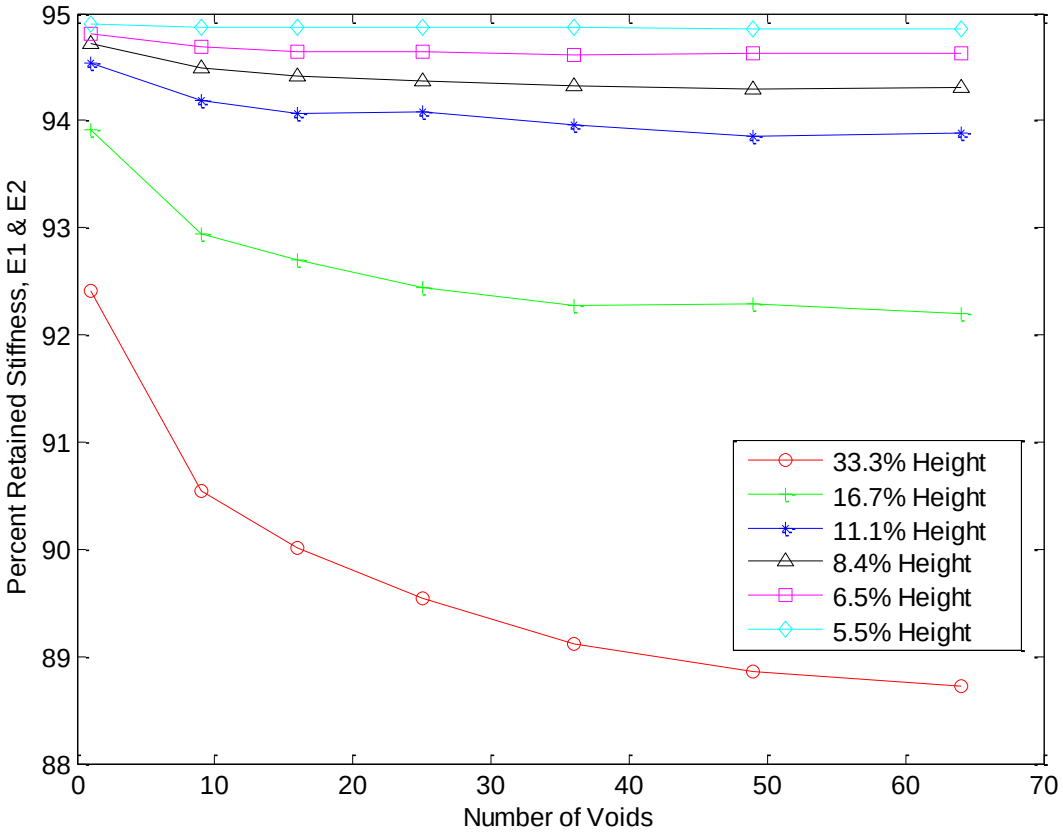

Figure B-1. In-plane stiffness as a result of varying void height and number of voids

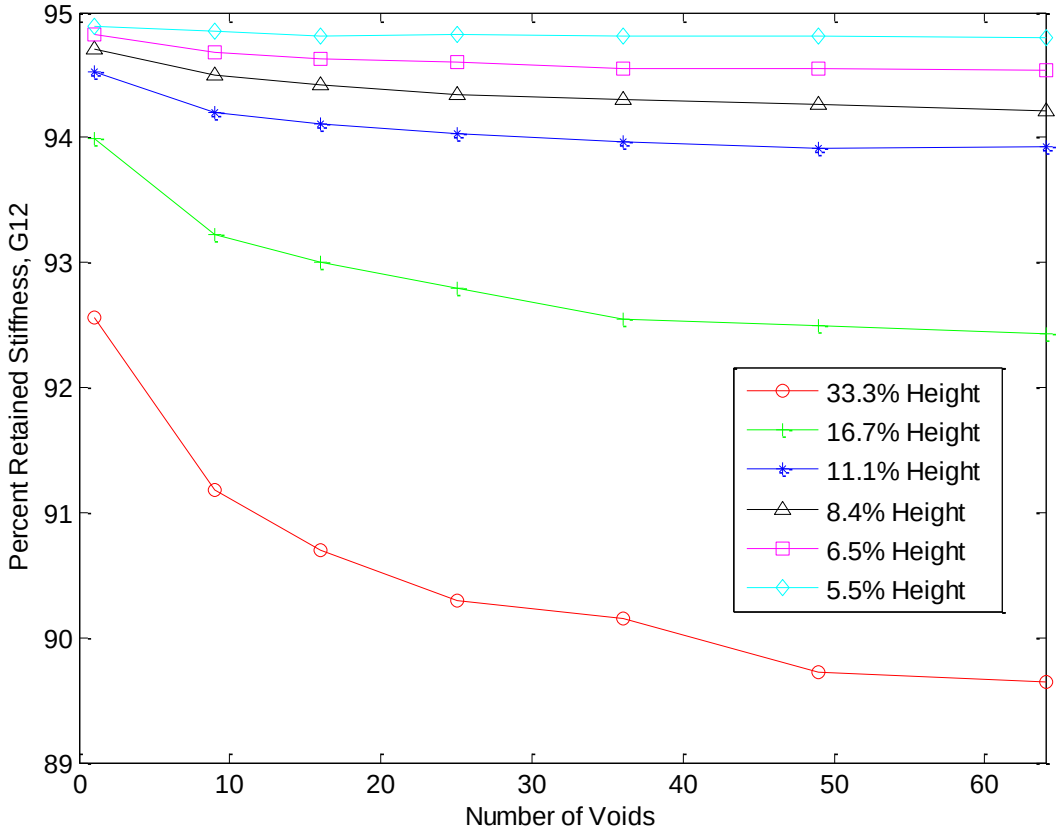

Figure B-2. In-plane shear stiffness as a result of varying void height and number of voids

APPENDIX C
TWO-DIMENSIONAL IMAGES OF COMPOSITE VOIDS

The images in this appendix are arranged as follows. For each ply, first the original 2D projection in the 1-2 plane of the voids is shown at the top. The middle image is an overlay of the original projection with the sketched voids. The bottom image is that of the 2D sketched voids, roughly representing the top image. Ply 1 and Ply 8 were not included because there were no voids in those plies.

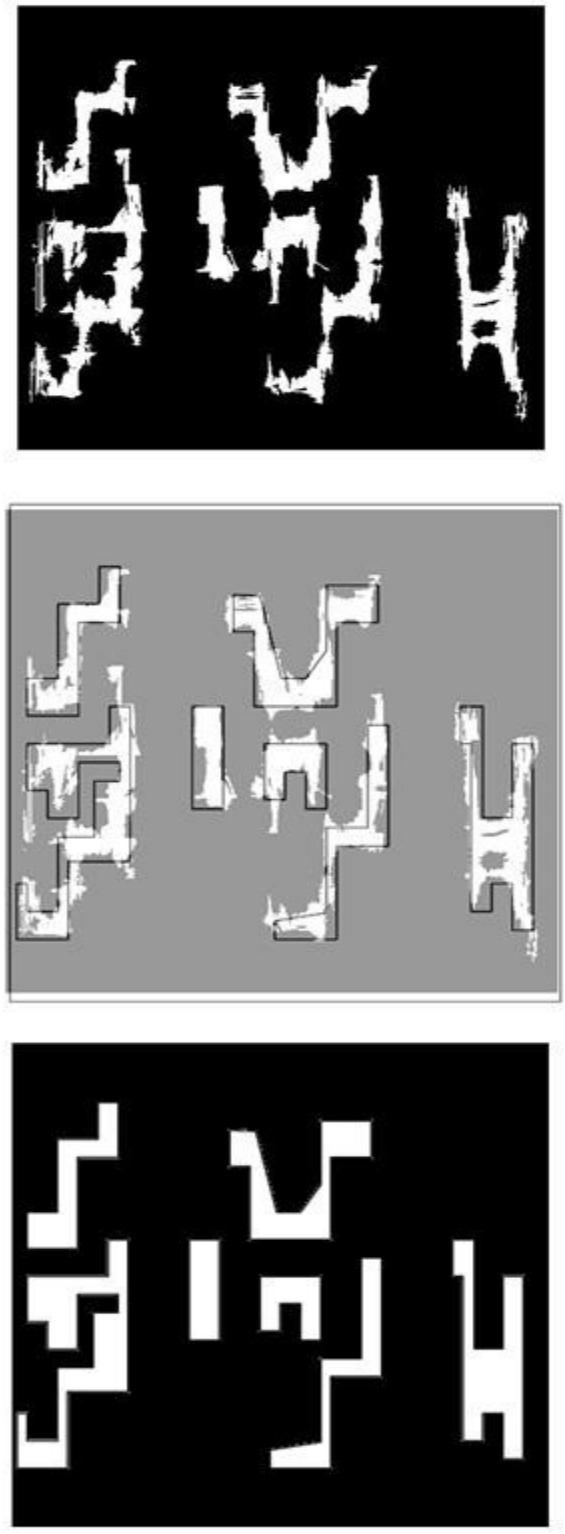

Figure C-1. Original void image and sketched voids for finite element model of ply 2

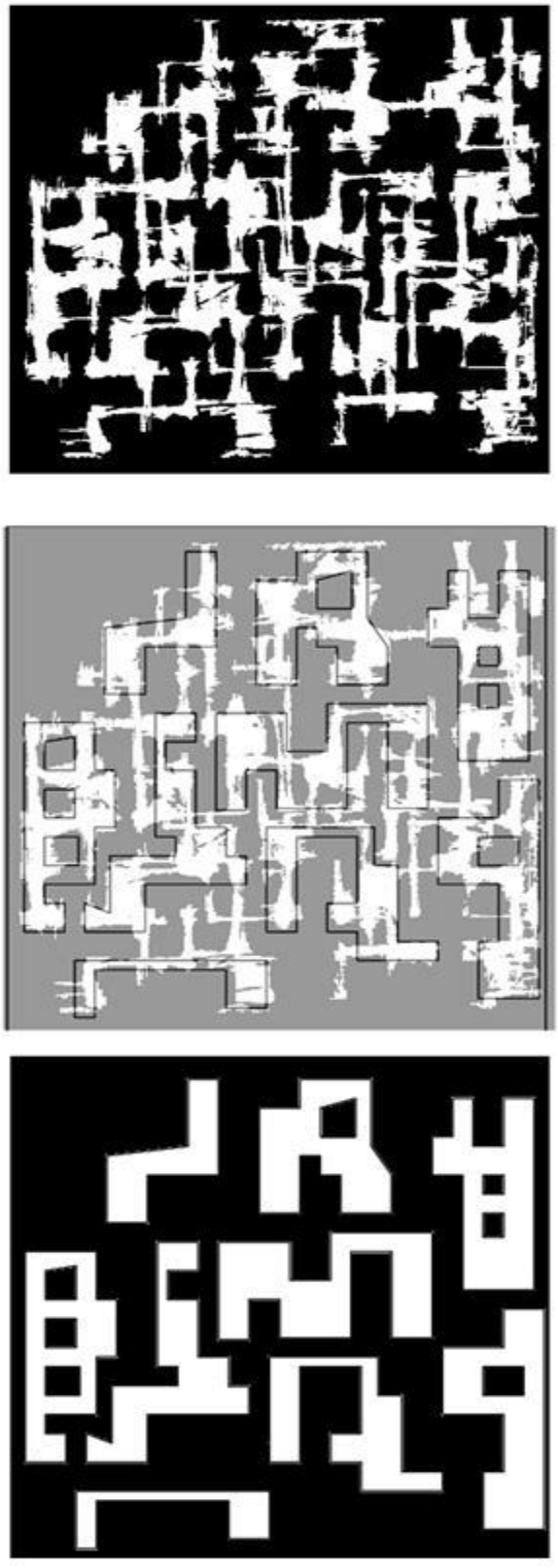

Figure C-2. Original void image and sketched voids for finite element model of ply 3

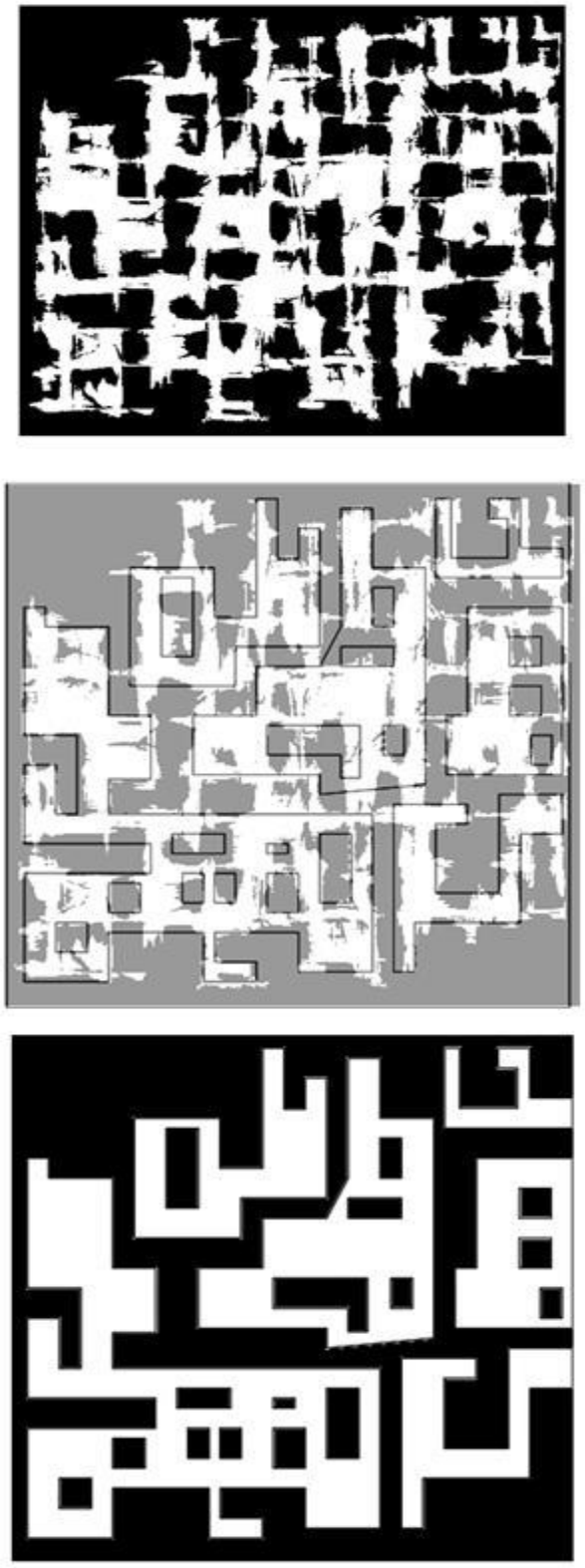

Figure C-3. Original void image and sketched voids for finite element model of ply 4

Figure C-4. Original void image and sketched voids for finite element model of ply 5

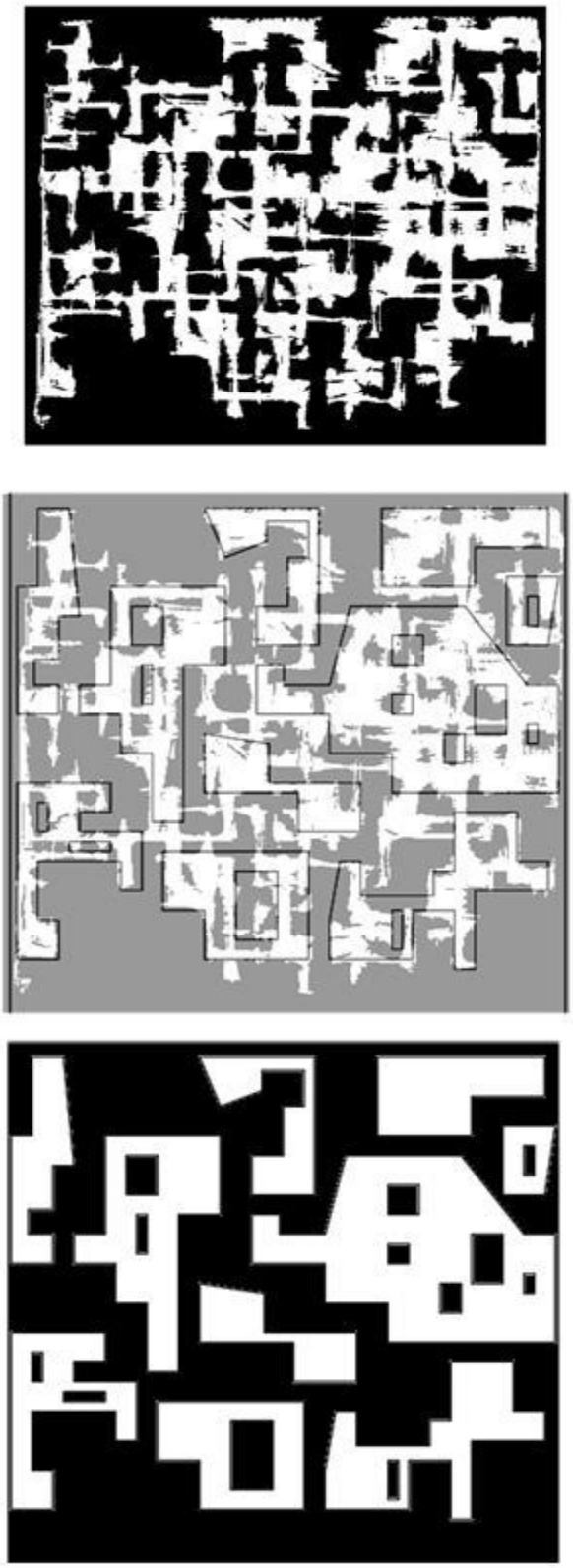

Figure C-5. Original void image and sketched voids for finite element model of ply 6

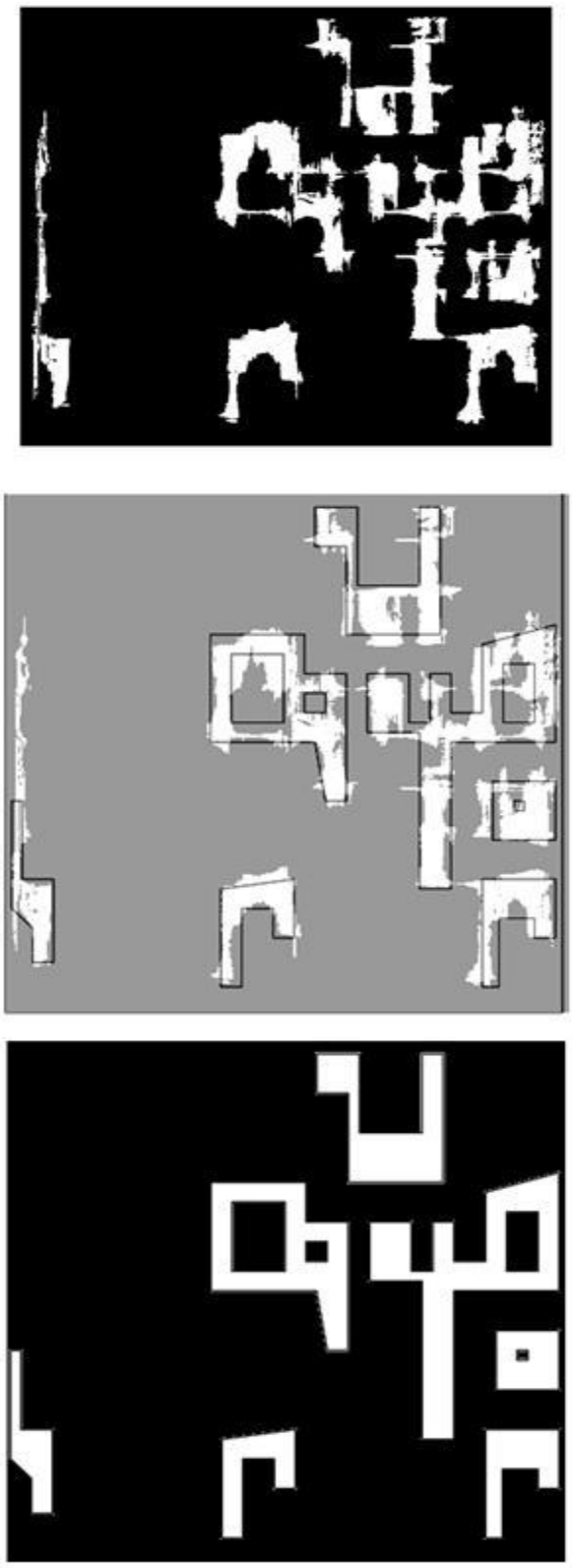

Figure C-6. Original void image and sketched voids for finite element model of ply 7

LIST OF REFERENCES

[1] Goldberg RK, Bonacuse PJ. Investigation of Effects of Material Architecture on the Elastic Response of a Woven Ceramic Matrix Composite. NASA/TM 2012-217269 2012.

[2] Charmpis DC, Schuëller GI, Pellissetti MF. The need for linking micromechanics of materials with stochastic finite elements: A challenge for materials science. Comput Mater Sci 2007;41:27–37.

[3] Kwon YW, Altekin A. multilevel Micro/Macro-Approach for Analysis of Woven-Fabric Composite Plates. J Compos Mater 2002;36:1005–22.

[4] Whitcomb J, Tang X. Effective Moduli of Woven Composites. J Compos Mater 2001;35:2127–44.

[5] Shah AR, Murthy PLN, Mital SK, Bhatt RT. Probabilistic Modeling of Ceramic Matrix Composite Strength. J Compos Mater 2000;34:670–88.

[6] Huang H, Talreja R. Effects of void geometry on elastic properties of unidirectional fiber reinforced composites. Compos Sci Technol 2005;65:1964–81.

[7] Ohnabe H, Masaki S, Onozuka M, Miyahara K, Sasa T. Potential application of ceramic matrix composites to aero-engine components. Compos Part A Appl Sci Manuf 1999;30:489–96.

[8] Dicarlo JA, Yun HM, Morscher GN, Bhatt RT. SiC / SiC Composites for 1200 ° C and Above. NASA T/M 2004-213048 2004.

[9] Composite Materials Handbook. Volume 5. Ceramic Matrix Composites. MIL-HDBK-17-5 2002.

[10] Sankar B V., Marrey R V. Analytical method for micromechanics of textile composites. Compos Sci Technol 1997;57:703–13.

[11] Murthy PLN, Chamis CC. Composite Analyzer (ICAN): Users and Programmers Manual. NASA TP-2515 1986.

[12] Skocek J, Zeman J, Sejnoha M. Effective Properties of Textile Composites : Application of the Mori-Tanaka Method. Model Simul Mater Sci Eng 2008.

[13] Ishikawa T, Chou TW. Stiffness and strength behaviour of woven fabric composites. J Mater Sci 1982;17:3211–20.

[14] Aboudi, J., M.-J. Pindera and SMA. Linear thermoelastic higher-order theory for periodic multiphase materials. J Appl Mech 2001;68:697–707.

[15] Choi S. Micromechanical Analysis of Composite Laminates at Cryogenic Temperatures. J Compos Mater 2005;40:1077–91.

[16] Šejnoha M, Zeman J. Micromechanical modeling of imperfect textile composites. Int J Eng Sci 2008;46:513–26.

[17] Tan P, Tong L, Steven GP. Modelling for predicting the mechanical properties of textile composites -A review. Compos Part A Appl Sci Manuf 1997;28A:903–22.

[18] Whitcomb JD, Chapman CD, Tang X. Derivation of Boundary Conditions for Micromechanics Analyses of Plain and Satin Weave Composites. J Compos Mater 2000;34:724–47.

[19] Chang SH, Sutcliffe MPF, Sharma SB. Microscopic investigation of tow geometry changes in a woven prepreg material during draping and consolidation. Compos Sci Technol 2004;64:1701–7.

[20] Lomov SV, Verpoest I, Peeters T, Roose D, Zako M. Nesting in textile laminates: geometrical modelling of the laminate. Compos Sci Technol 2003;63:993–1007.

[21] Woo K, Whitcomb JD. Effects of fiber tow misalignment on the engineering properties of plain weave textile composites. Compos Struct 1997;31:343–55.

[22] Liu KC, Arnold SM. Impact of Material and Architecture Model Parameters on the Failure of Woven Ceramic Matrix Composites (CMCs) Via the Multiscale Generalized Method of Cells. NASA/TM-217011 2011.

[23] Bonacuse PJ, Mital S, Goldberg R. Characterization of the As Manufactured Variability in a CVI SiC/SiC Woven Composite. Proc. ASME Turbo Expo 2011, Asme; 2011.

[24] Rao MP, Pantiuk M, Charalambides PG. Modeling the Geometry of Satin Weave Fabric Composites. J Compos Mater 2008;43:19–56.

[25] Nagpal V, Tong M, Murthy PLN, Mital SK. Probabilistic Material Sylramic Woven Modeling Fiber / CVI-SiC of High-Temperature Properties Composite of a 5-Harness 0/90 Sylramic Fiber/CVI-SiC/MI-SiC Woven Composite. NASA Tech Memo 1998;208497.

[26] Chamis CC. Probabilistic Design of Composite Structures. NASA/TM 2006-214660 2006.

[27] Chowdhury KA, Talreja R, Benzerga AA. Effects of Manufacturing-Induced Voids on Local Failure in Polymer-Based Composites. J Eng Mater Technol 2008;130.

[28] Mital SK, Bednarcyk BA, Arnold SM, Lang J. Modeling of Melt-Infiltrated SiC / SiC Composite Properties. NASA T/M 2009-215806 2009.

[29] Mital SK, Murthy PLN. CEMCAN—Ceramic Matrix Composites Analyzer User's Guide—Version 2.0. NASA TM–107187 1996.

[30] Murthy LN, Mital K, Shah R. Probabilistic Micromechanics Macromechanics for Ceramic Matrix Composites. NASA Tech Memo 1997.

[31] Madsen B, Lilholt H. Physical and mechanical properties of unidirectional plant fibre composites—an evaluation of the influence of porosity. Compos Sci Technol 2003;63:1265–72.

[32] Pal R. Porosity-dependence of Effective Mechanical Properties of Pore-solid Composite Materials. J Compos Mater 2005;39:1147–58.

[33] Peters P, Martin E, Pluvinage P. Influence of porosity and fibre coating on engineering elastic moduli of fibre-reinforced ceramics (SiC/SiC). Composites 1995;26:108–14.

[34] Wu Y, Shivpuri R, Lee LJ. Effect of Macro and Micro Voids on Elastic Properties of Polymer Composites. J Reinf Plast Compos 1998;17:1391–402.

[35] Christensen RM. Effective Properties of Composite Materials Containing Voids. Proc R Soc A Math Phys Eng Sci 1993;440:461–73.

[36] Tsukrov I, Kachanov M. Effective moduli of an anisotropic material with elliptical holes of arbitrary orientational distribution. Int J Solids Struct 2000;37:5919–41.

[37] Zhu H, Sankar BB, Marrey RV. Evaluation of Failure Criteria for Fiber Composites Using Finite Element Micromechanics. J Compos Mater 1998;32:766–82.

[38] Jones R. Mechanics of composite materials. 2nd ed. Philadelphia: Taylor & Francis; 1999.

[39] Schuecker C, Pettermann HE. Fiber Reinforced Laminates: Progressive Damage Modeling Based on Failure Mechanisms. Arch Comput Methods Eng 2008;15:163–84.

[40] Talreja R. Transverse Cracking and Stiffness Reduction in Composite Laminates. J Compos Mater 1985;19:355–75.

[41] Karkkainen RL, Sankar B V., Tzeng JT. Strength prediction of multi-layer plain weave textile composites using the direct micromechanics method. Compos Part B Eng 2007;38:924–32.

[42] Padhi GS, Shenoi RA, Moy SSJ, Hawkins GL. Progressive failure and ultimate collapse of laminated composite plates in bending. Compos Struct 1998;40:277–91.

[43] Ochoa O, Engblom J. Analysis of progressive failure in composites. Compos Sci Technol 1987;28:87–102.

[44] Knight NF. Factors Influencing Progressive Failure Analysis Predictions for Laminated Composite Structure n.d.:1–25.

[45] Blackketter D, Walrath D, Hansen A. Modeling Damage in a Plain Weave Fabric-Reinforced Composite Material. J Compos Technol Res 1993;15:136–42.

[46] Whitcomb J, Srirengan K. Effect of various approximations on predicted progressive failure in plain weave composites. Compos Struct 1996;34:13–20.

[47] Tang X, Whitcomb JD. Progressive failure behaviors of 2D woven composites. J Compos Mater 2003;37:1239.

[48] Camus G. Modelling of the mechanical behavior and damage processes of fibrous ceramic matrix composites : application to a 2-D SiC / SiC. Int J Solids Struct 2000;37:919–42.

[49] Barbero EJ, Lonetti P. An Inelastic Damage Model for. J Compos Mater 2002;36:941–62.

[50] Puck A, Schurmann H. Failure analysis of FRP laminates by means of physically based phenomenological models. Compos Sci Technol 2002;62:1633–62.

[51] Pineda EJ, Waas AM, Bednarcyk BA, Collier CS. Computational Implementation of a Thermodynamically Based Work Potential Model For Progressive Microdamage and Transverse Cracking in Fiber-Reinforced Laminates. NASA/TM 2012-217243 2012.

[52] Nairn J a. The Strain Energy Release Rate of Composite Microcracking: A Variational Approach. J Compos Mater 1989;23:1106–29.

[53] Wang ASD, Crossman FW. Initiation and Growth of Transverse Cracks and Edge Delamination in Composite Laminates Part 1. An Energy Method. J Compos Mater 1980;14:71–87.

[54] ABAQUS Software Package, Ver. 6.8, SIMULIA, Providence, RI. n.d.

[55] Hillerborg A, Modeer M, Petersson P-E. Analysis of Crack Formation and Crack Growth in Concrete by Means of Fracture Mechanics and Finite Elements. Cem Concr Res 1976;6:773–82.

[56] Barenblatt GI. The mathematical theory of equilibrium cracks in brittle fracture. Adv Appl Mech 1962;7:55–129.

[57] Yang Q, Cox B. Cohesive models for damage evolution in laminated composites. Int J Fract 2005;133:107–37.

[58] Goldsmith MB, Sankar B V, Haftka RT, Goldberg RK. Effects of Microstructural Variability on Thermo-Mechanical Properties of a Woven Ceramic Matrix Composite. NASA/TM 2013-217817 2013.

[59] Nemeth NN, Mital SK, Lang J. Evaluation of Solid Modeling Software for Finite Element Analysis of Woven Ceramic Matrix Composites. NASA T/M 2010-216250 2010.

[60] Reid A. Modeling Microstructures with OOF2. Int J Mater Prod Technol 2009;35:361–73.

[61] Woo K, Suh Y, Whitcomb J. Effect of Phase Shift on Engineering Properties of Plain Weave Laminates. J Compos Mater 2005;39:479–95.

[62] MATLAB 2011A Student Edition, The MathWorks Inc., Natick, MA, 2000). n.d.

[63] Lamon J. A micromechanics-based approach to the mechanical behavior of brittle-matrix composites. Compos Sci Technol 2001;61:2259–72.

[64] Morscher G, Singh M, Kiser J, Freedman M, Bhatt R. Modeling stress-dependent matrix cracking and stress–strain behavior in 2D woven SiC fiber reinforced CVI SiC composites. Compos Sci Technol 2007;67:1009–17.

[65] Evans AG, Zok FW. Review The physics and mechanics of fibre-reinforced brittle matrix composites. J Mater Sci 1994;29:3857–96.

[66] Lamon J, Thommeret B, Percevault C. Probabilistic-statistical Approach to Matrix Damage and Stress ± Strain Behavior of 2-D Woven SiC / SiC Ceramic Matrix Composites. J Eur Ceram 1998;18:1797–808.

[67] Http://www.ceramics.nist.gov/srd/summary/fthexsa.htm. NIST Property Data Summaries for Hexoloy SA (SiC) 2001.

[68] Http://www.ceramics.nist.gov/srd/summary/ftgsic.htm. NIST Property Data Summaries for Silicon Carbide (SiC) 2001.

[69] Mital SK, Goldberg RK, Bonacuse PJ. Two-Dimensional Nonlinear Finite Element Analysis of CMC Microstructures. Vol 1 Aircr Engine; Ceram Coal, Biomass Altern Fuels; Wind Turbine Technol 2011:491–6.

[70] Swaminathan S, Ghosh S, Pagano NJ. Statistically Equivalent Representative Volume Elements for Unidirectional Composite Microstructures: Part I - Without Damage. J Compos Mater 2006;40:583–604.

BIOGRAPHICAL SKETCH

Marlana Goldsmith is from Daytona Beach, Florida. She graduated with a Bachelor of Science in Aerospace Engineering from the University of Florida in 2009. That same year she joined the Center for Advanced Composites at The University of Florida where she previously participated in undergraduate research. During the summer of 2009 she held an internship at NASA Langley Research Center. She also spent several more months at NASA Langley Research Center and NASA Glenn Research Center as part of the NASA Graduate Student Research Program. She was awarded the Alumni Fellowship from The University of Florida, the Amelia Earhart Fellowship from Zonta International, and AIAA's Harry H. and Lois G. Hilton Best Paper Award in structures.